Stretchable electronics towards the fabrication of organic sensors for artificial skin

Bastien Marchiori

N°d'ordre NNT : 2018LYSEM025

THESE de DOCTORAT DE L'UNIVERSITE DE LYON

opérée au sein de
l'Ecole des Mines de Saint-Etienne

***Ecole Doctorale** N° 488*
Sciences, Ingénierie, Santé

***Spécialité de doctorat** : Microélectronique*

Soutenue publiquement le 19/11/2018, par :
Bastien MARCHIORI

STRETCHABLE ELECTRONICS TOWARDS THE FABRICATION OF ORGANIC SENSORS FOR ARTIFICIAL SKIN

DEVELOPPEMENT DE L'ELECTRONIQUE ETIRABLE POUR LA FABRICATION DE CAPTEURS ORGANIQUES POUR LA PEAU ARTIFICIELLE

Devant le jury composé de :

Président

John C. de Mello, Professeur, Norwegian University of Science and Technology, Rapporteur
Piero Cosseddu , Associate professor, Università di Cagliari, Rapporteur

Louis Giraudet , Professeur, Université de Reims, Examinateur
Escoubas Stéphanie, Maitre-assistante, Université d'Aix-Marseille, Examinatrice

Sylvain Blayac, Professeur, Ecole des Mines de Saint-Etienne, Directeur de thèse
Marc Ramuz Maitre-assistant, Ecole des Mines de Saint-Etienne, Encadrant

Spécialités doctorales	Responsables :	Spécialités doctorales	Responsables
SCIENCES ET GENIE DES MATERIAUX	K. Wolski Directeur de recherche	MATHEMATIQUES APPLIQUEES	O. Roustant, Maître-assistant
MECANIQUE ET INGENIERIE	S. Drapier, professeur	INFORMATIQUE	O. Boissier, Professeur
GENIE DES PROCEDES	F. Gruy, Maître de recherche	SCIENCES DES IMAGES ET DES FORMES	JC. Pinoli, Professeur
SCIENCES DE LA TERRE	B. Guy, Directeur de recherche	GENIE INDUSTRIEL	N. Absi, Maitre de recherche
SCIENCES ET GENIE DE L'ENVIRONNEMENT	D. Graillot, Directeur de recherche	MICROELECTRONIQUE	Ph. Lalevée, Professeur

EMSE : Enseignants-chercheurs et chercheurs autorisés à diriger des thèses de doctorat (titulaires d'un doctorat d'Etat ou d'une HDR)

ABSI	Nabil	MR	Génie industriel	CMP
AUGUSTO	Vincent	CR	Image, Vision, Signal	CIS
AVRIL	Stéphane	PR2	Mécanique et ingénierie	CIS
BADEL	Pierre	MA(MDC)	Mécanique et ingénierie	CIS
BALBO	Flavien	PR2	Informatique	FAYOL
BASSEREAU	Jean-François	PR	Sciences et génie des matériaux	SMS
BATTON-HUBERT	Mireille	PR2	Sciences et génie de l'environnement	FAYOL
BEIGBEDER	Michel	MA(MDC)	Informatique	FAYOL
BLAYAC	Sylvain	MA(MDC)	Microélectronique	CMP
BOISSIER	Olivier	PR1	Informatique	FAYOL
BONNEFOY	Olivier	MA(MDC)	Génie des Procédés	SPIN
BORBELY	Andras	MR(DR2)	Sciences et génie des matériaux	SMS
BOUCHER	Xavier	PR2	Génie Industriel	FAYOL
BRODHAG	Christian	DR	Sciences et génie de l'environnement	FAYOL
BRUCHON	Julien	MA(MDC)	Mécanique et ingénierie	SMS
CAMEIRAO	Ana	MA(MDC)	Génie des Procédés	SPIN
CHRISTIEN	Frédéric	PR	Science et génie des matériaux	SMS
DAUZERE-PERES	Stéphane	PR1	Génie Industriel	CMP
DEBAYLE	Johan	MR	Sciences des Images et des Formes	SPIN
DEGEORGE	Jean-Michel	MA(MDC)	Génie industriel	Fayol
DELAFOSSE	David	PR0	Sciences et génie des matériaux	SMS
DELORME	Xavier	MA(MDC)	Génie industriel	FAYOL
DESRAYAUD	Christophe	PR1	Mécanique et ingénierie	SMS
DJENIZIAN	Thierry	PR	Science et génie des matériaux	CMP
DOUCE	Sandrine	PR2	Sciences de gestion	FAYOL
DRAPIER	Sylvain	PR1	Mécanique et ingénierie	SMS
FAUCHEU	Jenny	MA(MDC)	Sciences et génie des matériaux	SMS
FAVERGEON	Loïc	CR	Génie des Procédés	SPIN
FEILLET	Dominique	PR1	Génie Industriel	CMP
FOREST	Valérie	MA(MDC)	Génie des Procédés	CIS
FRACZKIEWICZ	Anna	DR	Sciences et génie des matériaux	SMS
GARCIA	Daniel	MR(DR2)	Sciences de la Terre	SPIN
GAVET	Yann	MA(MDC)	Sciences des Images et des Formes	SPIN
GERINGER	Jean	MA(MDC)	Sciences et génie des matériaux	CIS
GOEURIOT	Dominique	DR	Sciences et génie des matériaux	SMS
GONDRAN	Natacha	MA(MDC)	Sciences et génie de l'environnement	FAYOL
GONZALEZ FELIU	Jesus	MA(MDC)	Sciences économiques	FAYOL
GRAILLOT	Didier	DR	Sciences et génie de l'environnement	SPIN
GROSSEAU	Philippe	DR	Génie des Procédés	SPIN
GRUY	Frédéric	PR1	Génie des Procédés	SPIN
GUY	Bernard	DR	Sciences de la Terre	SPIN
HAN	Woo-Suck	MR	Mécanique et ingénierie	SMS
HERRI	Jean Michel	PR1	Génie des Procédés	SPIN
KERMOUCHE	Guillaume	PR2	Mécanique et Ingénierie	SMS
KLOCKER	Helmut	DR	Sciences et génie des matériaux	SMS
LAFOREST	Valérie	MR(DR2)	Sciences et génie de l'environnement	FAYOL
LERICHE	Rodolphe	CR	Mécanique et ingénierie	FAYOL
MALLIARAS	Georges	PR1	Microélectronique	CMP
MOLIMARD	Jérôme	PR2	Mécanique et ingénierie	CIS
MOUTTE	Jacques	CR	Génie des Procédés	SPIN
NEUBERT	Gilles			FAYOL
NIKOLOVSKI	Jean-Pierre	Ingénieur de recherche	Mécanique et ingénierie	CMP
NORTIER	Patrice	PR1	Génie des Procédés	SPIN
O CONNOR	Rodney Philip	MA(MDC)	Microélectronique	CMP
OWENS	Rosin	MA(MDC)	Microélectronique	CMP
PERES	Véronique	MR	Génie des Procédés	SPIN
PICARD	Gauthier	MA(MDC)	Informatique	FAYOL
PIJOLAT	Christophe	PR0	Génie des Procédés	SPIN
PINOLI	Jean Charles	PR0	Sciences des Images et des Formes	SPIN
POURCHEZ	Jérémy	MR	Génie des Procédés	CIS
ROUSSY	Agnès	MA(MDC)	Microélectronique	CMP
ROUSTANT	Olivier	MA(MDC)	Mathématiques appliquées	FAYOL
SANAUR	Sébastien	MA(MDC)	Microélectronique	CMP
STOLARZ	Jacques	CR	Sciences et génie des matériaux	SMS
TRIA	Assia	Ingénieur de recherche	Microélectronique	CMP
VALDIVIESO	François	PR2	Sciences et génie des matériaux	SMS
VIRICELLE	Jean Paul	DR	Génie des Procédés	SPIN
WOLSKI	Krzystof	DR	Sciences et génie des matériaux	SMS
XIE	Xiaolan	PR0	Génie industriel	CIS
YUGMA	Gallian	CR	Génie industriel	CMP

Mise à jour : 03/02/2017

Acknowledgements

First, I want to thank Marc Ramuz, to have been a good supervisor. Thank you for sharing your vision, your ethic of the research and all the small tips that help with the project. These 3 years were tough, and I would not have been able to fabricate this stretchable OECT without your dedication. Thanks also to Sylvain Blayac for having many comments to make everything progressing, and especially to make this manuscript like a cocktail glass, and finally to Roger for being always available when I needed some help with machines.

Thank you to Stéphanie Escoubas, Souren Grigorian and Mouaad for teaching me the way of life in Synchrotron and helping me with this project. It was a great experience, and I hope my replacement will enjoy the experience as much as I enjoyed it, even though it was very exhausting. Thank you also to Lionel Fritsch and the other members from IRLYNX for helping me with the fabrication of the infrared sensor. The discussions about the PVDF were very interesting and very helpful.

Thank you to everyone else from FEL/former PS2 and particularly the open space. Thanks to Malika and Olivier for being my first office mates; to Simon, Mohamed, Omar, Aravind and all the other professors. I would also like to thank everyone from CMP, for their participation to make this happen, and particularly Jessica, Thierry, Jean Philippe, Anais, Michelle, Véronique… They were not involved directly in the project, however very helpful and dedicated. Thank you to the people from the other departments (BEL, SAS, SFL, Magali) and especially to Mary Donahue that was always there to answer my question and gave me the opportunity to participate to ELBYSIER. Thank you also to all my future colleagues from Panaxium and to Pierre for very helpful LabVIEW tips and for giving me the opportunity to join the company.

Remerciements

Je voudrais commencer par remercier mon père et ma mère. Vous n'avez pas toujours compris ce que je faisais exactement, mais parce que je n'ai pas toujours été clair dans mes explications. Mais je sais que vous avez toujours été derrière moi. Merci, du fond du cœur, de m'avoir soutenu (de loin). Je voudrais aussi en profiter pour vous remercier pour tout ce que vous avez fait avant. Financièrement, d'abord, je suis conscient que ça n'a pas été forcément facile pour vous, mais que vous avez fait des sacrifices pour m'offrir cet avenir. Pour le moment, je ne peux pas vous remercier comme il se doit, mais un jour, je saurais le faire ! Ensuite, je souhaite remercier mon frère et ma sœur. Même si je suis parti il y a un moment maintenant, quand je reviens, c'est comme si je n'étais jamais parti. Merci à vous pour votre soutien et j'espère que vous le savez déjà, je serai toujours là en cas de besoin.

Finalement, les derniers remerciements en français iront à mes amies et collègues: Séverine et Yanid. Séverine, merci d'avoir accepté de commencer une thèse en dépit de tout ce que j'ai pu te dire sur Aix. Je te souhaite bon courage, et particulièrement pour les prochains mois, et pour la fin de la thèse. Yanid, ce n'est pas seulement moi qui te remercie, mais aussi et surtout petit chat, pour avoir pris soin de lui avec amour. Merci pour ta bonne humeur et ton énergie.

Contents

List of Figures

Introduction

The development of flexible and stretchable electronics has opened the possibilities to many new outstanding applications. For wearable electronics, very thin flexible devices can conform to 3D surfaces and stretchable devices can go even further and follow any deformation. For application within the skin, this property is mandatory. The skin can stretch up to 15% and is constantly moving. These technologies are thus particularly suitable for developing sensing or actuating devices distributed directly onto human skin.

The feeling of touch and pressure within the artificial skin has been widely studied, but integrating temperature sensing capabilities remains a challenge and particularly the non-contact sensing. This thesis aims to understand the strategies for making stretchable devices; and then, to provide the tools to make stretchable sensors and integrate them into artificial skin. The different components of a stretchable sensor are analysed to select the appropriate materials and methods for this application. New processes for fast and easy fabrication of highly stretchable devices are introduced. To understand the challenges and develop processes for making soft sensors, a stretchable organic electrochemical transistor with high performance is fabricated. Its integration onto the skin would give the ability to sense various physiological parameters. Then, a stretchable infrared sensor with similar performance than rigid electronic devices is demonstrated.

Chapter 1 reviews the state-of-the-art stretchable sensors for electronic skin. A study of stretchable devices is carried out to understand the design structure of such systems. A stretchable sensor comprises 3 different blocks with different strategies to make the overall sensor stretchable: the substrate to carry the device, the interconnection integrated into the substrate to route the signal, and the active area between the interconnections to generate a signal.

Chapter 2 provides a method to make highly conductive stretchable interconnections. This process allows the fabrication of bulk metallic interconnections for a minimum resistivity under stretch and thus, high quality of the signal.

Chapter 3 presents the integration of interconnections compatible with classic microfabrication process, and application to sensor based on organic materials. First, a platform for electrical wound-healing is demonstrated to identify the key functionalities of the organic electrochemical transistor (OECT). Then, the optimisation of this device is shown in order to make it stretchable.

Chapter 4 is dedicated to the fabrication of the stretchable temperature and infrared sensor. By using the knowledge developed in the previous chapters, the sensor shows promising results for integration into electronic skin.

1. State-of-the-Art soft Electronics for sensing application

This chapter provides a general overview of the work done to make stretchable electronic devices for e-skin applications. The meaning of stretchable, in this thesis, has to be understood by the ability of an object (more specifically, a device, or a material) to be elastically elongated without being inelastically or permanently deformed. A stretchable device keeps its functionality by definition until a certain elongation defining its stretchability. A review of stretchable devices is provided in the first section. The different elements of a stretchable device are analysed and studied separately. The screening of the materials for the substrate, the interconnections and the active material is done. The materials and the processes are chosen according to the applications. Then, an introduction of the two sensors developed in this work is provided in order to understand the challenges.

Most of the electronics systems and applications rely on rigid electronic devices. Figure 1 displays the evolution of electronics from rigid calculators and computers to soft and conformal electronic devices. The technology from more than 100 years ago allowed the fabrication of cumbersome systems, with restrictive applications such as calculus with a simple computer or telephone. However, since the discovery of the transistor in 1925, more and more sophisticated devices have been developed. As described by Moore's law, the continuous miniaturisation of the transistors has led to shrinking of electronics. With the first mobile phone in 1973, people have been able to take electronic systems with them. As a step forward, devices fully and properly integrated on our skin or in textile are being imagined. The smartwatches are the perfect examples of what people want to achieve: they can monitor in live what is happening to our body. However, the devices are still limited. For now, most of the applications are restricted by the rigidity of the available devices.

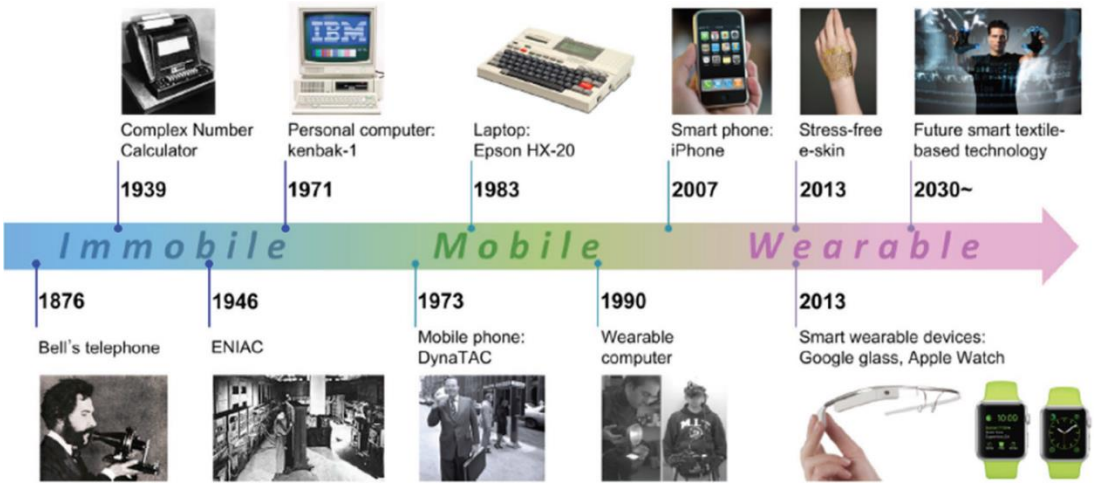

Figure 1: Evolution of electronics, from immobile to wearable systems. It implies the development of imperceptible soft and stretchable systems. Reproduced from [1].

The field of stretchable electronics is emerging to go beyond this limitation. Stretchable electronics concern electrical and electronic circuits that are elastically or inelastically stretchable by more than a few per cent while retaining function. To achieve this, devices tend to be laminar and usually thin. Compared with rigid, hard conventional electronic systems in planar formats, stretchable electronic systems can be stretched, compressed, bent, and deformed into arbitrary shapes without electrical or mechanical failure within the circuits.

For this reason, stretchable electronic systems have many important and emerging applications in new, soft and curved bio-inspired areas, such as tunable electronic eye cameras or epidermal electronics capable of mechanically invisible integration onto human skin. The human body is soft, always in movement and in evolution. Its skin can be stretched during movements up to 15%[2]. So, electronic systems have to match with the mechanical properties of the skin to fit with the body. Moreover, this evolution will lead to electronic systems more imperceptible, comfortable to use. For example, stretchable sensors for biomedical applications include various sensing capabilities such as temperature, touch/pressure, electrocardiogram, and motion detection. Stretchable electronic devices can also be attached to any organ in the body to monitor or assist functions of organs for health care. The use of very thin flexible sensors has

already been integrated and has shown good contact with the skin[3]. However, the use of stretchable devices, particularly for large scale applications will improve the reliability and the compatibility with the probed surface. Through the engineering of a matrix of sensors, it would be possible to re-create tactile and temperature sensing properties for robotic or prosthetic applications. The integration of these sensors in a large area is commonly known as electronic skin (e-skin).

Figure 2 shows an example of an e-skin design. The global device is organised with several layers of a matrix of sensors. The aim of this skin is to be integrated on prosthesis and to give back all the properties of the skin: touch, pressure and temperature. For this purpose, the e-skin is structured into layers. Each layer has one application. The outside layer is made out of tactile sensors for the feeling of the touch. The second layer is dedicated to infrared temperature sensing, and the last layer is for deep pressure sensing. Each sensor response is sent through the vertical interconnections to the last layer that receives and analyse the signal[4].

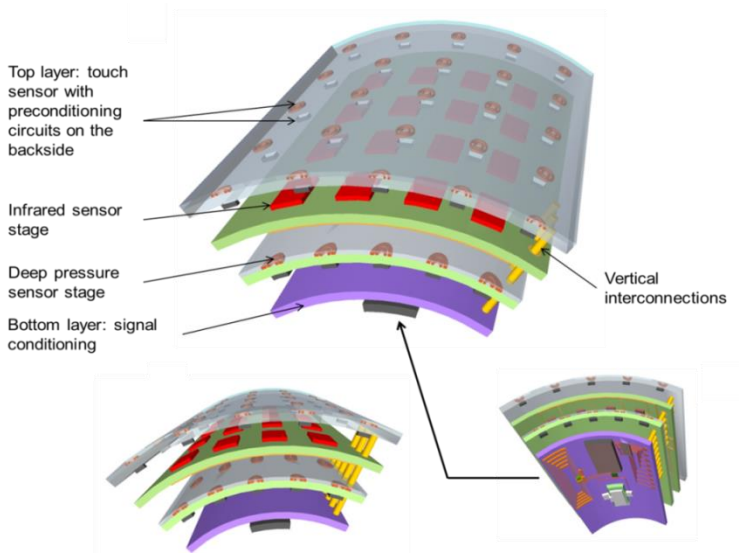

Figure 2: Illustration of the construction of a multifunctional e-skin. The skin is built from 3 layers of sensors: touch, infrared and pressure. They are all connected with vertical interconnections to the last layer which processes the signal.

A stretchable sensor, and more globally a stretchable device is built around three components: a substrate, interconnections and a sensitive material.

- The substrate is the first material to choose. It has to be stretchable because it is the material in direct contact with the deformation, and also the matrix containing the sensor. The substrate has to be compatible with the process of fabrication of the device. The stretchability of the substrate - its ability to deform before it breaks or lose its initial properties - is critical.
- The interconnections are defined by the stretchability and the conductivity. It is important to have a high conductivity to collect a proper signal from the device. Thus, a study of the conductivity regarding the stretchability of these interconnections is the key to choose the material and technique adapted to the application.
- The active material for sensing: inorganic and organic materials are potential candidates for this function. Inorganics are rigid, and thus, an effort to integrate a rigid material into a stretchable matrix is the appropriate strategy. For Organics, the material naturally possesses a better stretchability than metals. It is possible to improve the stretchability by different techniques, and also to study the strategy to minimise the elongation of the material: the strain. This strain is caused by the application of a stress: a tension which pulls the material. The material has a certain degree of resistance to the stress before being strained.

The fabrication of a stretchable device is always constructed around the same logic. The substrate is fabricated independently from the interconnections. Then, depending on the material used, a strategy is chosen to integrate the interconnections within this substrate. Finally, the active material is patterned through microfabrication techniques[5].

The goal of this work is to develop and fabricate stretchable electronic sensors for e-skin applications. For instance, a stretchable OECT - with physiological sensing abilities - has been developed. Moreover, a temperature sensitive layer was fabricated with an ability to sense infrared emission to reproduce the ability of the human body to feel the temperature and to “feel” temperature even in contactless approach. All of these devices have to stretch up more

than 15 % for an application in e-skin. Thus, an objective of 30% has been targeted for our devices; moreover higher stretchability improves the reliability of the device. One challenge with stretchable devices, however, is the limited availability of high-performance stretchable conductors, semiconductors and more generally devices with the same electrical properties than rigid electronic systems.

Additionally to a certain degree of flexibility, organic materials are potentially low cost and easy to integrate for large scale fabrication. For application in sensing, this mechanical flexibility and their mixed ionic/electronic conductivity are also more adapted to sense signals in interaction with the body, for physiological measurements[5]. Then, the development of organic sensors has been chosen as a focus for this work with two sensors:

- The OECT is a sensor which fits with the vision of the e-skin. It can be used as a multitask sensor for measuring physiological parameters on the body.
- An infrared sensor for contact/non-contact temperature measurement which aims to be integrated on the e-skin especially for prosthetic and robotic applications.

Section 1.1 reviews the existing work on stretchable devices for e-skin application. The development of the e-skin is an intensive topic of research. Many examples of pressure sensors are available in the literature, but stretchable temperature sensors are still marginal. However, examples of e-skin capable of sensing multiple characteristics can be found.

Section 1.2 presents the use of polymers in organic electronics and illustrates their superior stretchable properties.

Section 1.3 explains the choice of the substrate, compatible with the skin and with microelectronic processes.

Section 1.4 reviews the different strategies for making interconnections stretchable. Different approaches are presented. The stretchability of thick rigid materials is enhanced with a tuning of the design. For thin material, using strategy for processing the substrate such as pre-strain

during the fabrication of the interconnections is more adapted. Some composite materials can also be used as interconnections and are designed to be intrinsically stretchable.

Section 1.5 deals with the integration of the active area. The two strategies are introduced: the rigid-island method, by using a stiff material which is not deformed and the direct integration of the sensor on the stretchable substrate which deforms according to it.

Section 1.6 introduces the basics on the OECT and infrared sensor, which are developed and fabricated in the next chapters.

Section 1.7 sets the objective of the thesis and sum up the technological choices decided in this chapter.

1.1. Review of stretchable devices for e-skin applications

The skin is a complex metabolic active organ, which performs essential physiological functions. It is the largest organ of the body, making up 5-8% of body weight, with a surface area of $1.7m^2$[6]. Primary functions of the skin include barrier protections, temperature and tactile/pressure sensing. Sensing functions are carried out by a variety of sensors that transduce pressure, vibration, touch, stretch, strain, temperature, pain, and proprioception. Moreover, the skin can be stretched to perfectly fit to the shape of the body.

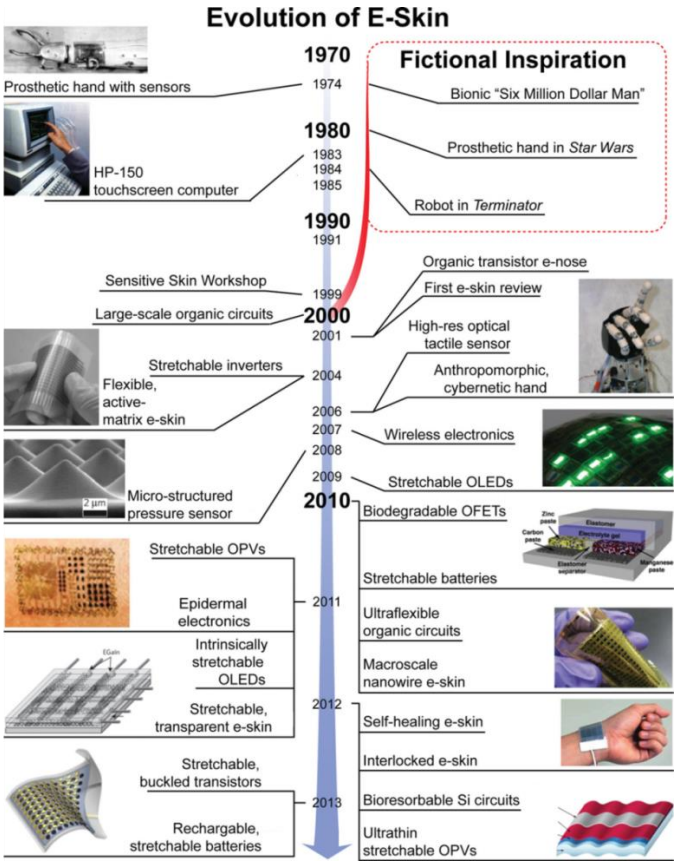

Figure 3: Big steps for the evolution of the e-skin from 1970 to 2013. Reproduced from [7].

Applications can go from mechanically invisible integration onto human skin to even surgical and diagnostic implementations. It naturally integrates with the human body to provide advanced therapeutic capabilities for prosthetics[8]–[11]. For example, stretchable sensors for biomedical applications have been attracting interest to develop various sensing capabilities such as temperature, touch, electrocardiogram and motion detection[8], [10], [12], [13].

Figure 3 presents an overview of the research on e-skin until 2013[7]. Extensive work has been achieved in the field regarding the recognition of nerves signal through movement of the fingers. Frank *et al.* reported the successful feedback of sensors for the movement of metallic fingers[14]. In 2001, after a workshop on sensitive skin, Lumelsky *et al.* introduce the first idea of an electronic/sensitive skin able to sense the surrounding environment based on LED and infrared detectors on a flexible substrate[15]. After, with the development of large scale organic

electronics, the research accelerated in the 2000's. The development of electronic skin with pressure sensing capabilities was shown by Someya *et al.*[16], [17]. Meanwhile, the development of the stretchable interconnections presented in the previous section is an intense subject of research to reach the first stretchable large area electronic system in 2009 with a stretchable matrix of transistors and organic light emitting diode (OLED)[18], [19]. Since 2010, the research in e-skin has been in constant progress. To reproduce the capabilities of the skin, the main developed devices are pressure and temperature sensors.

This section presents the integration of stretchable devices for e-skin, with pressure and temperature sensors. Then, the work on the integration of multiple sensors in the same device is introduced.

1.1.1. Pressure sensing

Over the last few years, examples of skin-like devices were achieved by focusing on the pressure sensor functionality onto a large area, flexible substrates such as PET[16], [20]. The use of stretchable material is adapted to the pressure sensing because it deforms according to the pressure. Figure 4 displayed an example of a transistor with a sensitive rubber used as a dielectric for the transistor. It can transduce the applied pressure into changes of the transistor output by the modification of the thickness of the dielectric. Bao *et al.* reported microstructured-rubber-based capacitive pressure sensors with a measured sensitivity up to $0.5kPa^{-1}$[21]. Despite being highly sensitive, these capacitive-based pressure sensors are neither conformable nor stretchable due to the required metallic interconnections. As a fully stretchable alternative for a pressure sensor, resistive modulation based on thin rubber films has been used but shows large hysteresis and reduced sensitivity in the low-pressure regime (<10kPa)[22]. Alternative technology incorporates capacitive sensing between adjacent or superposed electrodes, widely used for touch screens. This system has the advantage of technological simplicity for the sensor itself but requires the use of complex ultralow capacitance measurement and specific analogic acquisition circuits. It is highly desirable to

develop sensors which deliver direct voltage. Piezoelectric pressure sensors based on polyvinylidene fluoride (PVDF) are not strictly speaking stretchable but could be flexible. They exhibit a dynamic measurement range within [0-200kPa] and a response time around 100µs[23]. Moreover, they can be deposited by an additive process such as inkjet printing. They also demonstrate pyroelectric behaviour that has been exploited for temperature sensing.

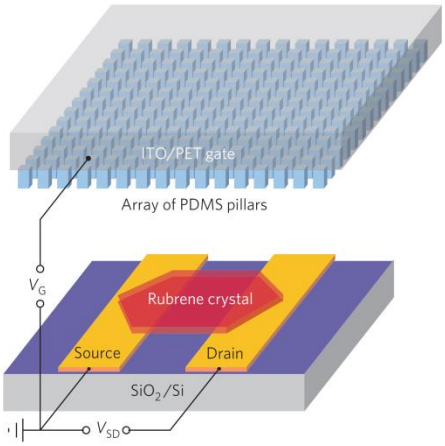

Figure 4: Schematic of a pressure sensor based on a gate with a thickness of dielectric depending on the pressure. Reproduced from[21].

1.1.2. Temperature sensing

Temperature sensing is a crucial functionality in e-skin that allows the body to be aware of the surrounding environment. However, most of the pressure/tactile sensors are also temperature sensitive so they can be used with an appropriate calibration for temperature sensing[24]. However, it is difficult to separate the contribution of the pressure from the one of the temperature as it often has the same kind response. By using two different pyroelectric materials with two different poling, Graz *et al.* have achieved materials with only either pyroelectric properties or piezoelectric properties[25]. Trung *et al.* have separated these two effects by using AC gate biasing on the sensitive material, with a transistor and the pyroelectric material as a dielectric. The pyroelectric voltage, the capacitance and the mobility were

measured to separate the two contributions[26]. A flexible large area matrix of sensors has been used for an e-skin application. Yu *et al.* have made a gold-based temperature sensor on a pre-strain substrate with a stretchability of 30%[27]. Then, several groups have developed e-skin with sensors using platinum[13] and gold[12] that can resist to the strain of the skin using meander shapes. Finally, Someya *et al.* have made a large area matrix of sensors using a metallic mesh with flexible transistors that shows stretchability up to 30%. The range of detection was from 30°C to 160°C[17].

1.1.3. Multisensory integration

Only a few examples of the integration of multiple skin functionalities have been reported. Recently, Javey *et al.* reported a flexible touch sensor with integrated output capabilities[28]. Rogers *et al.* described an array of thermal sensors integrated onto the skin that could be combined with other functionalities such as strain sensors or EEG recording[13]. Segev-Bar *et al.* have demonstrated a pressure, temperature and humidity sensor based on nanoparticles[29]. Finally, Kim *et al.* have demonstrated the engineering of a complete e-skin, capable of being used on a prosthetic hand illustrated by Figure 5. It was capable of reproducing almost all the properties of the skin such as pressure, temperature, humidity sensing, but also generation of heat and can be stretched up to 20%[30].

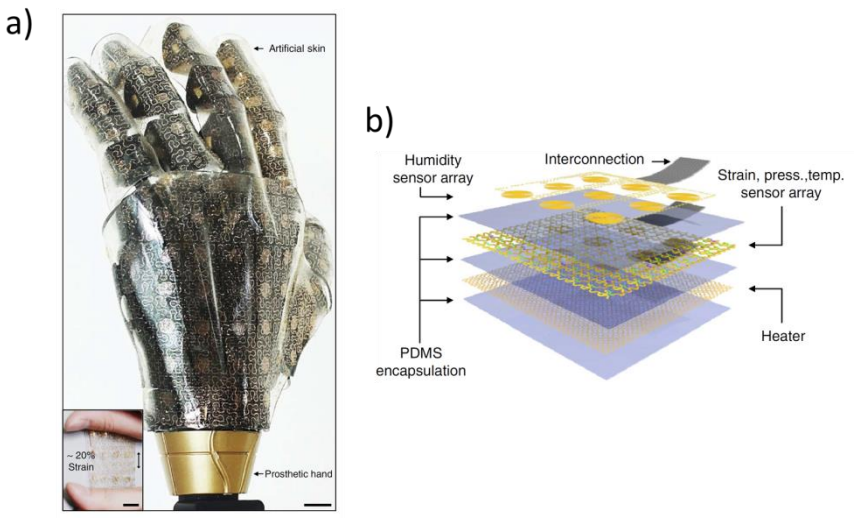

Figure 5: Artificial skin developed by Kim et al. a) Picture of the device on a prosthetic hand. b) The skin comprised a humidity sensor, strain, pressure and temperature sensor mapping and a heater encapsulated in polydimethylsiloxane (PDMS). Reproduced from [30].

The development of e-skin with an ability to sense multiple parameters is not entirely covered. The development of a multi-layered device presented in the introduction is a solution for the integration in prosthetics and robotics particularly. For this thesis, the focus is on organic electronics and particularly on the use of polymers as active materials.

1.2. Polymers in organic electronics

The organic electronics is a field comprising the use of small molecules and polymers for making electronic devices. Some of them can be used in a variety of situation because of the insulating, semiconducting and conducting properties. They possess the advantage of being mechanically flexible and stretchable more than inorganic materials due to their particular molecular arrangement.

This section summarises the applications of the conducting polymers. Then, a discussion about the stretchable properties in polymers compared to other materials is provided.

1.2.1. Applications of conducting polymers

Since the Nobel Prize for the discovery of the conduction of polyacetylene in 1977 by H. Shirakawa, A. Heeger and A. MacDiarmid[31], organic electronics has been an intense subject of research. This development has led in recent years to significant advances in the field of organic photovoltaics (OPV)[32], OLED[33] and organic thin-film transistors (OTFT)[34]. Indeed, compared to inorganic devices, the organic has the advantage of being easier to process with a low cost of fabrication. Applications in bioelectronics remain recent. The mechanical flexibility of organic devices would help for example to reduce the damaging of the tissues for applications *in-vivo* where rigid devices can cause inflammations to tissues[35], [36]. The ionic permeation of the conducting polymers combined with its electrical conductivity greatly improve the interface compatibility with biological systems, reducing the impedance of contact[37].

The main problem with all the applications concerns the stability of the material. Organic devices are often sensitive to the O_2 and H_2O present in the air. The UV light or the use of an electrical field can damage the active organic layer irreversibly[38]. In term of pure performances, organic materials are not able to achieve mobility and conductivity as high as inorganic materials. The semi-crystalline nature is a limiting factor in organic electronics; the charges do not move as fast as in the crystalline region, reducing the mobility[39].

1.2.2. Understanding the superior stretchable properties of polymers

In inorganic materials, as displayed in Figure 6a, the atoms are aligned depending on the material in a predefined arrangement. The stability is ensured by sharing electrons with neighbour atoms forming a covalent bond in the case of silicon for example. When the material is stretched, the deformation implies the break of a covalent bond and cracks appears directly in

the material[40]. Thus, their perfect crystal structure does not allow a high stretchability (typically less than 5%).

Figure 6b presents the structure of polymers, different from crystals. Usually, polymers are long chains of atoms, organised in clusters of crystalline structure in an amorphous matrix. It can spread from fully amorphous with disordered chains; to fully crystalline with perfectly oriented chains. Most of the polymers are either amorphous or semi-crystalline, and the ratio of crystalline /amorphous phases defines the degree of crystallinity of a polymer. This crystallinity can also enhance properties that depend on the arrangement of the chains. For example, a better crystallinity of poly(3,4-ethylenedioxythiophene):poly(styrenesulfonate) (PEDOT:PSS) improves its conductivity[41]. The crystallisation can be improved with the process of fabrication. A melted or solubilised polymer gives, for example, more crystallinity at high temperature than at low temperature[42]. Another example is to brush the polymer chains to orient them in the same direction, enhancing the crystallinity of a conjugated polymer artificially and at the same time their conductivity[43].

There is another method for inducing crystallinity of the polymer chains: so-called cross-linked polymers. This arrangement is constrained by a chemical reaction between a chemical group within the polymer chain and another one from a cross-linker agent. This agent can be another polymer or a small molecule. Figure 6c presents the structure of the resulting polymer. The agent is added to the monomer or polymer mixture in a liquid state and reacts to form a grid. It creates less mobility and thus higher stiffness.

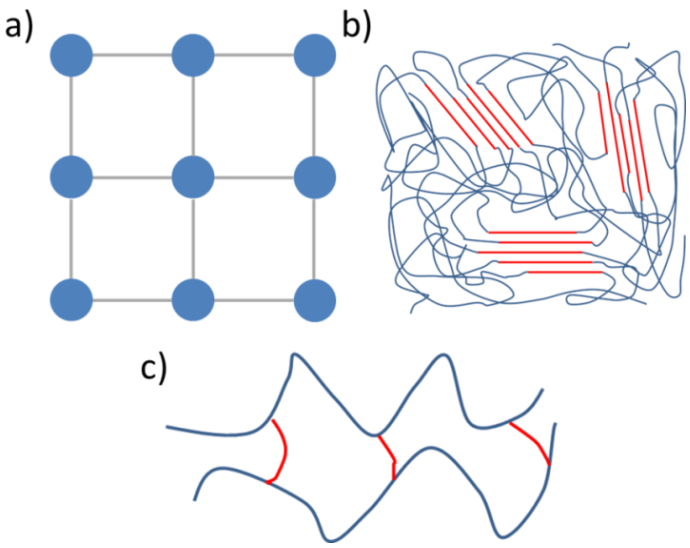

Figure 6: Crystalline structure of a) monocrystalline arrangement; b) polymer semi-crystalline structure, within red the crystallites and in blue the amorphous regions; and c) cross-linked polymers. The polymers have the particularity to possess a certain disorder at the mesoscopic phase. It gives him its particular mechanical properties.

The PDMS belongs to these cross-linked polymers. There are a lot of different PDMS formulations with different length and composition, resulting in different mechanical properties. It is made out of several components mixed containing silicone polymers of different length, a small polymer terminated by vinyl groups (double carbon bond) and a catalyst. When mixed, the vinyl and Si-H groups react together forming the three-dimensional network in an amorphous matrix. Depending on the length and the proportion of the polymers, the resulting copolymer has different mechanical properties. If more cross-linking agent is added (Figure 7b) or if the curing temperature is higher (Figure 7a), this increases the hardness of the PDMS because of more cross-linking reactions[44], [45].

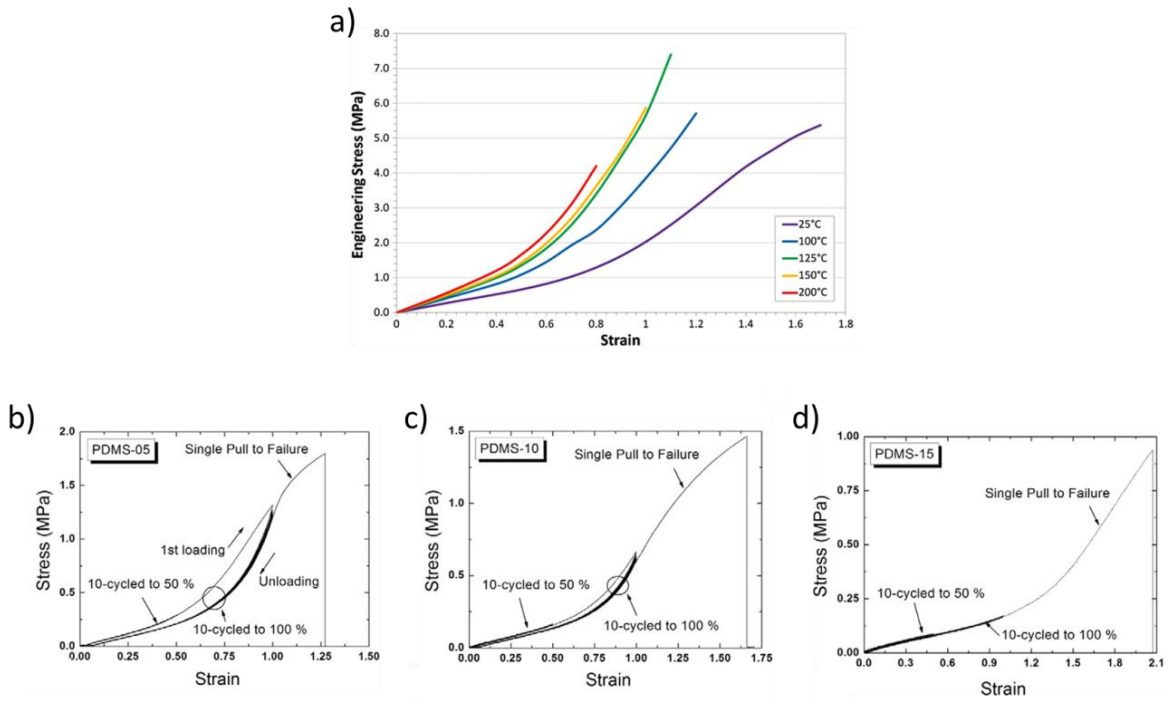

Figure 7: Mechanical properties of PDMS as a function of the process. a) Stress-strain curve as a function of the curing temperature. The strain at break is decreasing when the temperature of curing is higher. Reproduced from[44]. b,c,d) stress-strain curve with different ratio of initial polymer:cross-linking agent with b) 5:1, c)10:1 and d) 15:1. The strain at break is increasing with less cross-linking agent. Reproduced from [46].

It is possible to understand the effect of the crystallinity on the stretchability by studying the effect of the strain at the molecular level. Figure 8 presents this mechanism of stretchability in polymers. When the structure is stretched, the amorphous phases slide between themselves in the direction of the stretch, until reaching a certain rigidity and alignment. Then, when the tension is maximum, the crystalline regions start also to slide. The mechanism in cross-linked polymers is the same. The polymer-free chains slide and stretch the network until the structure is fully tight.

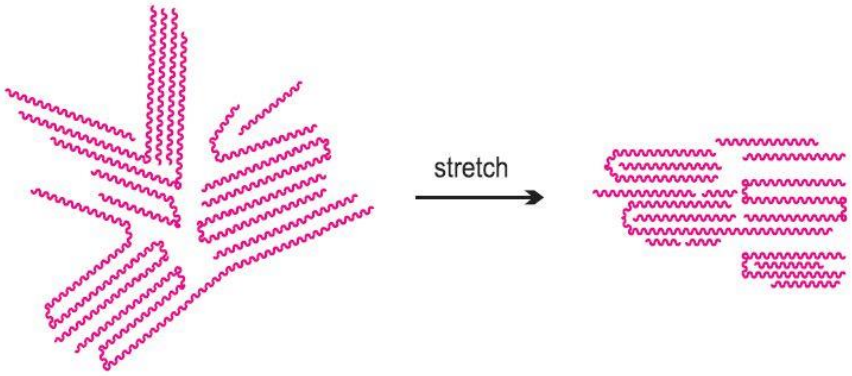

Figure 8: Movements of the polymer chains while stretching. The amorphous phases of the chains are sliding until being perfectly aligned. Reproduced from [47].

Obviously, there is a limitation to the strain. At a certain strain, the amorphous phase is completely aligned. At this point, the energy needed to displace the amorphous regions is equivalent to the crystalline phase. Thus, all the chains in crystalline and amorphous regions start to move, and the initial properties of the polymer are degraded.

The improvement of the crystallinity reduces the amorphous phase ratio. Thus, the stretchability is decreasing with this ratio. As a consequence, there is a need to find a compromise between electrical and mechanical properties when tailoring its properties. The difference of stretchability within materials is important to choose materials with desired properties. For the choice of the substrate, the only important factor is the stretchability of the material. So, the choice of a polymer with a maximum of amorphous phase seems to be ideal for stretchable properties.

1.3. Overview of substrates for e-skin

The choice of a material for the e-skin raises two problems. First, it has to be compatible with the properties of the skin. It has to be stretchable by more than 30% according to the objective cited previously. Until now, industrialised electronic and microelectronic devices fabrications

are mainly based on rigid silicon. So, it has to be compatible with the process developed on rigid substrates. This way, the ability to fabricate organic sensors is ensured.

This section is dedicated to the choice of the substrate, with a presentation of the different stretchable materials, and their compatibility with microfabrication techniques.

1.3.1. Screening materials for soft substrates use

A prerequisite creating stretchable electronic components is to develop materials that can withstand large mechanical constraints. Materials known as hyperelastic possess the desired properties of stretchability:

- they can undergo tremendous strains: between 100% and 700% with a pure elastic response
- they are also incompressible, the shape changes when stretched
- the volume does not change
- they have a nonlinear stress-strain relation

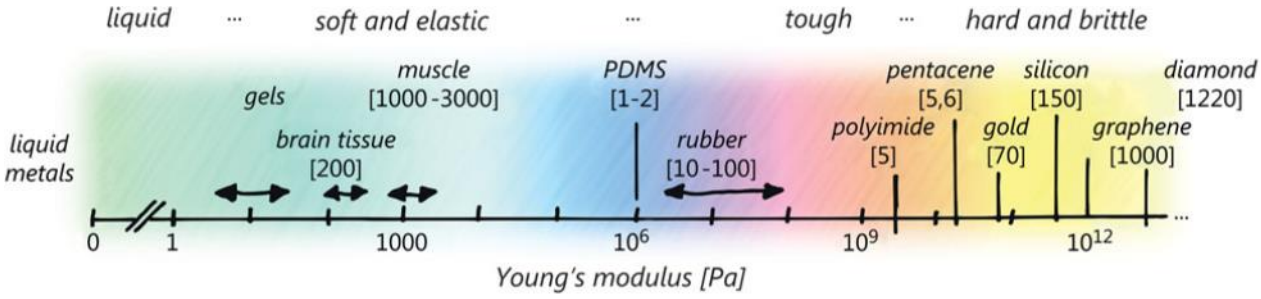

Figure 9: Young modulus scale for materials from liquid state to diamond. Young Modulus of PDMS and rubber are close to the one of the skin. Reproduced from [48].

For stretchable sensors in e-skin, the ideal substrate would be the one with the same characteristics than the skin. In Figure 9 is presented some materials with their Young's

modulus. The right area with tough, hard and brittle materials is not adapted. They need a high strength to be deformed, and their elasticity is low. These materials generally break around 5%. On the other hand, PDMS and rubber or more globally elastomers have Young's Modulus close to the human body. They are part of the hyperelastic materials, and the Young Modulus of the skin is around 0.1-1kPa. It can be stretched by more than 100%, making them a suitable material for our application[2], [44], [49]. Among substrate with adequate properties, PDMS and other silicone type rubbers are already widely used alongside with polyurethane (PU) based films[2].

1.3.2. A substrate compatible with microfabrication processes

As a matter of fact, when considering nano/micro-metric layer thicknesses of conventional electronic components, the use of ultra-flat, smooth and rigid substrate is more adapted. The mechanical deformation of soft substrates during manipulations restrains the precision or the reproducibility of the devices. It is easier to have a very flat substrate, making it more adapted to spin-coating for example. Moreover, the solvent compatibility of polymer substrates is not as good as most of the rigid materials. Organic solvents dissolute or make polymeric materials swelling, changing the topology of the material as a substrate[50]. Thus, the number of stretchable substrates is limited.

A big challenge concerning elastomeric substrates is its processability. To produce high-performance devices, the most conventional process is based on photolithography which provides high-resolution patterning. However, the use of photolithography directly on elastomers has shown limitations regarding the wettability of the resin and more globally any chemicals on PDMS[51]. Some alternative methods have been developed to pattern active materials on elastomers with transfer patterning[52], screen printing[53], inkjet printing[54] or stamping[55], but are limited in resolution and challenging to implement for multi-layer alignment.

The main advantage of PDMS over other substrates is its resistance to many solvents, so it is compatible with a lot of processes[50]. PDMS is widely used since it is a silicone-based and biocompatible polymer. It is commercially available, low cost, solution processable and it is stretchable more than 100%[44]. Other substrates used in the literature present significant drawbacks. PU is very stretchable, but its compatibility with solvent is very limited[56]. Stretchable fibre is also a common substrate used mainly for the integration in textile[57]. It is also very stretchable but is not compatible with 2D patterning such as photolithography.

The choice of the PDMS as a substrate fits with our objectives. It is stretchable by more than 30%, and it is compatible with microfabrication processes. Usually, the substrate is not the limiting material in term of stretchability. The limitations concern the active material and the interconnections.

1.4. Review on strategies for making stretchable interconnections

This section presents the different options for the choice of the interconnections. The development of highly conductive interconnections is mandatory in the field of electronics and more specifically for sensing applications. A change of resistance within a measurement induces changes in the response such as parasitic effects or artefacts of measurement. Then, the choice of the interconnections depends on the resistivity of the material, defining the resistance of the interconnections; along with the degree of stretchability. A trade-off between resistivity and stretchability is the main criteria of choice. The aim is to find interconnections with the lowest resistivity, but with a stretchability superior to 30%. It is preferable to get a stable resistance while stretching to avoid variations in the signal.

Three methods have been identified to reach these objectives:

- The stretchability obtained by the design of thick bulk conductive materials.
- The stretchability obtained by giving a specific design or by pre-stretching the substrate for the integration of the interconnection.
- The stretchability obtained by using stretchable conductive materials.

In a first part, the use of rigid materials as interconnections is presented. These materials need a special geometrical arrangement to be stretched. In a second part, the processing of the substrate to integrate interconnections is introduced, and interconnections using pure stretchable materials are presented. They are mostly based on conductive nanomaterials blended within a polymeric matrix. In the last part, a detailed discussion about the advantages and disadvantages is carried out to conclude on the use of each method. Then, a decision on the type of interconnections that are adapted for our application is made.

1.4.1. Stretchability of thick/rigid materials by design adjustment

Non-intrinsically stretchable interconnections deal with the use of material with high Young Modulus, typically in the range of hundreds of GPa and with low resistance to the strain. As a consequence, stiff materials cannot be used directly as interconnections; some strategies are applied to make it stretchable. For thick materials, the design is tuned in order for them to relax the constraints independently from the substrate. The stretchability in thin films is different; the material cannot be free-standing. Thus, the stretchability comes from the pre-strain of the substrate for the deposition of the metal.

1.4.1.1. Mechanical behaviour of horseshoe designs

In order to provide stretchability for such materials, one way is to use a specific geometry of metallic lines on an elastomeric matrix. This method is more effective with thick material that has a certain self-standing ability and is not strongly bonded to the elastomer. This displacement freedom allows the material to move inside the substrate matrix and relax the constraints[58], [59]. Figure 10a presents the parameters for the so-called horseshoe design. This design was introduced by Gray *et al.* in 2004 with 5µm thick gold lines electroplated on PDMS[60]. After quick optimisation, these lines were able to get 54% strain while maintaining a stable resistance. There are four parameters to describe the design of the horseshoe interconnection:

- the width of the line w
- the radius of the arc of circle R
- the angle of the arc of circle θ
- the length of the connection between two arcs of circle L.

All of these parameters can be tuned in order to improve the stretchability of the line.

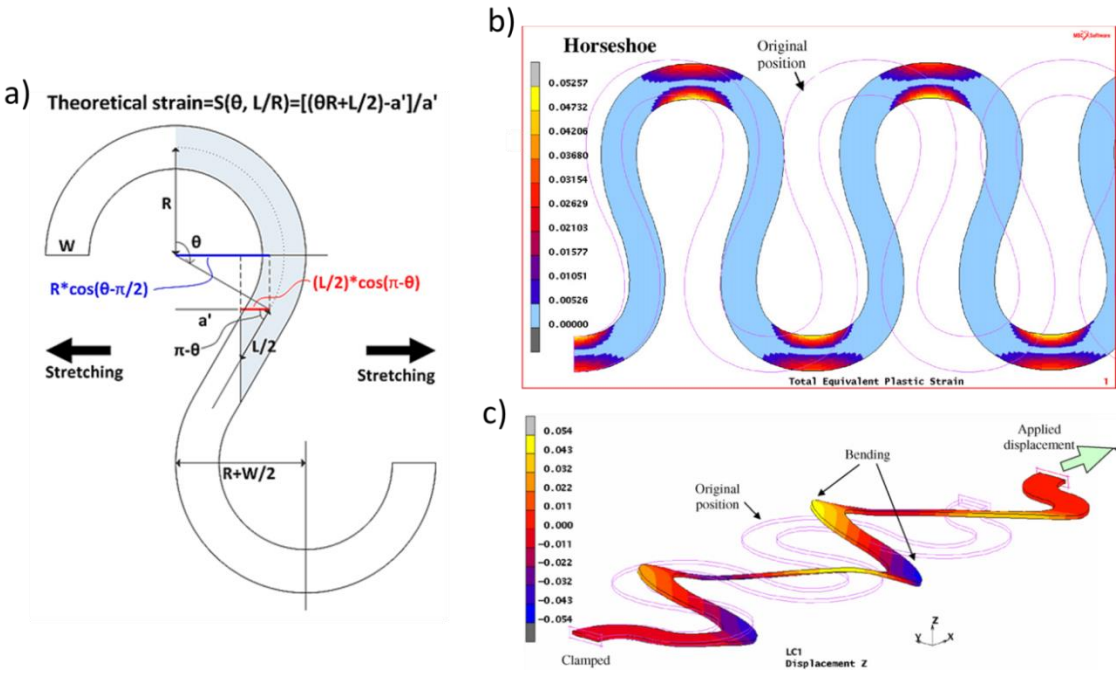

Figure 10: Geometry and mechanism of deformation of a horseshoe line. a) Serpentine routing parameters, reproduced from [61]. b) Visualisation of the constraints into the horseshoe-shaped electrodes. The scale represents the relative plastic strain. c) Non-constrained deformation of a line with a horseshoe shape. The scale represents the displacement in the z-axis. Reproduced from [62].

The mechanism of relaxation has been extensively studied using simulation. In a first approach to understand how the line is deformed, Gonzalez *et al.* have done a simulation of a line free in the air[62]. Figure 10c presents the results of the simulation. When the interconnections are stretched, the presence of the horseshoe allows the metal to twist and then go out of the plane of the 2D structure, releasing the stress.

To reach the criteria of stretchability, the line has to recover its initial shape. The delamination of the line has to be limited as it is considered as a mechanism of failure. Encapsulation of these interconnections in an elastomeric substrate limits the out-of-plane movement able to relax the stress. In Figure 10b, when the line is constrained in the plane, the accumulation of deformation is noticed. Plastic stress is accumulated in the circular areas when stretched. In real conditions, when the line is encapsulated, the interconnection is constrained, but also deform out of the

plane. The ratio depends on the thickness of the substrates, of the metal and the encapsulation. These effects have been studied by Hsu *et al.* from the same group[63].

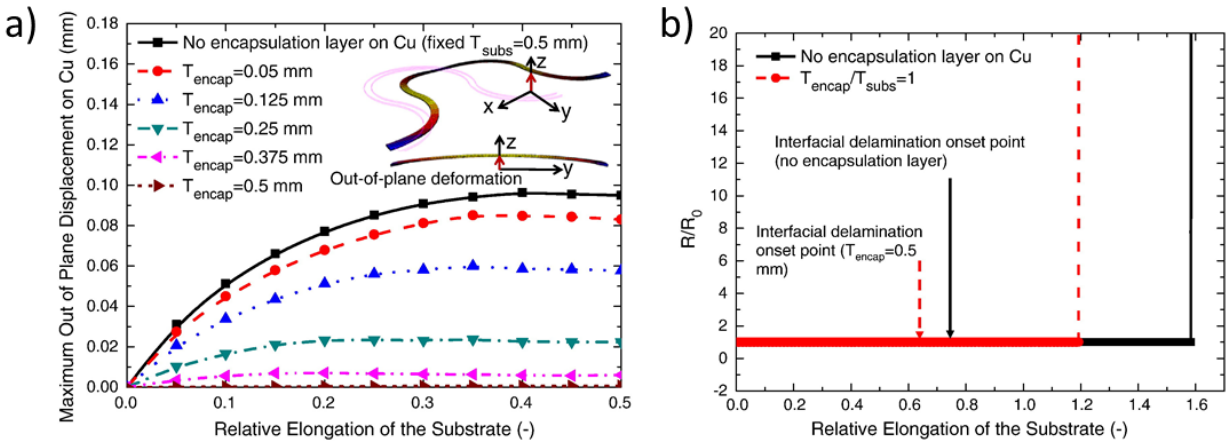

Figure 11: Effect of the encapsulation on a) the mechanism of deformation and b) Variation of resistance as a function of the elongation and failure of the interconnection. The encapsulation of the lines decreases the out-of-plane movement of the interconnections and thus, decreases their stretchability. Reproduced from [63].

Figure 11a shows the effect of the encapsulation thickness on the out-of-plane deformation. Without encapsulation, the line is pushed out of the plane of the substrate. The more the substrate thickness is increased, the more the line is constrained into the 2D plane until the substrate, and the encapsulation reached the same thickness. In this configuration, the metallic line is completely constrained in the plane. In Figure 11b, the impact of the encapsulation layer on the mechanism of failure is observed. Without encapsulation, the line breaks at 160% of strain whereas the encapsulated line breaks before at 120%. The same trend was observed with the delamination of the line from the substrate.

So, the horseshoe-shaped interconnections encapsulated in a thick enough elastomeric substrate is an appropriate base for the device. It is stretchable by more than 30% with a stable resistance while stretching. The stretchability can be further enhanced by a study of the parameters of its design. More stretchability means less stress induced in the line. Then, the reliability of the materials is improved.

1.4.1.2. Optimisation of the horseshoe geometry

Some studies have been made on the geometry of the horseshoes to understand the effects on the stretchability of the device[61], [64], [65]. However, it is difficult to compare because it depends, as seen before, on the encapsulation thickness but also on the material. Hocheng *et al.* have studied this effect by the simulation of a 5µm gold line embedded in PDMS displayed in Figure 12a [61].

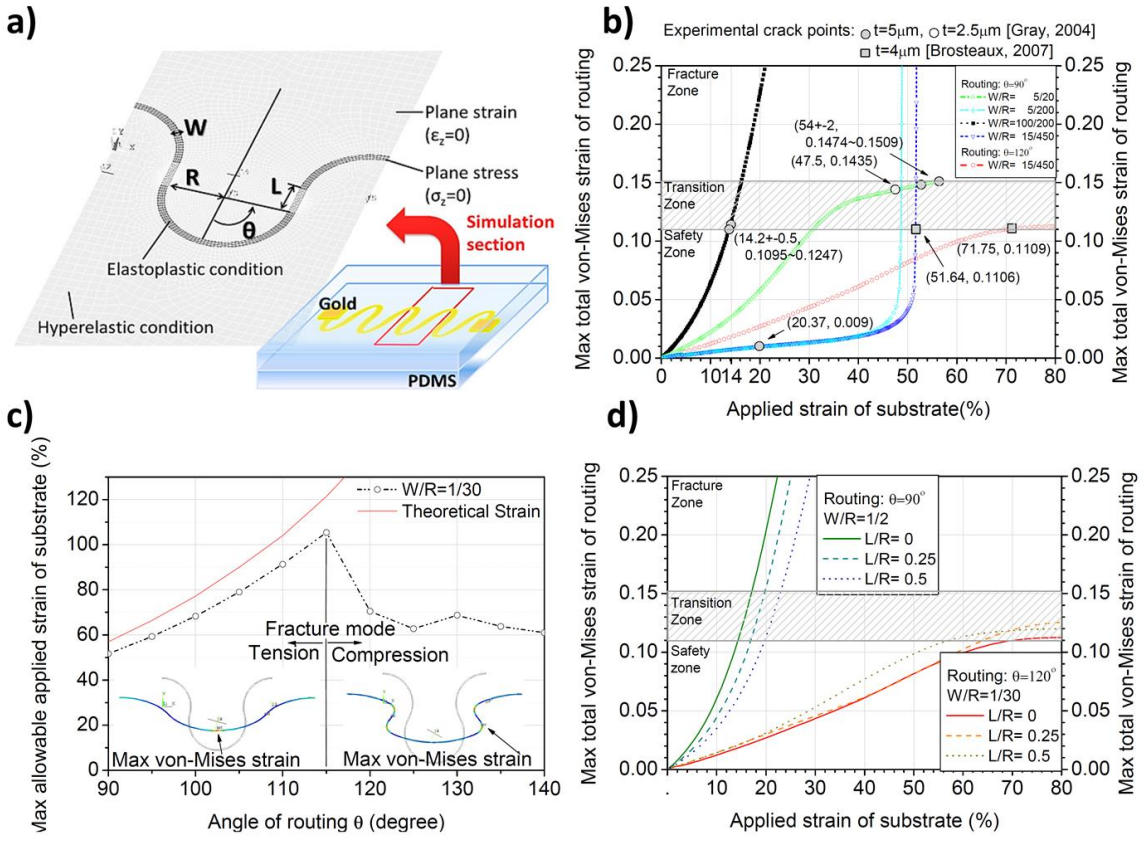

Figure 12: Simulation of the device in a), a gold horseshoe-shaped line embedded in PDMS. Impact of b) the ratio W/R, c) the angle of routing ϑ and b) the ratio W/R on the stretchability of the interconnections. There are different modes of fracture when tuning the angle α that decreases the stretchability after a certain value. Reproduced from [61].

Figure 12c illustrates two different failure mechanisms: in tension or compression. For an angle of routing before θ=115°, the max strain before the break increases with the angle of routing.

The line is breaking due to tension in the material. However, once this critical angle is passed, the strain at the break of the device is reduced and stays constant with the increase in angle of routing. This is attributed to the accumulation of compression stress in the line. When the substrate is stretched in one direction, following the Poisson effect, the substrate is compressed on the sides, compressing the line and breaking it if the geometry is not adapted. In Figure 12b, is presented the effect of W/R ratio on the stresses induced in the lines. Reducing W/R increases the possible applied strain before entering the fracture mode, mostly for higher values of W/R. Figure 12d presents the maximum Von-Mises strain as a function of the applied strain for different values of L/R. This ratio increases the stretchability of the device for low angles of routings or decreases it for low values of angle of routings.

So, it is possible to improve the stretchability of the horseshoe interconnections by using an appropriate angle of routing, by improving the W/R ratio and by choosing an appropriate L/R. However, the data presented are valid for this case, with these particular materials. Thus, by changing the materials, a study on the angle of routing particularly is necessary to optimise it. Moreover, only a few examples of experimental data are available (in Figure 12b). So, an empirical study would be more adapted to analyse the impact of these parameters.

1.4.1.3. Fabrication of interconnections with horseshoes

Gray *et al.* showed that it is possible to create in-plane electroplated gold stretchable interconnections via photolithography. The horseshoe shape encapsulated interconnections able to withstand a strain up to 50% has been fabricated[60]. They optimised the geometry but did not probe the resistance of the resulting line. Then, optimisation of the geometry has led to embedded copper lines in PDMS with a stretchability up to 100% and a change in resistance of less than 5%[64].

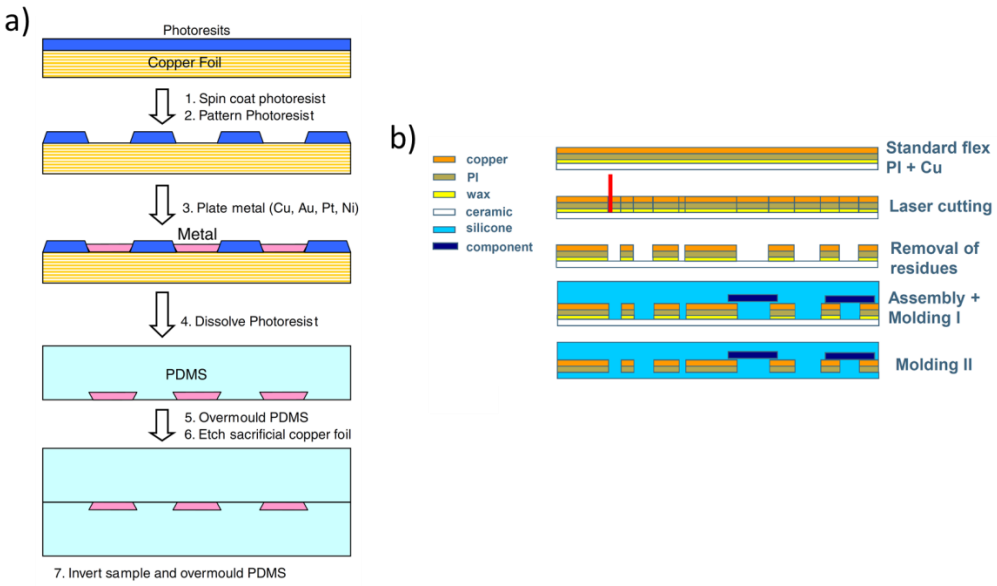

Figure 13: Two process to fabricate interconnections encapsulated in an elastomer. a) Electroplating of metal is patterned by photolithography and is covered PDMS. Reproduced from[62]. b) A wax layer carries a flexible circuit board and is patterned with a laser. Only the patterned lines are kept, and the remaining board is removed. Reproduced from [66]

Most of the work found in the literature is based on electroplating for making thick layers of metals (>1µm) combined with photolithography presented in Figure 13a. An alternative has been found with the design of flexible polymeric serpentines as a substrate for the deposition of thin films is shown in Figure 13b. Vanfleteren group has already demonstrated the use of laser patterning of a flexible circuit board embedded within PDMS for stretchable applications[67]. Initially, a thin metal layer is evaporated on a flexible polymer such as polyimide (PI) or polyethylene terephthalate (PET). Next, a temporary adhesive is used to fix and flatten the substrate. Finally, a laser beam is used to selectively pattern the interconnection. The lines exhibit between 80% and 100% stretchability. A study of the optimisation of the interconnections parameters (geometry, materials) has been partially investigated[68]. Using a technique based on laser cutting, Yang *et al.* have demonstrated Indium Tin Oxide on PET serpentines displaying stretchability up to 100%. Despite the high stretchability of the film, the resistance increases rapidly due to the appearance of cracks in the thin-film[59].

The laser patterning appears to be a good alternative to electroplating and photolithography. It is faster and cheaper. However, the only examples available in the literature did not take advantage of this process for bulk metallic materials for a low resistivity. They only used thin films evaporated on polymers. This part was focused on the design of interconnections to be integrated into the substrate. The process of the substrate does not change the final stretchability of the device.

1.4.2. Stretchability using design and substrate buckling

The stretchability of some other materials can be introduced by using different strategies with the substrate. For thin film materials, the thermal or mechanical buckling provides stretchability. Other minor strategies to pattern the substrate have also been studied and can be used for thick films.

1.4.2.1. Buckling for thin film patterning

Thin film materials (typically below 1µm) have not the same mechanical behaviour than self-standing thick materials. Thin-films metals are often thermally evaporated; the force of cohesion within the film is weaker compared to the stronger force of adhesion to the substrate. Then, the material directly suffers from the deformation of the substrate. So, serpentines shape is not adapted to these materials.

A strategy has been found by using thermal buckling of thin films. In 1998, Whiteside group observed thin metal films evaporated on a heated PDMS substrate. It was leading to random wavy structures in a sinusoidal shape[69]. In Figure 14 are displayed examples of methods to induce thermal buckling. The size and periodicity of the waves induced in the film depend

mainly on the difference of height in the substrate. The patterning of the material is possible to control the orientation of the waves.

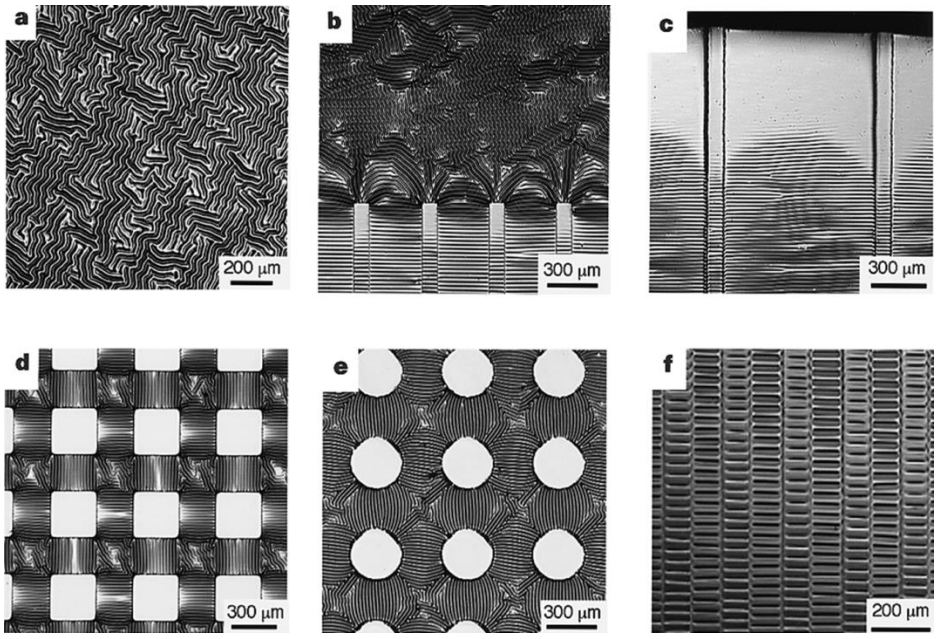

Figure 14: Micrographs of metallic thin film buckled, induced by heating. a) Metal evaporated on PDMS heated at 110°C. b,c) Oriented buckles due to rectangular shaped PDMS elevated by 10-20µm from the rest of the substrate. d,e) Effect of elevated PDMS by 10-20µm. There are no buckles on the elevated area. f) Oriented buckles from rectangular ridges, 10-20µm high and aligned. Reproduced from [69].

Then, Watanabe *et al.* introduced the use of pre-strain during the deposition of materials, so induced mechanically. The pre-strain is the cause of larger and oriented wrinkles on the surface of the materials when released, improving the stretchability of the material[70]. This pre-strain method is widely used today for stretchable electronic devices because it can increase the stretchability of any thin-films materials. Taking advantage of this property, Lacour *et al.* have shown the first reported stretchability of gold evaporated lines on PDMS, whereby the resistance increased by a factor of 8 after 8% strain was applied[71]. In a further step, they demonstrated three mm-wide gold lines showing no increase in resistance up to 100% stretchability by using a substrate pre-strain method during evaporation[72]. These interconnections are completely biocompatible and are widely used for stretchable biosensors. Recent work has introduced the use of Gallium as a liquid metal at the interface of gold to make

it stretchable without requiring pre-strain, displaying stable resistance after multiple cycles at 50% strain[73].

As mentioned before, this pre-strain method is more adapted for thin films. Zhang *et al.* have studied the effect of the thickness of the metal. They used serpentine metallic interconnections and showed that the pre-strain is less efficient for materials thicker than 1µm. Moreover, it does not induce any buckles in the metal after 4 µm of thickness. Thus the effect of pre-strain is limited[65].

The buckling for thin films and the tuning of the geometry for thick films are not the only strategies. Some methods taking advantage of the geometry of the substrate have also been studied, but their application is marginal.

1.4.2.2. Patterning of the substrate

One of the strategies to make stretchable interconnections is to take advantage of the ability of the material to bend without breaking. Using a pre-strain based technique, Sun *et al.* have been able to transfer silicon ribbons on PDMS that could be used with other materials(Figure 15a)[74]. By tuning the adhesion on some parts of the substrate, the silicon is bonded regularly and when the substrate is released, not bonded parts bend due to the compression of the substrate. The stretchability then depends on the ability of the material to bend. The same approach can be made by 3D printing of metallic lines (Figure 15b)[75]. The lines are stuck regularly on the substrate and printed in the air to be able to move during the elongation.

Different tests of geometries have been done for interconnections such as spiral structures that unfolds when stretched[76]. Fractal structures are also capable of improving stretchability of curved lines.

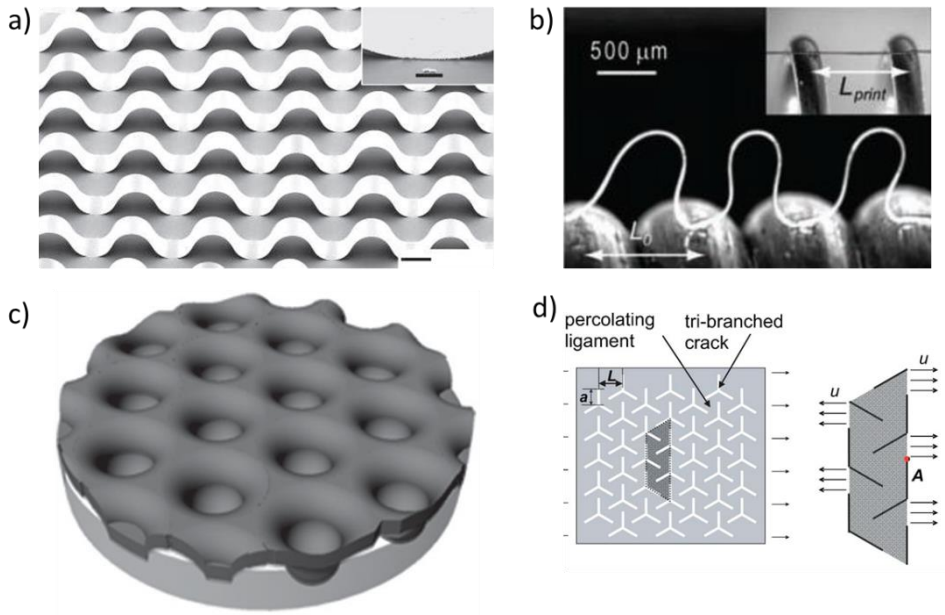

Figure 15: Other strategies to make stretchable interconnections a) with 3D sinusoidal shape extracted from [74]. b) with 3D printed wires, reproduced from [75], c) Mogul pattern of the substrate extracted from [77] and d) Tri-branched cut of the substrate, reproduced from [78]

All the previous methods focus on the ability of the interconnections to deform in a different way than the substrate. However, in this approach, the substrate is modified to be able to deform preferentially without stretching the interconnections. In Figure 15c, the substrate is modified by incorporating some valleys. When stretched, the dug areas are more prone to strain, and the flat zones in between are more protected[77]. In Figure 15d, the substrate is cut in a tri-branched pattern. When stretched, the substrate twists out of the plane to reduce the stress[78].

This part has presented the different strategies to use the process to induce stretchability. This method is mainly interesting for thin films, with the buckling of the substrate. By mechanically stretching the substrate during the deposition, it is possible to reach up to 100% stretchability for gold lines[72]. Moreover, this method is also useful not only for interconnections but also to improve the stretchability of organic thin films of active materials. In the next section, the last category of stretchable interconnections is introduced.

1.4.3. Intrinsically stretchable conductive materials

Researchers have developed highly stretchable elastic conductors made from hyperelastic materials. These materials are mainly fabricated by incorporating conductive nanoparticles in a stretchable elastomer matrix. Some examples of the best materials in this field are presented in Table 1. The conductivity mainly depends on the filling percentage of the particles inside the matrix. The more particles and the more contact between the particles there is, reducing the resistivity. For the same material and different filling, there is an impact on the conductivity and on the stretchability[79], [80].

Conductive material	Matrix	Max strain	Conductivity $S.cm^{-1}$ at max strain (Initial)	Fabrication	Ref
Single-walled carbon nanotubes	PDMS	40%	100 (100)	Printing	[19]
	PDMS	120%	10 (10)	Printing	[19]
	PDMS	150%	2200	Spray-coating	[81]
Ag nanoparticles	Fibre	140%	610 (5400)	Dipping	[82]
Ag nanowires	PDMS	80%	2500(8130)	Drop-casting	[83]
Au nanoparticles	PU	115%	2400 (11500)	Dipping	[79]
	PU	486%	94 (1800)	Dipping	[79]
Multi walled carbon nanotubes	PVDF	140%	20 (5710)	Drop-casting	[80]
Polyaniline	Elastomer (SEBS-g-MA)	215%	10 (1100)	Printing	[84]

Table 1: Comparison of the characteristics of some stretchable composites. The initial resistance reached can be high, comparable to ITO, but dramatically decreases when stretched.

Some studies have been done using long nanowires to improve the stretchability, leading to resistivity comparable to the ITO with stretchability more than 300%. The ability to maintain a good conductivity upon strain depends on the percolation threshold of the conductive particles. The more particles, and the more it is stretchable before losing the conduction. These interconnections are compatible with the buckling method, and it can thus improve the above-mentioned techniques, in term of stability of the conductivity.

1.4.4. Summary of screening methods and design rules

Composite polymeric materials have the advantage of being highly and intrinsically stretchable, but offer lower conductivity (in the range of 10-1000 $S.cm^{-1}$) than bulk metals (6×10^5 $S.cm^{-1}$ for copper and silver). Moreover and as seen in the previous example, the resistance increases consequently when stretched. Composite stretchable interconnections are mainly adapted for devices in which the change in the interconnections resistance is not a problem. Moreover, if there is a fixed targeted stretchability, it is easy to maximise the conductivity by adding conductive particles. Since the material is solution processable, it makes it easy to fabricate. Other techniques of patterning such as inkjet, screen printing or transfer patterning are also possible.

By using thin conductive films, the problem of stability in the resistance can be solved by processing the substrate to induce buckling[19]. This method presents some problems regarding the conventional processes used in microelectronics. Indeed, it is difficult to implement a pre-stretched substrate in an evaporator or a mask aligner.

For more convenient processability and lower resistance, a solution is to use bulk metallic interconnections, by tuning the geometry. Serpentines architecture can make interconnections stretchable up to 100 % and results in a low variation of resistance until break (<5 %). These kinds of interconnections are well adapted for devices requiring low resistance and low stretchability. However, the fabrication of these metallic interconnections mainly relies on

electroplating with photoresists, expensive and tedious to carry out. Thus, there is a need of providing a faster and easier method for bulk metallic stretchable interconnections.

For applications in e-skin, a high stretchability is not necessary for the application. Moreover, a low and stable resistance during the stretch is preferred. So, the choice of metallic interconnections with a serpentine shape is preferable. However, the development of a faster and cheaper method for the fabrication is necessary. The choice of the substrate and the interconnections are now clear. Then, the next section is devoted to the integration of the active material, to make a stretchable sensor.

1.5. Sensing material integration

The integration of a sensor on the stretchable substrate with the interconnections is the last step for a functional device. This section aims to presents the two approaches for this purpose:

- The rigid-island method, which consists of a stretchable device, with a rigid part where there is the active material. This prevents the materials to deform and be stretched.
- The fully stretchable device, on which, the whole device is stretched. The main challenge of this technique is to give the material the ability to deform without losing its properties.

1.5.1. Rigid-island method

All the stretchability comes from the interconnections and the substrate. The active area is made of a rigid material or is deposited on a rigid material. This is easier to integrate as there is no need to tune the stretchability of the active material. The main advantage of this method is its compatibility with rigid and conventional electronics; providing superior performances. Even for organic materials, the fabrication of high-quality devices with no or a few changes in

performance while stretching has been demonstrated[85]. Figure 16a displays an example of such a device with 3D interconnections made out of flexible materials. The active area called island is rigid, this area is not able to deform. The stretchability comes from the bridge structure that is done in this case by pre-strain of flexible material. The maximum stress is located at the transition between the stretchable interconnections and the island. This stress decreases with the pre-strain of the substrate[86]. Experimentally, the island can be made directly out of a silicon device[87], or with a stiffening material as an island on the substrate with the material on top[88]. With the last choice, it is possible to incorporate any rigid materials. Kim *et al.* have also shown the possibility of incorporating the device directly on a serpentine device in Figure 16b[30].

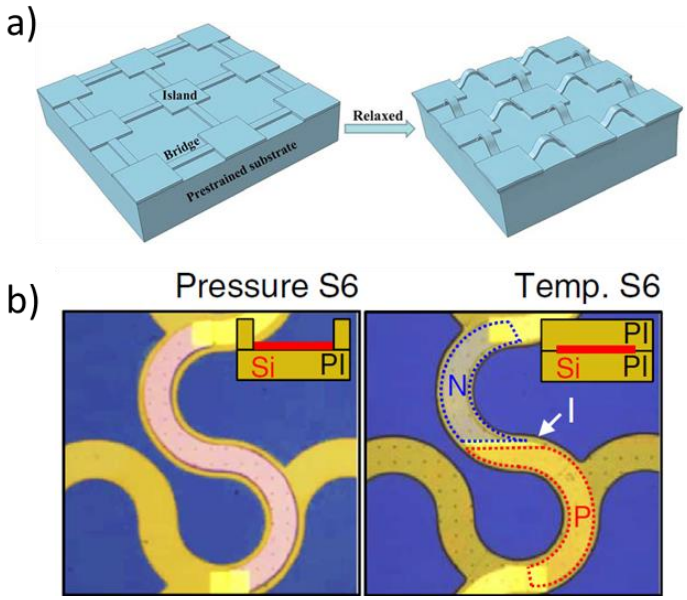

Figure 16: Rigid island devices. a) With a rigid material and stretchable interconnections, reproduced from [86] and b) with the active material on the interconnection, reproduced from [30]. This method allows the use of inorganic rigid high performing devices.

1.5.2. Fully stretchable devices

Fully stretchable sensors are required for strain sensors, *e.g*. the deformation of the active material provides the recorded signal. Most of them are based on the use of the polymer

composites presented in section 1.4.3. For interconnections, the change in resistance is not wanted, because it disrupts the signal carried. However, for strain sensors, the change in resistance directly gives the response[89], [90].

The engineering of fully stretchable devices relies on the ability of the active area to withstand the strain. For thin film materials, the main technique for the integration is based on the buckling effect, induced by the pre-strain of the substrate. This allows the fabrication of sensors based on thin inorganic materials. For example, Yu *et al.* have shown an example of a temperature sensor based on gold evaporated on a pre-strained substrate[27].

For organic material, especially for polymers, section 1.2.2 referred to its superior stretchable properties, polymeric materials can be stretched due to their long chains tangled together. So, in a thin film on an elastomer, the buckling technique can also be used. It increases even further the stretchable properties of the polymer. The film is compressed by the pre-strain of the substrate. The increase in mechanical stretchability comes from the properties of the amorphous area. After deposition, when the substrate is released, the chains are compressed especially in the amorphous area. This method has the advantage of providing good stability in term of performances, until the pre-strain value is reached, but is difficult to combine with fabrication processes.

The chosen strategy depends on the type of material and sensor used. The presence of a rigid material improves the reliability of the device globally and prevents any stretching to interfere with the measurement. However, for strain and pressure sensing, this deformation is necessary to give the response of the sensor.

In this section, the different materials and strategies for making stretchable active devices have been presented. The next part deals with the two sensors aimed to be fabricated during this thesis.

1.6. Integration of OECT and infrared temperature sensor for e-skin

The three characteristics of a stretchable sensor for e-skin have been established. The use of metallic serpentines in a stretchable substrate is the base of the device. For the integration of the sensor, the method depends on the sensor. For this thesis, the focus on the fabrication of two sensors is presented: the OECT and the infrared temperature sensor.

The choice of the OECT has been motivated by the knowledge on the material and the process of our laboratory. So, it is a good proof of concept for the development of the materials and the process. Moreover, it possesses all the reasons to be integrated into an e-skin. It is a multitask sensor able to sense various physiological parameters (ECG, glucose, sweat…); which are highly interesting for wearable application onto skin. The development of the infrared sensor is more related to the global project of this work. As presented in the introduction, the aim is to recreate the properties of the skin and to integrate a layer of these sensors as part as e-skin.

In this section, is presented the construction and working principle of the OECT and the infrared sensor.

1.6.1. OECT working principle

The OECT is a recording device widely used in bioelectronics. It was first described by White *et al.* in 1984 as a device with behaviour similar to a transistor[91]. The active layer is based on a conducting polymer patterned between two electrodes. Its resistance changes by applying a signal through the gate. The OECT is a three-terminal device. The construction is displayed in Figure 17. The source and the drain are made out of gold and are in contact with PEDOT:PSS that constitute the channel. Then, the third terminal is commonly made out of an external electrode that is in electrical contact through an electrolyte. It is also possible to make a fully planar device with a golden gate[92].

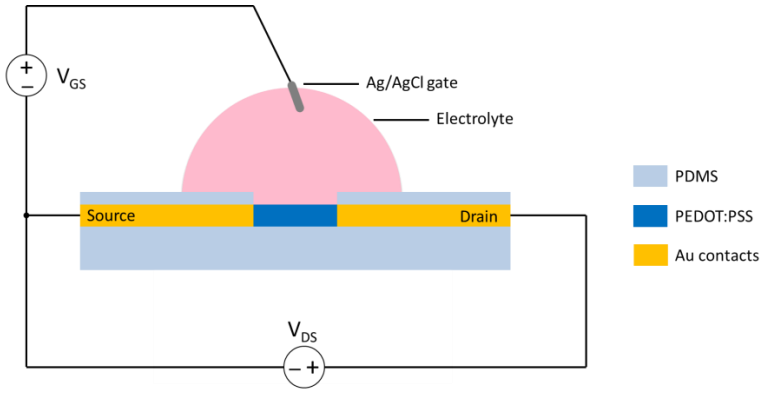

Figure 17: Schematic of an OECT in operation. The PEDOT:PSS layer is deposited between two contacts: the source and the drain and the gate, from an external Ag/AgCl electrode, is on top and in contact with an electrolyte

In operation, the current is measured through the channel (source to drain current: I_{DS}) upon application of a voltage through the gate (gate to source voltage: V_{GS}). The application of a positive voltage V_{GS} forces the cations from the electrolyte to enter into the PEDOT:PSS film recombines with negative PSS parts, dedoping the active layer. The penetration of the ions thus modulates the drain current I_{DS}, making this device an ion to electron transducer. It makes it an excellent sensor for measurement at the interface between biological and electronic worlds.

1.6.2. Infrared sensing: definition and construction of a device

As part of e-skin, the ability to sense the temperature is crucial. It protects the user against potential harmful environments. The sensing in a non-contact approach is even a step further in mimicking the skin. Indeed, our body is also able to detect the radiations emitted by warm heat sources. It is important to understand what is behind the infrared radiation to understand how works the infrared detection for temperature and detection of movement. Temperature and infrared sensing are closely related and cannot be dissociated.

1.6.2.1. Definition of an infrared radiation

The infrared belongs to the light radiation above 800 nm. As described by Planck, an ideal black body is a matter, able to absorb all the electromagnetic incident radiation and at a temperature T, emits radiations in all directions.

Figure 18 illustrates the distribution of the spectral radiance; the black body emits in a broad band of wavelength depending on the temperature of the black body and with a maximum wavelength given by the Wien's law (Equation 1), with λ in µm and T in Kelvin.

$$\lambda_{max}(T) = \frac{3000}{T}$$

Equation 1: Wien's law

An emitter like the sun has a temperature around 6000 K and has a maximum of emission around 500 nm. For objects close to the body temperature, around 300 K, the maximum is around 10 µm. So there is a direct link between the temperature and the maximum of intensity. Thus, the determination of the temperature of an object is made by measuring its emission.

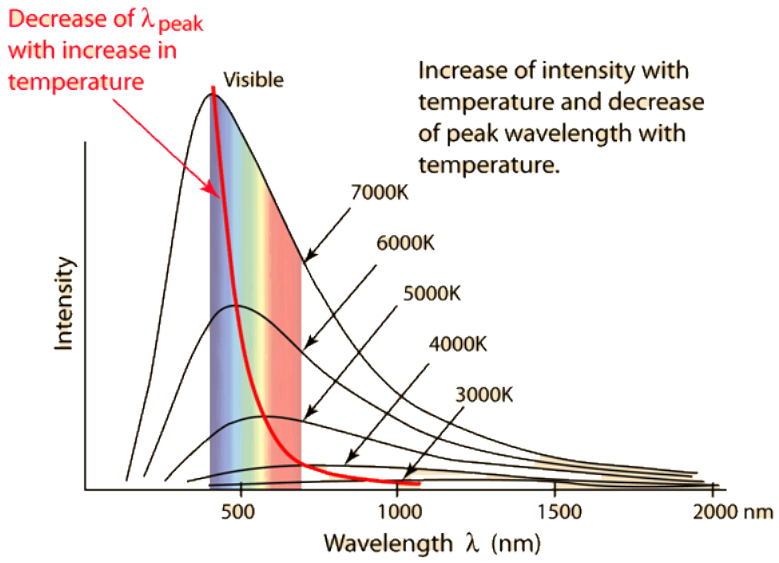

Figure 18: Distribution of the energy as a function of the wavelength. Reproduced from [93]

All the materials with a temperature above absolute zero emit radiations depending on their temperature, but they are not perfect black body, they have a proper emissivity. The spectrum is the same but weighted by a factor ε=1 for perfect black body and ε<1 for others. Then, different technics and applications are used.

1.6.2.2. Device construction

There are two kinds of infrared sensors differentiated by the mechanism of detection. The active infrared sensors are often used for the detection of objects and persons passing into a specific area. It is made out of two parts: an emitter that emits an IR radiation and a detector that detects this radiation. The source is either placed in front of the detector for direct detection of the break of the source radiation, or by reflectance, with the source reflecting onto the object and goes to the detector. In both cases, when something blocks this radiation, the detector knows there is a movement. On the other hand, passive infrared sensors (PIR) are based on only one sensor that can detect infrared radiation in a specific field of view.

Infrared sensors can also be distinguished based on how works the detector. First, the quantum infrared sensors are based on the energy transition with low band gap materials. They are generally fast, highly sensitive and wavelength dependent. However, the devices need to be cooled down to reach these performances. On the other hand, thermal detectors are based on the absorption of infrared energy to produce heat, usually not wavelength dependent. They are not as accurate and fast as the quantum detectors, but they remain cheap and easier to produce.

In the case of the e-skin, the precision of quantum detectors is not necessary. The simple detection of a heat source is enough, and the human body does not need ultra-high accuracy and speed. Then, the focus on thermal detectors with a passive infrared sensor construction adapted to the detection of temperature is carried out. The active sensors are only adapted for movement and proximity detection.

1.7. Aim of this thesis

The development of complete e-skin goes alongside with the development of stretchable sensors. Examples of stretchable sensors are mainly covered by touch sensing. The development of a multi-sensing e-skin is not widely studied. The approach presented in the introduction lies in the development of large areas of sensors. For this application, an objective of at least 30% stretchability is set, which corresponds to the double of the estimated maximum elongation of the skin. The different blocks for making stretchable sensors were analysed:

- The substrate is made out of PDMS, for good compatibility with microfabrication processes.
- The interconnections are based on bulk metal for a low and stable resistance during elongation.
- The active material has two options depending on the material. If it cannot endure strain, the integration of a rigid material into the stretchable substrate limits the deformation. If the material possesses a natural high stretchability, the optimisation of the process of fabrication is possible: by tuning the formulation of the material, or by using different fabrication methods.

The main issue of this work is to provide stretchable sensors with similar properties than on glass and wafers. Moreover, compatibility with processes for large scale fabrication is appreciated as the next step is to integrate the devices in the form of a matrix.

So, in the next chapter, the process for interconnections based on laser patterning is presented. The fabrication of encapsulated interconnections with a stretchability of 80 % is demonstrated with similar or superior to what is achieved in the literature. The process is cheaper and faster than the literature based mainly on photolithography, with a good lateral resolution of 25 µm for the channel of the sensor. As a way to explore the potential use of OECT as well as understanding their working principle, the development of this device for an application in wound-healing is presented. Once done, by tuning the process presented in the literature, the

fabrication of an OECT that is stretchable by almost 40% while keeping high performance is presented. Then, a stretchable infrared based temperature sensor has been developed in order to complete the sensing capabilities of the artificial skin. The device can be stretched up to 35% without performance changes for temperature sensing. The sensor is based on PVDF as a pyroelectric material for temperature detection with a conducting polymeric material using the previously developed PEDOT:PSS as an absorber and top electrode of the device.

2. Development and evaluation of laser patterned stretchable interconnections

This chapter is based on the publication:

"Laser-patterned metallic interconnections for all stretchable organic electrochemical transistors."

Bastien Marchiori, Roger Delattre, Stuart Hannah, Sylvain Blayac, Marc Ramuz

Scientific Reports, volume 8, Article number: 8477 (2018), DOI: 10.1038/s41598-018-26731-8

The development of horseshoe-shaped metallic interconnections is more effective for thick metallic materials. These materials have the advantage of being highly conductive. However, the literature does not provide a process optimised for bulk metals. The reviewed technology in chapter 1 is either based on photolithography, expensive and tedious; or laser patterning of thin-films on polymeric flexible substrates, so more resistant. Moreover, the literature does not provide clear rules for the design of horseshoe interconnections.

The objective of this chapter is to develop a fast and simple process to low resistance and stretchability optimised for at least 30% strain. In this purpose, a process based on laser patterning for the fabrication of metallic interconnections encapsulated in PDMS is described. Different materials for the interconnections are studied, and the design is optimised for a maximum stretchability.

Section 2.1 introduced the measuring device for the combination of mechanical/electrical characterisation of the stretchable interconnections. The commercially available setups are not

adapted for both measurements at the same time. Therefore, a new setup was built as part of this thesis.

Section 2.2 illustrates the innovative process developed during this thesis for the fabrication of the bulk metal interconnections. The process is based on the combination of laser ablation, and thermal release tape ensures the fabrication of highly stretchable metallic lines–encapsulated in PDMS.

Section 2.3 explains the choice of material and design to maximise the stretchability of the interconnections. The choice of aluminium tape allows a stretchability up to 80%

Section 2.4 presents the results of the characterisation of the interconnections

Section 2.5 concludes on the chapter. State-of-the-art stretchability up to 80% combined with ultra-low mOhms resistance is demonstrated.

2.1. Measuring device for mechanical/electrical evaluation

The measurement of stretchable substrates needs the development of special tools for the characterisation. Commercially available devices are either adapted to electrical measurement of rigid substrates or to mechanical characterisation. Therefore, the coupling of electrical and mechanical characterisation needs the development of a homemade program and setup. In this section, the devices and programs developed for the characterisation of stretchable interconnections are presented

Figure 19 illustrates the setup. In Figure 19a, the former setup was constituted with an INSTRON, a classical tensile test machine, copper tape and a Keithley. This setup was fully manual, and not tuneable for other measurements needed for the future work. The new setup is presented In Figure 19b. It was based on a Keithley 2636A for the measurement of electrical

properties combined with a motor that moves a plate on which the sample was fixed. The motors used were ETEL DynX LM155, with a precision of 5µm, and were able to pull a maximum of 18N. In order to do later X and Y stretching, there were two of the same motors in both directions. The sample was placed horizontally on two metallic supports, and the device was clamped with two jaws. The measurement of the resistance was coordinated with the movement by a custom LabVIEW setup developed during this thesis. For the measurement of the resistance of the line, a four-wire measurement was used.

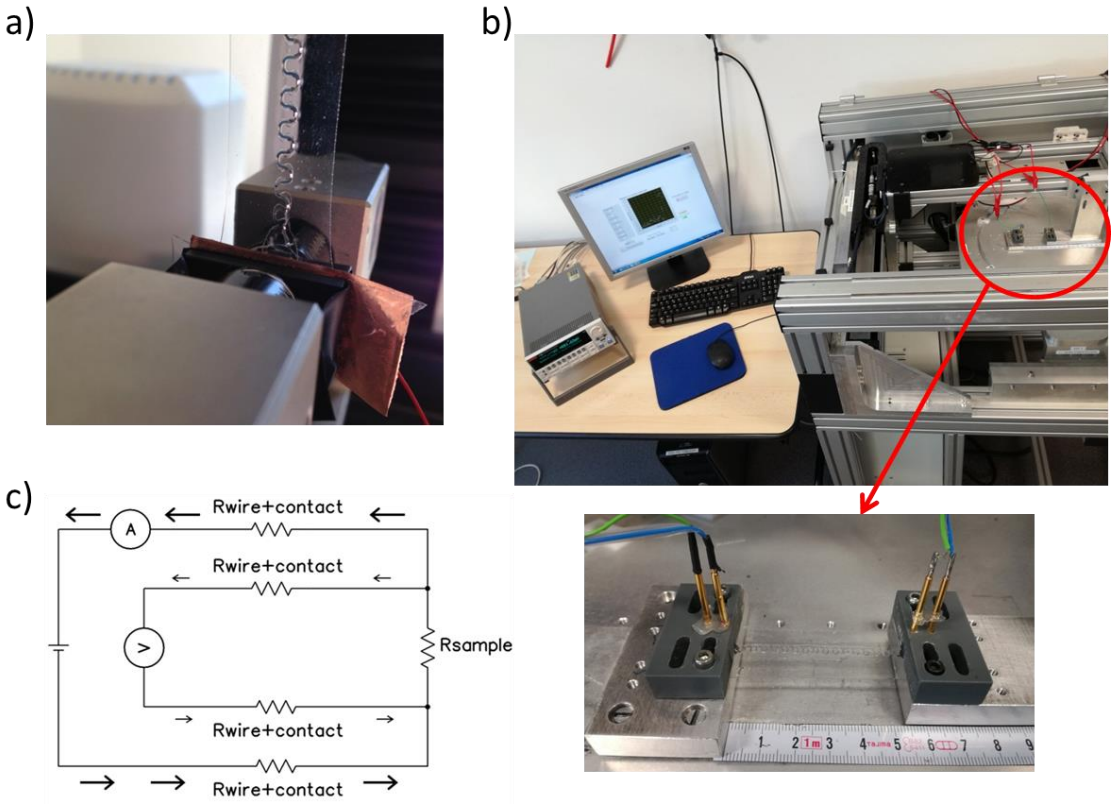

Figure 19: Setup of the mechanical/electrical characterisation of a stretchable line. In a) the former setup and in b) the new setup with the zoom on the sample c) Schematic of the 4-point probe measurement. With the new setup, very accurate resistance was measured while stretching devices.

The LabVIEW setup allows multiple experiments. A program has been developed for measuring the performances of a transistor as a function of the strain for the work of the next chapter.

More globally, it was possible to coordinate any measurement to the strain with a precision of 5µm in the motion.

In Figure 20 is displayed an example of a window for a 4-wire measurement as a function of the strain (the LabVIEW code is available in annexe 1). For this measurement, a range for the sweep of current has to be specified. For the XY table, the size of the sample, the maximum strain, the number of cycles, the number of measures for one cycle and the speed of the table were input. At each step, the program takes a measurement, displays it and goes to the next step. To place the sample, the jaws are moved using the "Away" and "Close" buttons by specifying the step for the movement. Then, once the sample is placed, the electrical contact is ensured by the R_0 measurement corresponding to one measurement without movement. When ready, the "Measure" button is pressed to launch the experiment. The program displays in real time the results and saves it as a table at the end of the measurement.

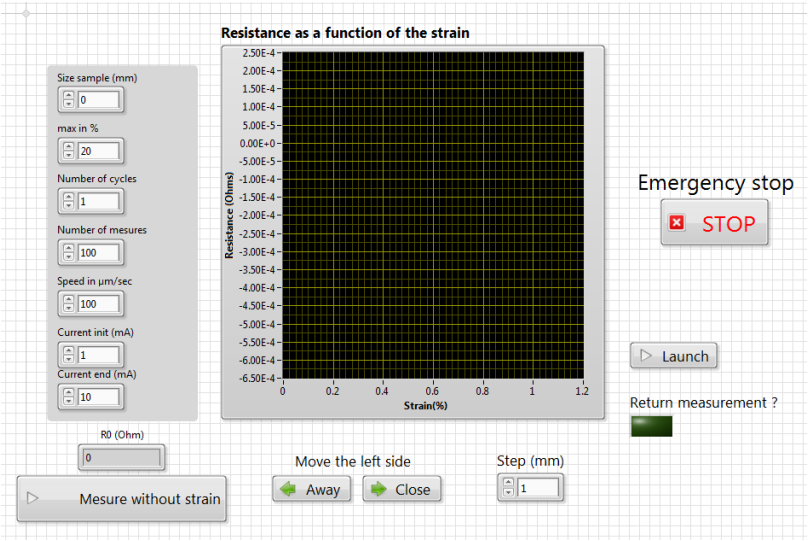

Figure 20: LabVIEW user window for the 4-wire measurement as a function of the strain. In input the length, the maximum strain, the number of cycles, the number of measures, and the speed of the displacement and the sweep of current for the electrical measurement.

By adding the corresponding sub-VI, it is easy to tune the program to adapt it with other measuring devices. Indeed, other different programs for capacitance measurement, transistor characteristics, 2-wire measurement has been made.

The jaws were 3D printed, and the electrical measurements were made through 4 gold plated pins. In order to measure the resistance of the lines, a 4-wire measurement was carried to get rid of electrical contact resistance, but also wire resistance and thus to get the pure resistance of the lines. A schematic of this technic is presented in Figure 19c.

In this configuration, the current is provided by the outer electrodes, and the voltage is measured through the inner ones. The current needed to measure the voltage is really low; the impact of the resistance of the wire and the contacts between the pin and the sample is then negligible in the measurement. In the outer pins, the current does not drop because of the resistance in a serial circuit. The calculus of the resistance by Ohm's law is therefore not affected by these parasitic resistances.

These tools allowed the measurement and characterisation of the stretchable interconnections. In the next section, the process of fabrication is presented.

2.2. Process for highly stretchable interconnections fabrication

The fabrication of the interconnections is based on an innovative process for the fabrication of stretchable interconnections encapsulated in PDMS, involving a laser patterning of bulk metal foils.

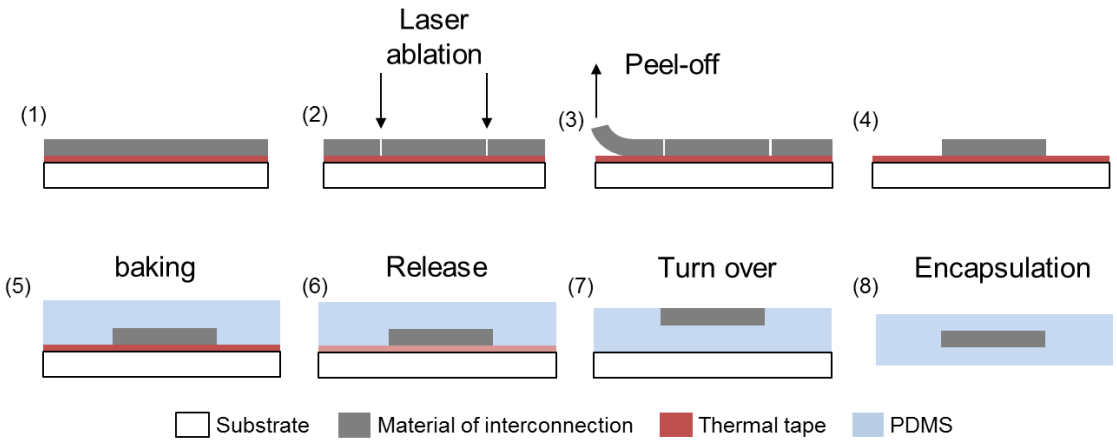

Figure 21: Schematic of the process of the metallic line based on a laser cutting of metallic foil stuck on a thermal release tape. Once patterned and peeled off, the line was encapsulated in PDMS. Finished device is the metal patterned and sandwiched within PDMS layers, which offer a high degree of stretchability.

The overall process is displayed in Figure 21:

1- First, a metallic bulk material was laminated on a thermal release double-sided 3195 Nitto RevAlpha® tape on a glass slide. This tape is a transfer tape used generally in the microelectronic industry to fabricate and cut dyes on a silicon wafer. One layer has a permanent sticky side while the other can be released with a minimum heating step at 90°C. After a few seconds, the tape loses all its glueing properties at this temperature.

2- The material was cut with a laser beam. Figure 22a displays a picture taken during the laser cutting, performed using LPKF Protolaser S equipment. The radiation was at 1064 nm with a frequency of 75 MHz and a power of 10 W. The diameter of the laser beam was 25 µm.

3- Subsequently, the unwanted metallic regions were peeled off from the thermal release tape substrate as illustrated in Figure 22b using a tweezer.

4- Only the design of the line was left on the substrate and ready for encapsulation

5- PDMS was poured on the device and baked at a temperature below 80°C to avoid thermal release tape to release. Otherwise, the PDMS merged with the tape and was impossible to separate. The thickness of the substrate was 350µm

6- The tape was thermally released at 95°C.
7- The resulting device was laminated upside down on another glass substrate
8- The device was encapsulated with a spin-coating of PDMS. The encapsulation layer was 100µm thick. This layer was thick enough to prevent the line to detach from the substrate and to be sure this layer is not broken due to out-of-plane movements as discussed in the introduction[63].

The patterning of high-resolution stretchable bulk metal interconnections with outstanding repeatability has been demonstrated using this procedure. The resolution of the line is limited by both the dimension of the laser beam (25 µm) and the thickness of the metal. For material thickness larger than the laser beam diameter, it is difficult to reach a width below the thickness of the metallic foil. Higher resolution can be achieved using advanced laser cutting techniques[94].

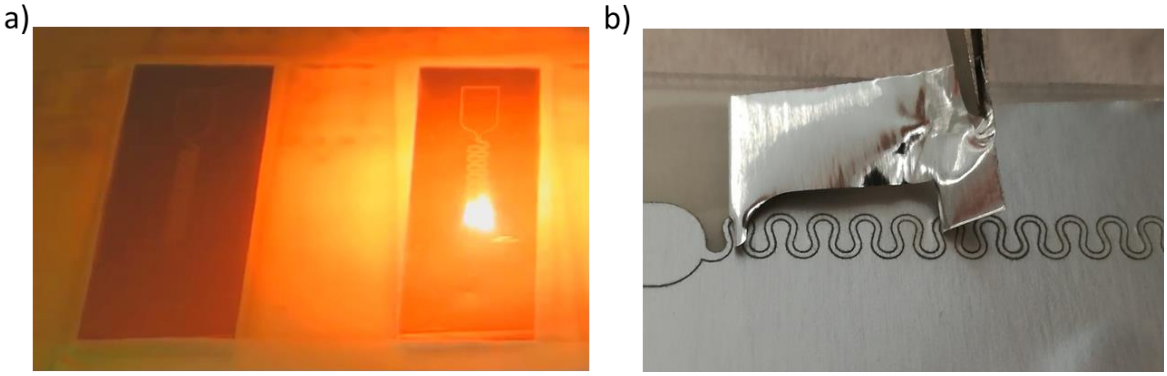

Figure 22: Patterning of the interconnections. a) Picture taken during laser patterning, b) illustration of the peel-off process. The unwanted regions of metals were either manually removed or fully removed by the laser to have a process compatible with conventional thin film microelectronic fabrication.

The transfer tape allows the metal to be perfectly planar on the surface during the fabrication process. The PDMS layer is also at the same level than the aluminium. This is very important for the compatibility with microelectronic processes such as photolithography, and when thin active areas are patterned. The layers of active materials in organic sensors are very thin (in nm range) compared to the thick layer of bulk foils (more than 10µm).

Compared to others fabrication processes of stretchable metallic connections, the advantages of this process are its simplicity since the process does not use a mask, the compatibility with microfabrication at an industrial scale-production and its versatility. This process is compatible with different metallic foils, such as aluminium, copper or titanium since it can be cut with the laser. For this thesis, only the patterning of aluminium has been completely studied.

2.3. Material and design optimisation of interconnections for maximum stretchability

The process for stretchable bulk metal interconnections has been presented before. The choice of the metallic material for the interconnections is critical for the device. This section focuses on the use of bulk aluminium as a material. It has the advantage of being low cost, and it is easy to find different kinds of foils. Various parameters on the material have been studied:

- Different thickness of aluminium foil
- The use of an aluminium foil or aluminium tape

Then, once the choice of the best material established, the optimisation of the design has been done to maximise the stretchability of the interconnections.

2.3.1. Material optimisation for interconnections

In this section, is presented the different types of aluminium tested for the interconnections. Different thickness has been investigated as well as two forms: pure foil or tape.

The graph of Figure 23a illustrates the stretchability of the encapsulated lines. For a 15µm thick line, a slight increase of the resistance before the breaking was observed. This was due to the deformation inside the metallic layer before rupture. In the case of 30µm and 60µm thick

aluminium, no increase was noticed because the line is not breaking, but the PDMS was torn, illustrated in Figure 23b. The only exception occurred with aluminium tape which lasted until 90% of strain.

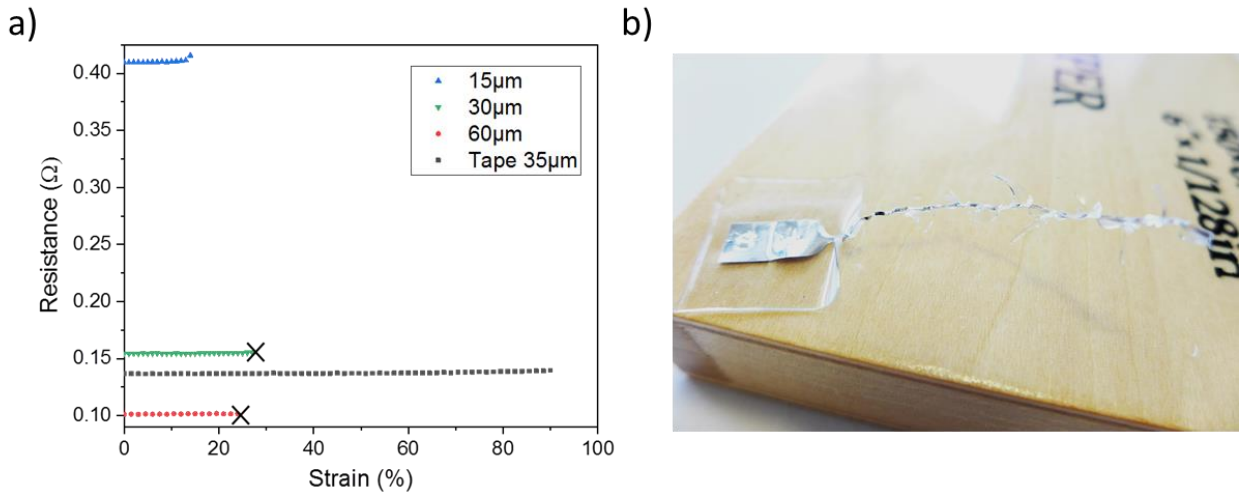

Figure 23: a) Resistance of the encapsulated Aluminium lines as a function of the material. The cross indicates that the PDMS breaks. b) Picture of the 60µm thick aluminium line after tensile test. The PDMS was cut, and thus, the line was free in the air.

Figure 24 depicts the SEM picture of the aluminium of different thickness after laser ablation. For the thinner layer of 15µm and 30µm Aluminium (respectively Figure 24a and b), there was less matter alongside the cut than for thicker aluminium of 60µm and 100µm (respectively Figure 24 c and d). The irradiation of a laser with sufficient energy induced the localised melting metal where the laser is focused. This melted matter was ejected outside the area of the laser beam[95]. It created a re-deposition of metal outside of the laser beam and also reduced the precision of the ablation. For thicker aluminium, more repetitions and slower mark speed rate have been used, so more energy and then more ejected droplets were observed.

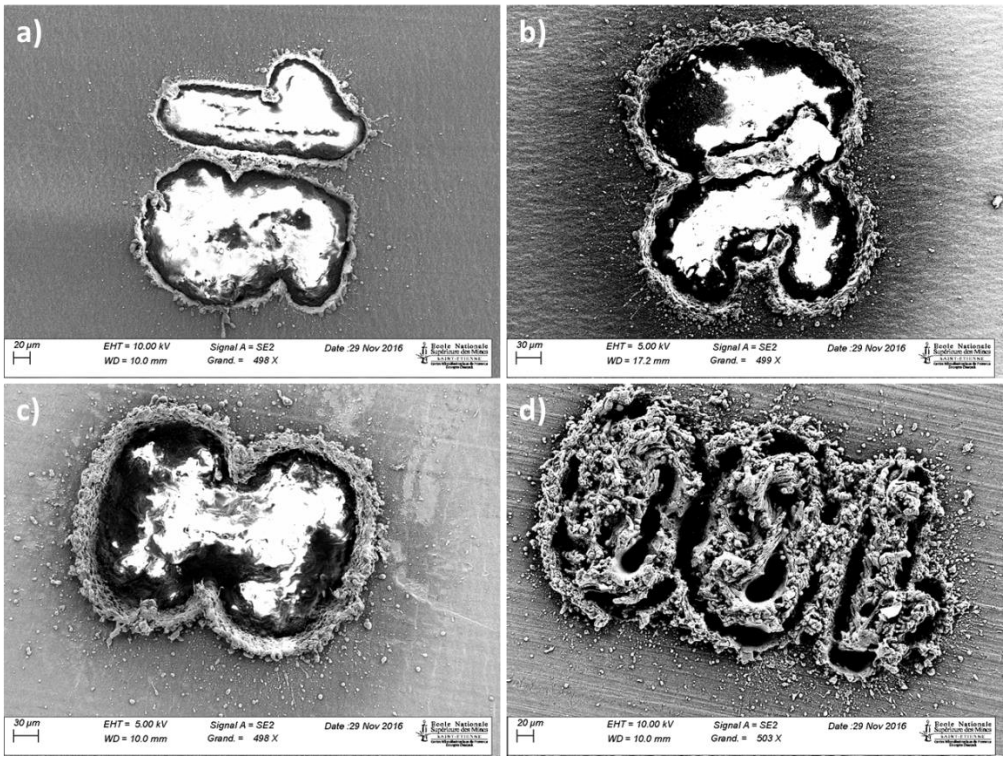

Figure 24: SEM picture of laser-cut aluminium at different thickness: a)15µm, b)30µm, c)60µm and d)100µm. On the edge of the cut, there was an accumulation of sharp aluminium that breaks the PDMS.

This matter constituted sharp spikes of aluminium making weakness points that damaged the PDMS. As a matter of fact, PDMS was inclined to get torn around these spikes. Several methods have been found in the literature to reduce the creation of these spikes that broke the PDMS prematurely. The use of a confinement layer of 400nm PMMA in the literature has shown good improvement of the definition of single pulse of picosecond impulsions, preventing the drops to be ejected[95]. Laser ablation of Aluminium in water has been shown to reduce the number of this re-deposition in a water medium. The localised ablation leads to the creation of bubbles, ejecting the fragments to avoid re-deposition[96].

However, the use of thin films confinement is not adapted to a laser cutting of thick films, with more energy and more projections. Different confinement layers have been tried to adapt this method to the use of glue or tape without success. The water-immersed ablation needs a

particular frequency to allow the creation of bubbles at the appropriate rate. It appears that it is not possible to achieve this frequency with our laser.

So, the best solution was to use aluminium tape with the layer of glue that acts as a confinement layer and also a protective layer from the aluminium to the PDMS.

Even if some work presented in chapter 1 has been done in order to optimise the geometry of the interconnections, no research group has used thick bulk metal, especially in the form of a tape and thus, there is no comparison with the literature.

2.3.2. Design optimisation of interconnections

A study through the simulation would be complicated with the glue. Therefore, an empirical study of the impact of the parameters of the horseshoe is provided in this section. First, an optimisation of the transition between the interconnections and the pads is presented, to ensure an effect of the geometry on the device. Then, a sweep on these parameters is done to determine the combination giving the highest stretchability.

2.3.2.1. Optimisation of transitions between pads of measure and interconnections

A large pad area is required in order to achieve good contact with the pogo-pin, to take the measurements. However, a regular point of rupture was observed when doing the tensile tests. In Figure 25b, is presented the first layout used. There was no smooth transition between the line and the pad. As a result, a regular point of rupture at this transition area was observed (Figure 25a). Whatever was the other geometry of the horseshoe, the maximum stress was located in this area, and the line broke.

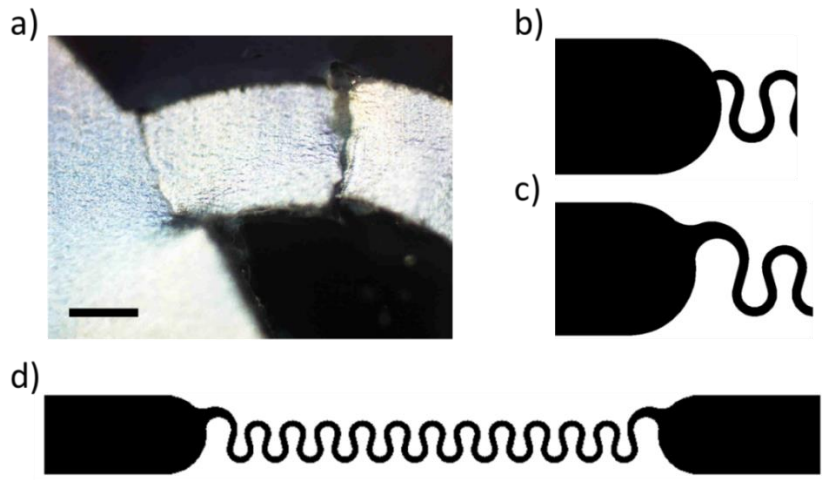

Figure 25: Optimisation of the transition from the pad to the line. In configuration a,b) the aluminium broke at the edge of the pad, revealing a weak zone. In configuration c), the break was more random and not located in the pad area. d) The design of the line with the pad optimised. Scale bar is 200µm, and the width of the interconnections is 400µm.

So, the transition was improved as illustrated in Figure 25c. The line width increased regularly and then finished in an inverted circle to match the circle of the pad. This led to a more random point of rupture located away from the pad. So the influence of horseshoe geometry is much more relevant. The final line which was used for the optimisation of the geometry of the horseshoe is displayed in Figure 25d.

2.3.2.2. Horseshoe parameters optimisation for maximum stretchability

To maximise the extension applied to the system, the geometrical parameters of the horseshoe described in the introduction and presented in Figure 26 were optimised: the angle of the arc α called angle of routing, the radius of the arc R and the length of the connection between two arcs L.

In order to ensure reproducibility and to tune the geometry of the interconnections easily, a code in Ruby has been developed, used in the software KLayout. This code is available in Annexe

2. The code offers the possibility to tune the angle, the radius and the length of the horseshoes. It is also possible to change the size of the pads for the electrical contacts, the number of horseshoes, and the shape of the transition between the pad and the horseshoe. The software designs one horseshoe according to the entered parameters and copies the pattern to reach the number input. Then, it makes the transition to the pad according to the characteristics the user selects.

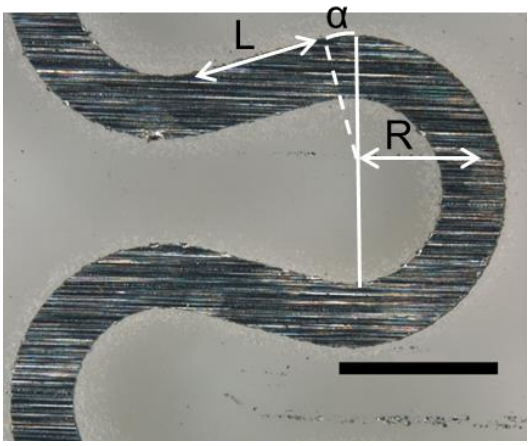

Figure 26: definition of the angle α, the length of the connections L between two arcs of the circles and R, the radius of the arc of a circle. The aluminium thickness is 50 µm, and the width of the lines is 400µm. The scale bar represents 1mm.

While varying one of the parameters, the others were fixed to either α=15°, L=800µm, or R=800µm. From this variation, it is possible to calculate the maximum theoretical stretchability ε that can undergo a free serpentine from a coplanar stretch without substrate. The maximum theoretical stretchability is defined as the maximum percentage of its elongation before becoming completely unfolded. It is expressed by Equation 2; the normalised ratio of the line stretched out to the length of the equivalent straight line[61]:

$$\varepsilon = \frac{2\left(\alpha + \frac{\pi}{2}\right) + \frac{L}{R}}{2\sin\left(\alpha + \frac{\pi}{2}\right) + \frac{L}{R}\cos\left(\alpha + \frac{\pi}{2}\right)} - 1$$

Equation 2: Maximum stretchability equivalent to the normalised ratio of the line stretched out

This ratio is equal to 0 when the line is completely flat; and if the total length of the line is the double of the equivalent straight line, it is equal to 1. In the following study, this ratio is called theoretical stretchability but converted in percentage.

The mechanical study performed on the lines shows a difference between the theoretical and experimental behaviour as presented in Figure 27. For each parameter and over ten separate samples, the impact of the shape of the constrained horseshoes on the maximal point of rupture was studied, which was correlated to the theoretical stretchability.

Referring to Figure 27a, the changes in the radius R had a limited impact on the strain at break of the line. The stretchability of the line with R=1000µm was the highest, nevertheless showing a moderate impact of this parameter in this range of data. Concerning the length L, Figure 27b shows the effect on the mechanical properties for $L \leq 1200\mu m$. The strain at break was improving (increasing) as a function of increasing L up to 400µm. However, after this value, the point of rupture was becoming more constant. For the last parameter α shown in Figure 27c, there was an increase in the mechanical properties, up to 15°. However, for α=20°, the line was breaking earlier at a lower strain at break value. While the total length of the line was longer, the interconnection was expected to be more stretchable with such an angle; this confirmed the observation of Hocheng *et al.* described in the introduction[61].

The theoretical stretchability (Equation 2) associated with the data was then calculated, shown in the graphs Figure 27a,b,c, and compared to the experimental strain at break as seen in Figure 27d. The geometry was improving the mechanical performance for equivalent theoretical stretchability up to 140%. After this value, the impact was negligible, except for the last data point at 210% which had a lower resistance to strain due to the same reasons explained previously for α=20°.

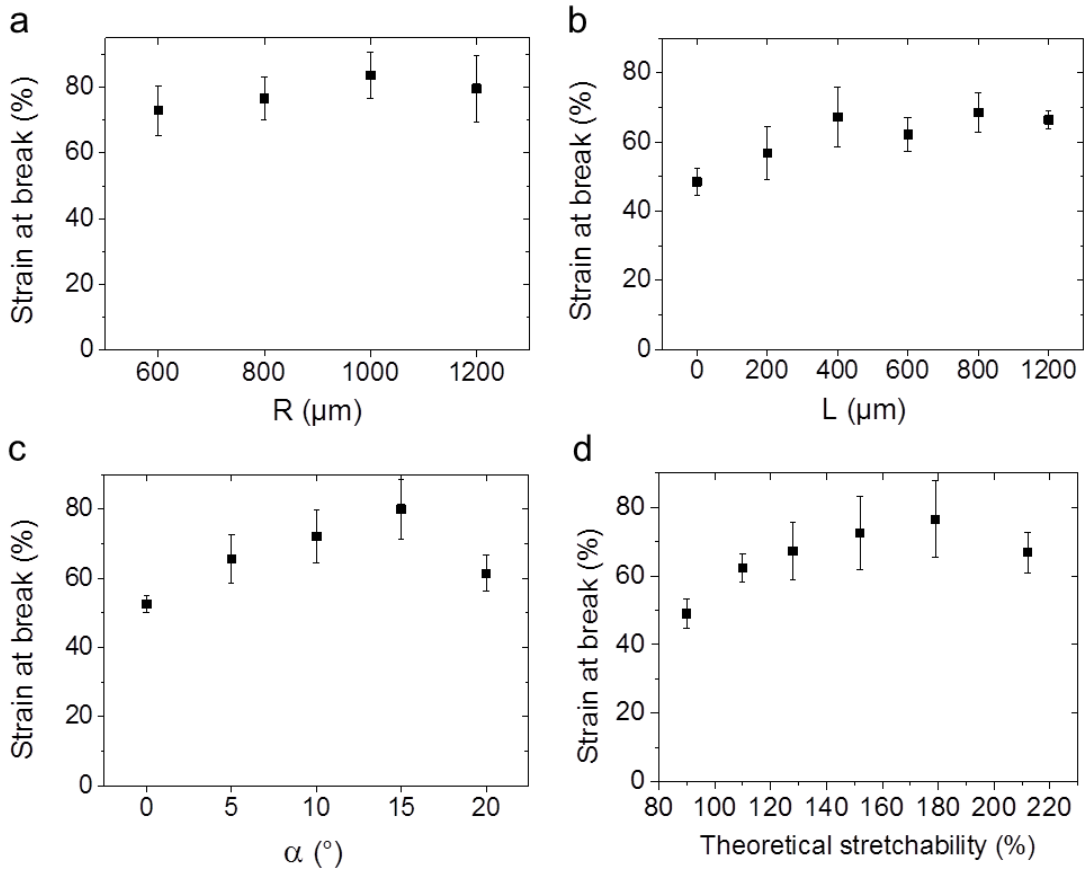

Figure 27: Optimisation of the stretchability of the interconnections. a,b,c) Experimental strain at break of the line for each parameter over 10 samples. The strain was applied at a speed of 100µm/s, and a measurement of the electrical resistance was taken at every 0.5% strain with a Keithley® using a four-terminal measurement setup. d) Compilation of the previous results representing the strain at break as a function of the calculated theoretical stretchability which is equivalent to the maximum strain the line can undergo before becoming straight. It is possible to design stretchable interconnections with an average point of rupture of 70%.

The key parameters of the geometry for the horseshoes were identified to achieve maximum stretchability with the interconnections. The tuning of the angle of routing α has the highest impact on the break of the lines, with an optimum angle of 15°. The parameter L must also be greater than 400µm to achieve the best stretchability. Finally, even if the choice of the radius of the horseshoe has a reduced impact on the mechanical performance of the line, R=1000 µm can be chosen to maximise the stretchability. By linking these parameters to the resulting

theoretical stretchability, an estimate of the strain at break of the interconnections is made possible.

There is a range between 140% and 180% of theoretical stretchability in which the rupture of the line stays similar when tuning the geometry. These interconnections have a measured average stretchability of 80%. This value is roughly half of theoretical stretchability. It is mainly attributed to the encapsulation of the line. During the strain, the line tends to deform out of the plane, which the encapsulation layer does not allow. This results in an increase of the stress in the line and explains the earlier break[63]. For the characterisation of the interconnections, the parameters chosen are α=15°, L=800µm, R=800µm, giving a theoretical stretchability of 180%, within the range determined.

2.4. Characterisation and performances of stretchable interconnections

Figure 28 illustrates the electrical behaviour of a stretchable line during a uniaxial tensile test. During the stretch, the resistance increased by only 1% from 183mΩ to 185mΩ up to 60% elongation. This value and variation of resistance for stretched interconnections represent state-of-the-art achievements. Then, the resistance stayed stable during the relaxation period of the line. The resistance was increasing due to the development of irreversible deformations in the line such as cracks[63].

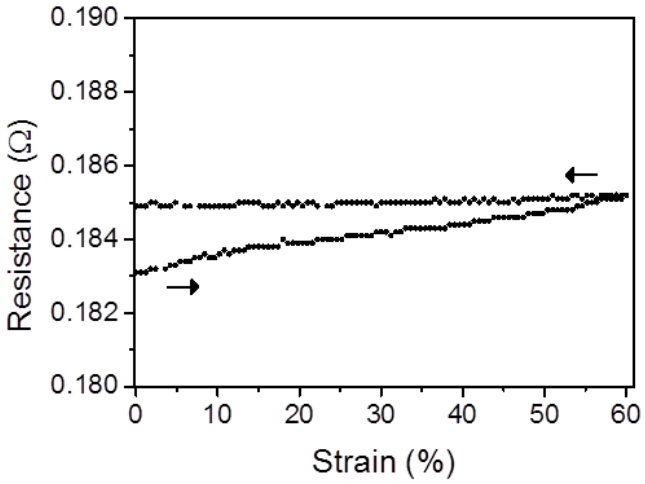

Figure 28: Example of electrical/mechanical characterisation of a line with the resistance as a function of the strain up to 60% for a line with width = 400 µm, α=15°, L=800µm, R=800µm, metal thickness=50 µm for a total length of the serpentines of approximately 95mm. The distance between the jaws was 40mm. The strain was applied up to 60% and goes back to 0%. There was an increase of 1% in the resistance while stretching due to small strain in the metal, but afterwards, the resistance stayed constant during relaxation from 60 to 0 %.

Comparing this behaviour to the literature[64], [72], the resistance is 10 to 100 times lower and is stable while stretching because the pure metallic sheets are highly conductive and thick. It is also possible to get high stretchability using composite polymers. However the conductivity is around 1000 times smaller, and it decreases under stretching[79], [84].

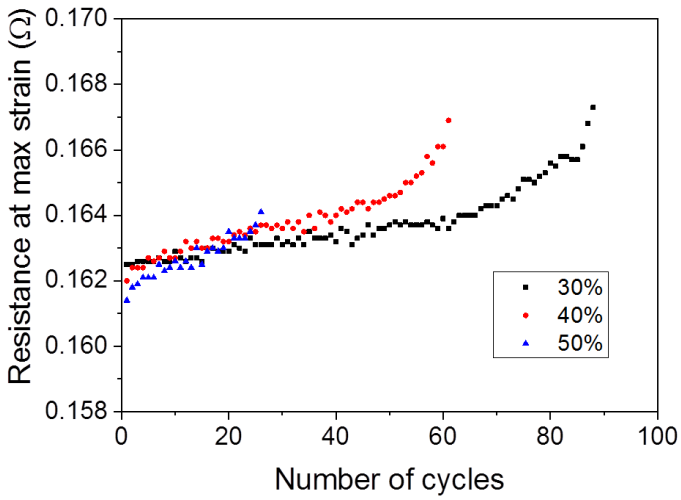

Figure 29: Cycling of the interconnection for a line with width = 400µm, α=15°, L=800µm, R=800µm, metal thickness=50. As expected, the device was more stretchable at small strain and could be stretched up to 90 times at 30% before breaking.

These interconnections have been characterised with cycling measurements in Figure 29. On this graph, logically, the line could endure fewer cycles if it was stretched more. At 50% strain, the interconnections cannot handle more than 30 cycles, at 40%, around 60 cycles and at 30%, near 90 cycles. Globally, at each cycle, the resistance increased slightly until the break to reach 3% of the initial value. As mentioned before, this rise is related to dislocation in the material. This effect is more important as it approaches the rupture of the interconnections because the line is at the edge of the rupture.

2.5. Conclusion on the interconnections

Very stable and state-of-the-art interconnections under strain have been developed. The low resistance allows precise measurement for the sensors. The process used is compatible with the microfabrication techniques and makes the substrate flat and ready for the next step of sensor integration. The interconnections are stretchable up to 80% which is more than the objective of 30%. However, the cycling measurements show roughly 90 cycles of stretching before the break

of the line. These performances are good enough for laboratory tests but need improvement for e-skin applications. Improvement of the stretchability is possible through a study of the encapsulation layer. Thinner encapsulation would help the line with going out of the plane. However, the line could also break the integrity of the PDMS by pushing the encapsulation layer. Therefore, a study of the encapsulation integrity and the stretchability of the line are necessary to optimise the thickness of this layer.

3. OECT for biosensing and artificial skin applications

This chapter is based on the publications:

“Organic transistor platform with integrated microfluidics for in-line multi-parametric in vitro cell monitoring.”

Vincenzo Curto, Bastien Marchiori, Adel Hama, Anna-Maria Pappa, Magali P. Ferro, Marcel Braendlein, Jonathan Rivnay, Michel Fiocchi, George G. Malliaras, Marc Ramuz and Róisín M. Owens

Microsystems & Nanoengineering (2017) 3, 17028; DOI:10.1038/micronano.2017.28

“Laser-patterned metallic interconnections for all stretchable organic electrochemical transistors”

Bastien Marchiori, Roger Delattre, Stuart Hannah, Sylvain Blayac, Marc Ramuz

Scientific Reports, volume 8, Article number: 8477 (2018), DOI: 10.1038/s41598-018-26731-8

In the previous chapter, the characterisation of the interconnections has demonstrated the possibility to be cycled up to 30% around 90 times before the break. The OECT is a sensor that allows multiple measurements and can be integrated into a skin to measure real-time parameters of the human body. On top of this, the process is well mastered and the integration of PEDOT:PSS on top of the interconnections is a technological challenge for the fabrication of organic fully stretchable devices.

The OECT is a transistor often based on PEDOT doped with PSS as active material, a conducting polymer which is widely used for its ability to transduce an ionic flow into current flow. To summarise the section 1.6.1, the OECT is a three terminals transistors working in depletion mode. In the case of p-type PEDOT:PSS channel, a high current is flowing in the channel between the source and the drain. When a positive gate voltage is applied to the electrolyte (between Gate and Source); cations penetrate into the channel and drastically reduce its conductivity.

The first demonstration of a highly stretchable, albeit out of plane OECT was shown five years ago (Figure 30a)[97]. Despite its high stretchability up to 270%, the non-coplanar structure of the OECT makes biointerface applications complicated. The PEDOT:PSS was printed in 3D between the electrodes through the shape of nanowires. When the substrate was stretched, the wire was elongated until being fully tight and then broke.

A fabrication process for an in-plane stretchable OECT on PDMS has recently been developed. The patterning of interconnections was based on evaporated gold through a shadow mask of parylene on a pre-strained substrate. After, photolithography of PEDOT:PSS by using an orthogonal photoresist on the pre-strained substrate led to an OECT which was stretchable up to 30% without cracking as a result of a pre-strain step before fabrication in Figure 30b[98]. However, for this device, only a modest transconductance of 0.6mS was achieved. The process of fabrication was long and needed to pre-strain the substrate during the fabrication. Moreover, the use of photolithography directly on PDMS is not totally reproducible. Finally, OECTs were stretchable only up to the initial pre-strain load. Past this value, the mechanical integrity of the device was compromised, leading to the apparition of cracks. Thus, a development of an accurate process for the fabrication of this device and a work on the material to make it stretchable without pre-strain is relevant.

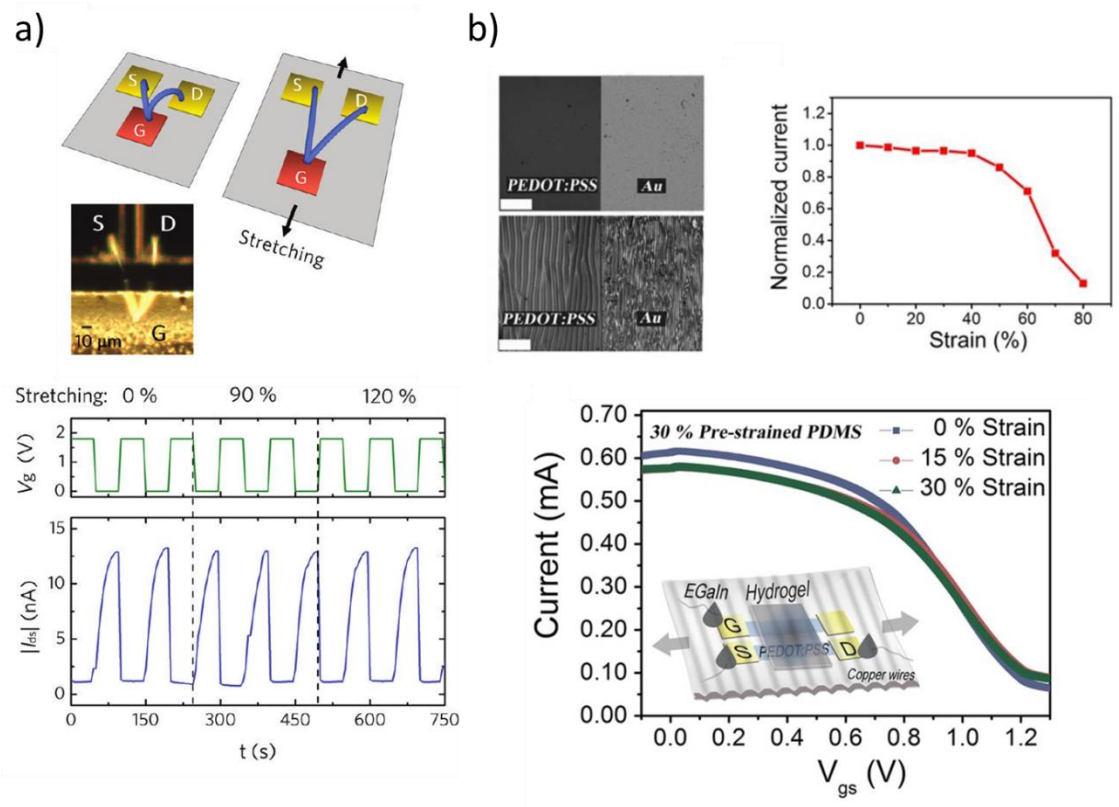

Figure 30: Demonstration of stretchable OECT in the literature. a) Non coplanar stretchable OECT up to 120%. It displays high stretchability, but is not planar, so tricky to use for e-skin and biosensing. Reproduced from [97]. b) Stretchable OECT with no variation in the output characteristics up to 30-40% strain. The device shows low current and relies on mechanical buckling. Reproduced from [98].

The objective of this chapter is to adapt the process of the rigid OECTs and to integrate the stretchable interconnections. For this purpose:

Section 3.1 reviews the applications and process of a rigid OECT, to understand the issues of its fabrication and use.

Section 3.2 presents the methodology for the characterisation of the stretchable devices.

Section 3.3 shows the development of a wound-healing assay on a rigid substrate as a way to master the process.

Section 3.4 presents the optimisation of the formulation of PEDOT:PSS and the process to render the device fully stretchable.

Section 3.5 concludes on the results of this chapter and question on the relevance of these interconnections for fully stretchable sensors.

3.1. OECT fabrication on rigid substrates

In this section, the PEDOT:PSS is presented as a conducting polymer and the formulation optimised for maximum stability and conductivity is introduced. Then, the standard process of fabrication is described.

3.1.1. PEDOT:PSS as conducting polymer for OECTs

The PEDOT:PSS is an intensively used conducting polymer due to its highly conductive properties. Its formulation is well understood for use as a rigid thin film.

3.1.1.1. Structure of the PEDOT:PSS

The highest conductivity of PEDOT:PSS reported in the literature is around 1400 S.cm^{-1} by Kim *et al.*[99], that makes it relevant for use as electrodes. Combined with low absorption of the light in the visible range, the PEDOT:PSS has found a particular use in electrodes for organic solar cells[100], [101].

As shown in Figure 31, the polymer is made of a PEDOT backbone doped with PSS. The presence of PSS induces a delocalisation of the electronic bond in the PEDOT, making it hole-conducting.

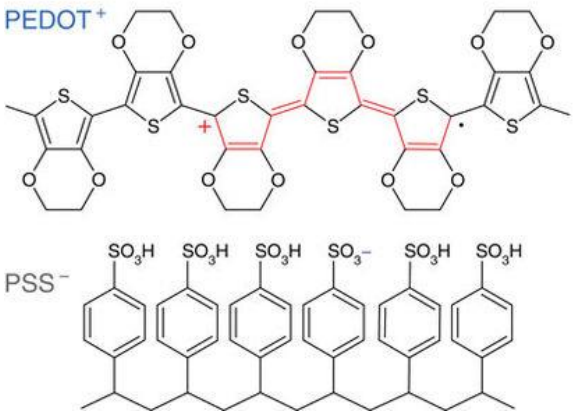

Figure 31: Chemical Structure of PEDOT and PSS.

Apart from its conductivity, PEDOT:PSS is well known for its mixed ionic and electronic conductivity[102], [103]. The polymer is used for bioelectronics applications because of its permeability to ions. Most of the signals from the body come from ionic currents. The material can transduce ionic current through electronic current to interpret biological signals. Initially, PEDOT:PSS was deposited by electrochemical polymerisation[104]. A solution of EDOT monomer and PSS was deposited on an electrode. Then, upon an electric field, the monomer is oxidised producing a radical that reacts with another one, forming a polymer chain. The PSS acts as a counter-ion to stabilise the reaction.

3.1.1.2. Applications

The high optical transparency of thin PEDOT:PSS and its high electrical conductivity make it really attractive as transparent electrodes, and its colour can be easily tuned, making it blue or transparent by oxidation or reduction. Taking advantage of this particular change, electrochromic windows have been investigated, to use it as a darkening layer in the automobile industry for example[105]. Kim *et al.* have increased its conductivity to 1400 $S.cm^{-1}$ and used it for organic solar cells[99]. Moreover, the work function and the ability of PEDOT:PSS to conduct holes makes it attractive as a hole injector in OLED[106].

As an organic electrode and due to its high conductivity, PEDOT:PSS is widely used for bioelectronic applications. For recording bio-signals, this polymer has the same advantages than other conducting polymers over rigid metallic electrodes. For example, microelectrodes made of platinum and indium has shown improved performance for deep brain stimulation with a coating of PEDOT[107]. Due to its mixed conductivity, dry flexible electrodes of PEDOT:PSS has shown similar performances than commercially available wet electrodes for electrocardiography (ECG) for heart monitoring[108] and electroencephalography (EEG) for brain monitoring[109]. The penetration of ions inside the layer makes it an excellent non-polarisable electrode[109].

The OECT is an important application of PEDOT:PSS, measuring a variety of physiological signals. For ion detection, the OECT has shown variations in its electrical properties with different ionic concentrations in its electrolyte[110]. Sessolo *et al.* have also shown the possibility of coupling an OECT with a polymeric membrane that is permeable to specific ions, for ion-selective OECT sensors[111]. Another field of use is in enzymatic sensors. By immobilising a specific enzyme onto the gate, it is possible to detect and measure a concentration of various molecules such as glucose[112], lactate[113], adrenaline[114]...

The second branch of application for the OECT is the recording of cells properties *in vivo* or *in vitro*. For the detection of non-electrogenic cells, without any natural electrical activity, the mechanism of detection is based on the natural ability of the cell to act as a barrier for ions. For in vitro models, cells are seeded and grown either directly on the devices, or on filters, suspended on top of the OECT. A voltage is sent through the gate to measure the properties of this layer. The cell layer induces a delay in the dedoping process of the OECT, acting as a parasitic capacitance. Depending on the frequency of the gate voltage, the response through the channel is different. It is determined by several parameters[92]: the integrity of the tight junctions between the cells, the integrity of the membrane, the coverage of the device and the adhesion of the cells. Then, the properties of the cells can be measured with the addition of different drugs or toxins[115].

The OECT has also shown good results for the recording and the stimulation of electrogenic cells such as neurones and nerves. For in vivo applications, Khodagholy *et al.* have shown a superior

signal-to-noise ratio than a penetrating silicon probe using an OECT for recording the activity of the brain for electrocorticography (ECoG). They demonstrated good results for long-term measurement showing its biocompatibility and also confirming that the mechanical flexibility of the device reduces injuries in the brain[116], [117]. The low-temperature process of the OECT also allowed the fabrication on a bioresorbable substrate for implantable electrodes[118].

The ability of the OECT to measure the properties of the cells is used for the development of the wound healing assay.

3.1.1.3. Formulation

Nowadays, the PEDOT:PSS is commercially available as a dispersion in water (Clevios PH1000 from Heraeus, e.g.). This formulation of PEDOT:PSS is highly conductive and perfectly suitable for spin coating or inkjet printing. Figure 32 is a schematic of the molecular structure of a film of PEDOT:PSS. The deposited material has a natural arrangement of PEDOT rich domains as crystallites (surrounded by dash points) which is the electronic charge transport in an amorphous PSS rich region. This second region helps with the mobility of the ions.

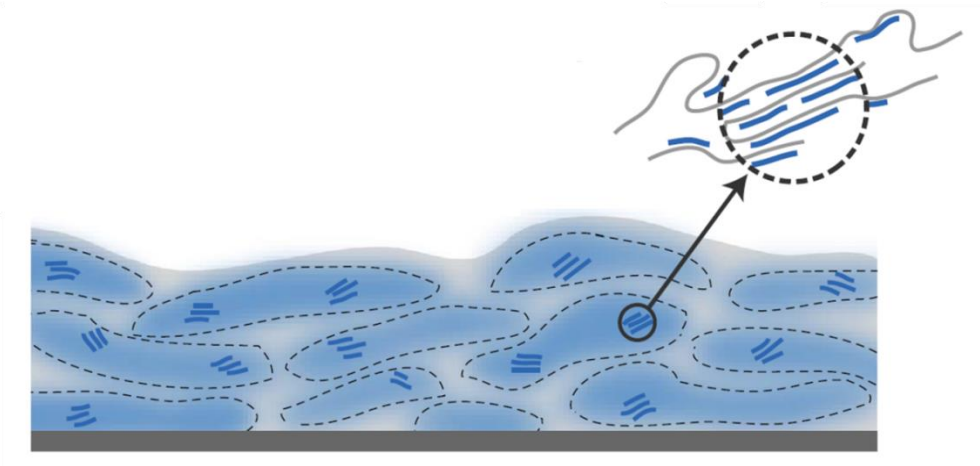

Figure 32: Crystallites arrangement of PEDOT:PSS on a substrate with PEDOT rich area in blue and PSS in grey. The PEDOT rich areas form regions with a certain degree of crystallinity in a matrix of PSS amorphous rich areas. Figure copied from [102]

To enhance the conductivity of the film, a technique consists in increasing the crystallinity of the PEDOT:PSS arrangement with the addition of a high boiling point solvent such as methanol or dimethyl sulfoxide or ethylene glycol[119], [120]. The addition of such a solvent allows a better organisation of the rich PEDOT area by pushing the PSS out of the crystallites[121]. Thus, it also decreases the ion mobility inside. For ethylene glycol (EG), the best ratio has been found around 5% v/v, for the best ratio ionic/electronic mobility[102].

The dodecylbenene sulfonic acid (DBSA), an anionic surfactant enhances the film formation as well as the conductivity, by acting as a counter anion on distorted PEDOT chains[122]. The best ratio has been found at 0.5%v/v to avoid phase separation[123].

Silanes, such as 3-glycidoxypropyltrimethoxysilane (GOPS), are used to avoid the problems mentioned above of stability by using organic materials. The material bonds to the substrate and avoids delamination, particularly in a liquid environment, mostly for bioelectronic applications. This formulation, introduced by Sessolo *et al.* is now widely used. It is particularly adapted to the measurement in an aqueous environment with the OECT[124].

3.1.2. Fabrication process of standard OECTs

There are several fabrication methods for the patterning of organic materials. For industrial use, the most effective is probably spray coating, inkjet or spray coating because they are easily scalable. However, they suffer from a lack of patterning resolution, and the development of compatible formulations is necessary. So, for our purpose of research, photolithography has been a compromise and is available in all cleanroom facilities.

The most used process used for OECT relies on the patterning of gold interconnections with photolithography and lift-off and then peel-off of parylene for the patterning of PEDOT:PSS by photolithography[125]. This is illustrated in Figure 33.

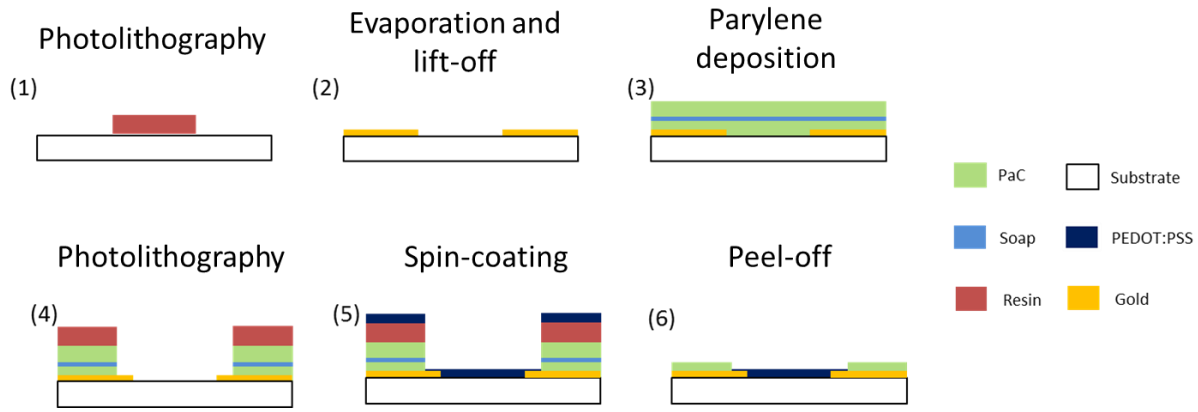

Figure 33: Schematic depicting the fabrication steps. The gold lines are patterned by lift-off of the resin after evaporation and PEDOT:PSS area is patterned with peel-off of parylene.

1- The patterning of gold is done by lift-off of the photoresist with acetone. Few micrometres of photoresist are spin-coated on the substrate at a certain rotation speed. After spin coating of the resist, a soft baking is necessary to evaporate the solvent and thus fix the photoresist to the substrate. In this process, a positive photoresist S1813 is used and baked for 1 minute at 110°C. After exposition to UV light, the sample is immersed in an MF26A developer to remove the resin from the part of the slide where there will be the gold lines.

2- The next step is to evaporate the metal onto the substrate. The metal is heated in a crucible with current by Joule effect. Once above its melting point temperature, the metal is ejected to the samples placed upside down and condenses on the cold substrate. Then, the unwanted parts of the gold are removed by immersion in acetone. This solvent has a high solubility power and goes underneath the gold to solubilise the resin entirely after a few hours.

3- Two layers of Parylene-C (PaC) are added by vapour phase deposition. The PaC is an excellent insulating material, so a first layer of 1.5µm is deposited to insulate the interconnections. A second layer of 2.5µm is used later for the patterning of the conducting polymer. 2% soap (Microchem90) is spin coated acting as an anti-adhesive to prevent adhesion between the two layers. PaC thickness is controlled by the quantity of initial dimer loaded inside the furnace.

4- The two layers of PaC are opened where the polymer is deposited, for electrical contacts and at the gate. A second photolithographic step with a thick layer of AZ9260 is used. The subsequent patterned device is placed inside a reactive ion etching system (RIE). A plasma is created in a vacuum chamber by the ionisation of O_2 and CHF_3 gas.

5- The deposition of PEDOT:PSS is done by spin-coating. The solution discussed previously is deposited on the substrate with a controlled rotation speed which determines the thickness. The device is baked a first time at 110°C for 1.

6- The peel-off is the step following this 1st baking. With tape, the top layer of PaC is removed from the bottom one, removing the photoresist and the PEDOT from the non-patterned areas. After, the device is baked for 1h at 140°C to dry completely the PEDOT:PSS layer, remove all traces of solvents and help the cross-linking process that provides stability of the device in water and adhesion to the substrate.

A picture of the final device is displayed in Figure 34a and a zoom in the design in Figure 34b. The two big squares are the gate, and the small lines reach the transistors. There are 6 transistors per well, with different sizes, to get different sizes of wound. The well is stuck with biomedical silicone glue to ensure no leaks and biocompatibility since cells are cultivated inside.

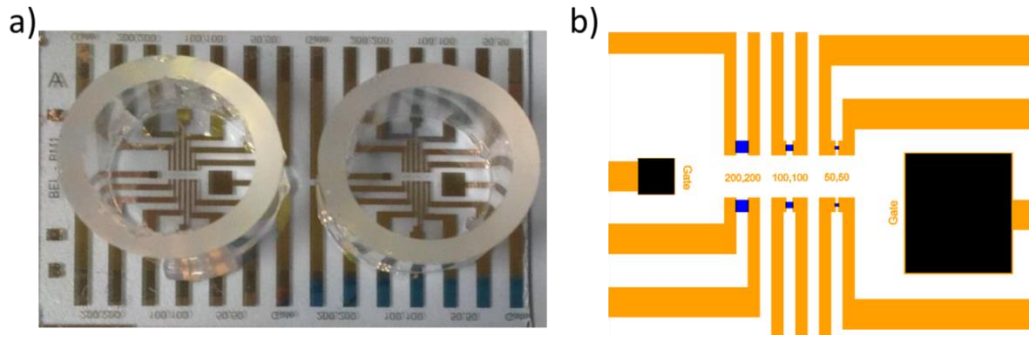

Figure 34: a) Picture of the final device on glass with glass well on top of the transistors to cultivate cells on top and b) design of the device zoomed in the well. In orange the gold lines and in blue/black: the PEDOT:PSS layer.

3.2. Characterisation methodology

This section is dedicated to the tools and the methods used to characterise the OECT. First, the two main methods to characterise the OECT are introduced. Then, the setup used to characterise the PEDOT:PSS on a stretchable substrate is presented.

3.2.1. Output and transfer transistor characteristics

For further measurement of the OECT, the setup for the characterisation has been associated with the displacement table. Figure 35 presents the electrical output characteristics of an OECT. Figure 35a displays the output curve of the transistor, with the drain current (I_{DS}) as a function of the drain voltage (V_{DS}) for different values of gate voltage (V_{GS}). V_{DS} was varied from 0V to -0.6V for values of V_{GS} from -0.6V to 0.6V. In this curve, the two regimes of the transistor are distinguished. In the linear regime, I_{DS} increases linearly with V_{DS} for low values of V_{DS} and, when the voltage tends to -0.6V, the saturation regime is reached. The current cannot be higher and is thus independent of the voltage. The current of saturation increases from V_{GS}=0.6V to V_{GS}=-0.6V. When going towards V_{GS}=-0.6V, the channel is more and more doped because there are more and more cations inside the PEDOT:PSS layer and then, the current decreases.

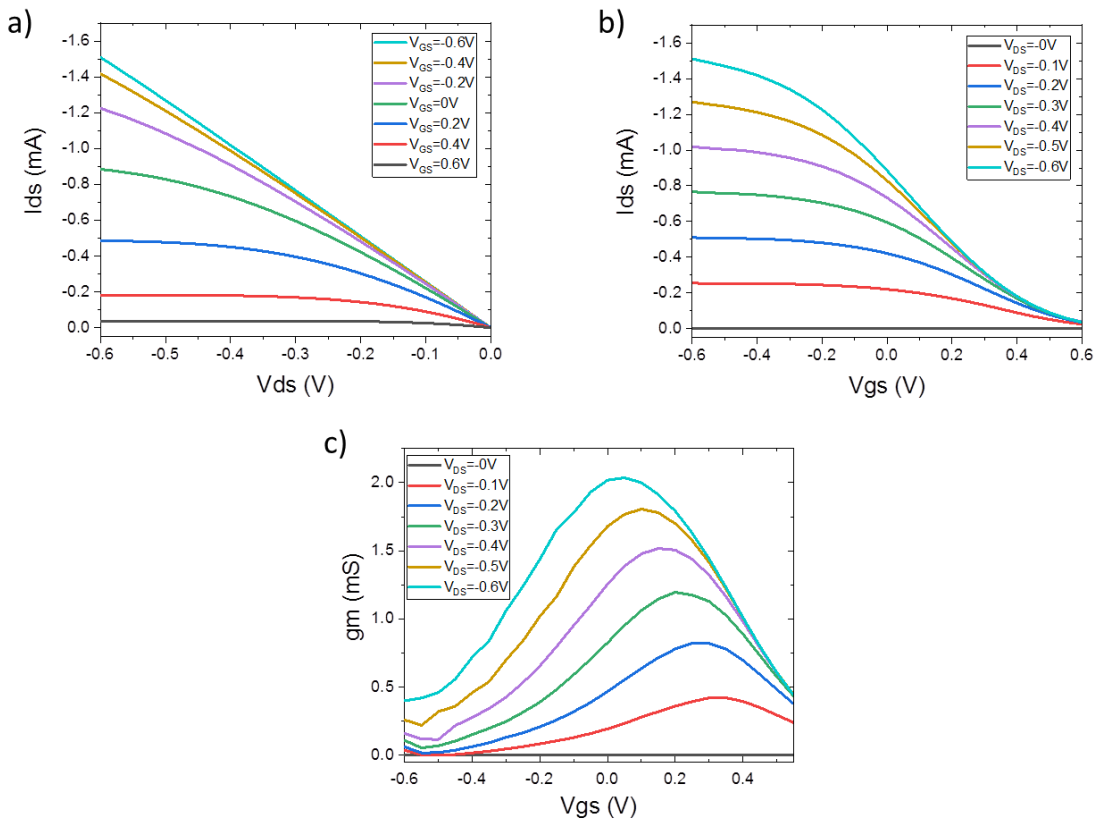

Figure 35: electrical characteristics of an OECT. a) Output curve of the device with different values of V_{GS} from -0.6V to 0.6V and b) Transfer curve of the device with different values of V_{DS} from 0V to -0.6V and c) the associated transconductance. The OECT channel is 50µm length and 50µm width and the electrolyte is a KH_2PO_4 solution at 0.01M

Another way to plot the transistor characteristics is presented in Figure 35b. The transfer curve represents I_{DS} as a function of V_{GS} from -0.6V to 0.6V for different values of V_{DS} from 0 to -0.6V. For high positive V_{GS}, the channel is almost full of cations, and so, the current is very low whatever the value of V_{DS}. From this transfer curve, the transconductance gm can be extracted and is plotted in Figure 35c. The transconductance is a useful figure of merit and corresponds to the ability of the OECT to be de-doped under gate bias. A high gm ensures a high OECT gain, and thus a high sensitivity when used as a sensor. It is calculated from the variation of current divided by the variation of gate voltage ($\Delta I_{DS}/\Delta V_{GS}$) for a given V_{DS}. Depending on the drain voltage, the transconductance has a maximum value for one gate voltage. This value is getting closer to V_{GS} when increasing drain voltage.

3.2.2. Measurement of OECT characteristics on the XY table

The device was clamped on the tensile test table described previously to proceed to the electrical characterisation of the device under strain. Programs developed to measure the characteristics of the transistor were used. Figure 36 shows a picture of the setup. The electrolyte was dropped on the channel, and the gate was in contact with the liquid on top. This gate is attached to a 3D printed plastic

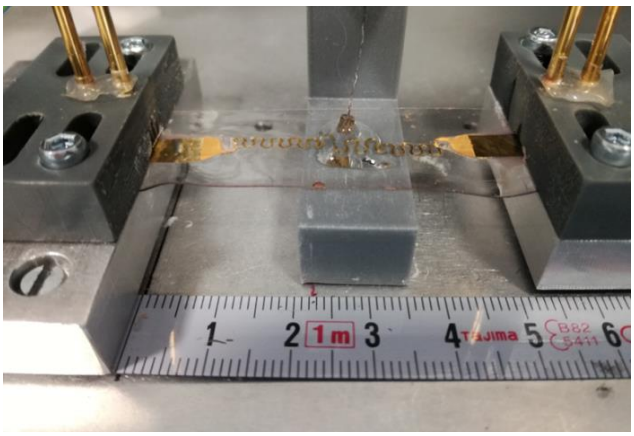

Figure 36: Photograph of the setup used to characterise the OECT. The device was clamped at either end. One output from the Keithley® was connected to the source and the drain. A second output was connected to an Ag/AgCl electrode immersed in an electrolyte. The strain and the electrical measurements were synchronised with LabVIEW.

The electrolyte used was a KH_2PO_4 solution at 0.01M. The device was not compatible with a classic phosphate buffer saline solution (PBS). An electrochemical reaction occurred on the aluminium, damaging the PEDOT:PSS layer.

3.2.3. Conductivity measurements

For the conductivity measurement on flexible/stretchable substrates, a four-wire measurement setup has been developed. Commercially available setups have the main drawback of using sharp pins to be very precise in the placement of the contact. In the case of soft substrates, the small pins were damaging the substrate and were not able to measure thin layer materials. Figure 37 displays our system. It had larger and smoother pins to reduce the damage done to the layer.

Figure 37: Conductivity measurement setup for soft substrates. The pins were large to avoid the substrate to be pierced.

As mentioned in the previous section, the current was applied through the outer pins with a Source Measurement Unit (NI PXIe-4141), and the voltage was measured with a Digital Multimeter (NI PXI-4071).

The configuration used is known as the Kelvin technique. The probes are aligned and equally spaced. Equation 3 is used to calculate the sheet resistance R_s if the two following conditions are satisfied[126]:

- The space between the probes is larger than the thickness
- The distance between the edge and the probes is larger than the distance between the probes

$$R_s = \frac{\pi}{\ln(2)} \frac{\Delta V}{I}$$

Equation 3: Formula for the calculation of the sheet resistance in the Kelvin configuration

Then, the conductivity of the layer is calculated if the thickness is known by dividing the resistivity by the thickness e in Equation 4.

$$\sigma = \frac{1}{R_s * e}$$

Equation 4: formula for the calculation of the conductivity σ with the sheet resistance R_s and the thickness e

The samples evaluated were squares of 17mm by 25mm of a PEDOT:PSS layer on PDMS. The solution was spin-coated on a PDMS sample after treatment with O_2 plasma.

3.3. Development of an OECT as a wound healing assay

In this section, a device inspired by electrical wound-healing is described. Classic methods rely on gold electrodes to make the wound and to follow the healing by electrical impedance spectroscopy (EIS). The fabrication of an OECT, used in a standard two electrodes system to make the wound is demonstrated. Then, the device is used as a transistor to measure the healing. Contrary to conventional methods used to monitor cell layer integrity, OECT allows the coupling with microscopy techniques as this polymer is transparent. Moreover, with the OECT configuration for the healing, the properties of the cells that are covering it are followed electrically.

3.3.1. OECT as a platform for the wound healing assay

Wound-healing is a technique commonly used to observe the migration of a cell monolayer. Following the formation of the wound, cells in the proximity are monitored over time using a microscope to study their ability to heal and migrate over the damaged area. This is the best method to study the displacement of the cells and their interaction during the migration with other cells or with the extracellular matrix.

In a classic wound-healing assay (or scratch assay), cells are grown in a confluent monolayer, and then the layer is 'wounded' using a pipette tip or razor blade. However, the scratch assay does not offer precise control of the size and the shape of the wounded area. Moreover, it lacks reproducibility, as the scratch assay is generally a manual technique. To overcome some of these limitations, Keese *et al.*[127], [128] first proposed an alternative method to obtain precise control of the wound size and shape by using AC electrical currents to achieve electroporation of cells (wounding) in a well-defined region corresponding to the area of a micro-sized gold electrode. It is highly reproducible, but it is difficult to follow the healing with classic microscopy, with a non-transparent gold electrode.

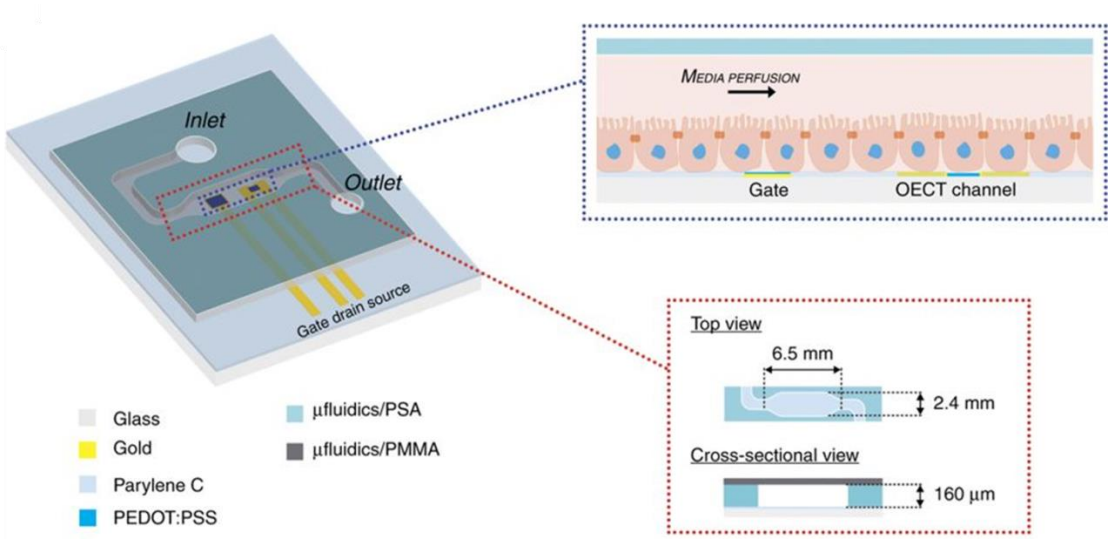

Figure 38: Schematic of the microfluidic device, comprising an OECT in a microfluidic channel. A cell layer is grown on top, and the media is perfused in the microfluidic channel.

One of the key advantages of using the OECT technology for testing the cells is the possibility for easy integration of micron-sized electrodes with a microfluidic structure in a compact manner, illustrated in Figure 38. As further evidence of our capabilities of using the OECTs to perform standard biological assays, an electric wound-healing assay for the cell layer cultured has been developed in the microfluidics. The device comprised an OECT in a microfluidic channel cut in poly(methyl methacrylate) (PMMA) and is covered by a pressure sensitive adhesive (PSA) to ensure sealing. Inspired by these findings, an electrical wound healing assay based on the use of the OECT to generate a wound in the cell layer covering the transistor channel has been developed. Conversely, OECT technology is fully compatible with high-resolution microscopy as the PEDOT:PSS active layer of the transistor channel is optically transparent[92]. In this scenario, the use of the OECT to perform an electrical wound healing assay can provide a unique tool to overcome the current limitations on the use of micron-sized gold electrodes, making this method fully compatible with standard microscopy tools.

3.3.2. Results of the wound healing on the OECT

An electrical wound assay has been developed using the OECT channel and the gate electrode in a slightly different operation mode compared to the classic transistor configuration[116], as shown in Figure 39a. The source and drain of the transistor are shorted together to obtain an equipotential distribution of the applied AC voltage in the transistor channel, while a second, bigger, electrode is used to close the electrical circuit and act as the counter electrode for the wound generation. It should be noted that by shorting the source and drain of the OECT channel, effectively an electrode is generated, which, used together with the bigger second electrode (gate electrode), was employed for the generation of the electrical wound in the cell layer.

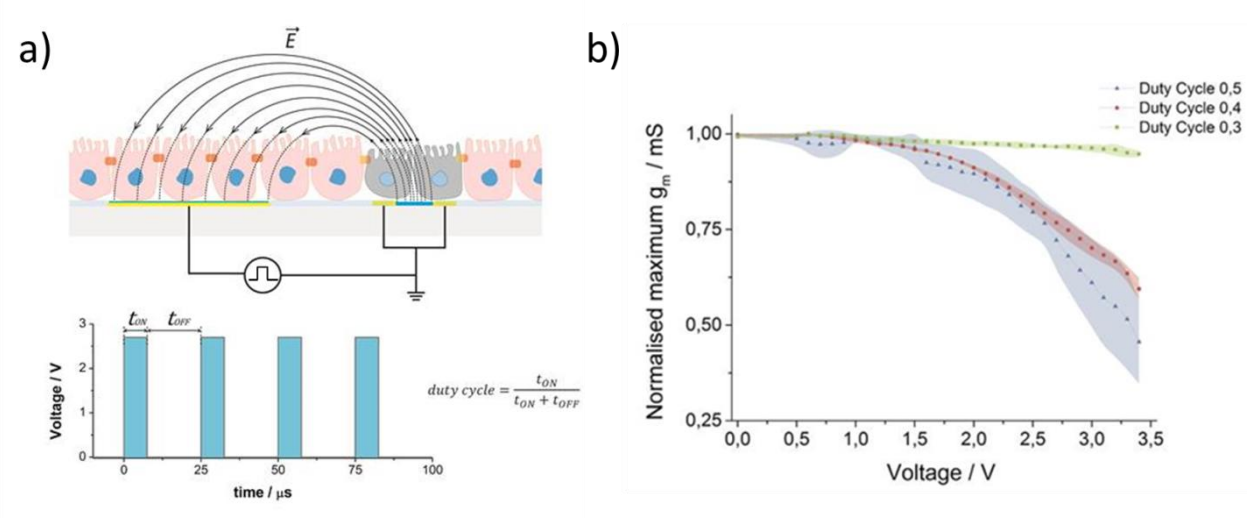

Figure 39: A microfluidic electrical wound-healing assay with the OECT. a) Schematic of the experimental set-up of the developed OECT-based electrical wound-healing assay. A confluent cell layer covering the transistor channel area is electroporated with an oxidative square voltage, typically below 3 V, resulting in an electrical wound of the same dimension as the transistor channel. The semicircle lines represent the electric field distribution at the electrode/electrolyte interfaces across the cell layer, while the two grey cells covering the transistor channel represent the electrically wounded cells. b) The impact on the OECT maximum transconductance (gm=ΔID/ΔVG) caused by the application of oxidative potentials for duty cycles equal to 0.3 (green), 0.4 (red), and 0.5 (blue), n=3.

The alternating potential applied to the system is schematically represented in the bottom diagram of Figure 39a. For the generation of the electric wound, a square wave pulse is applied from zero to the desired voltage (typically below 3V) at a frequency of 40kHz (period of 25µs). The schematic of Figure 39a shows the direction of the electric field across the two electrodes in the electrolyte. As the transistor channel is a much smaller electrode, the potential drop at the electrode/liquid interface across the cell layer covering this region is above the critical cell membrane rupturing value (4200 mV)[129], resulting in a localised cell electroporation and lysis, schematically represented by the grey cells, Figure 39a.

For the OECT wound-healing assay, one crucial parameter is the stability of the PEDOT:PSS organic conducting layer upon the application of a high oxidative potential needed to induce the electroporation of the cells. In addition, higher potentials (>1 V) in an aqueous environment can lead to electrochemical reactions within water associated to the oxidation and thus the

formation of other cytotoxic species, such as chlorine[127]. Interestingly, the use of AC currents at high frequency (>10kHz) can easily bypass these undesirable conditions even for potentials up to 5V[128]. Nonetheless, it is well known that the irreversible electrochemical oxidation of PEDOT:PSS-conjugated polymer leads to structural changes in the polymer backbone and loss in its conductivity[130]. Figure 39b shows the variation of the maximum transconductance value of the OECT (gm = ΔID/ΔVG) when sequentially stepping the potential from 0 to 3.4V at 40kHz for 30s each time, using the electrical configuration and the wave signal shown in Figure 39a. By evaluating the variations in the maximum transconductance of the OECT, it is possible to obtain useful information on possible degradation processes induced in the PEDOT:PSS layer. For a duty cycle of 0.5 (blue line/triangle, t_{ON}=12.5µs, t_{OFF}=12.5µs), a rapid decrease of the OECT transconductance is observed for a potential above 1.5V, resulting in a total loss of ~50% at 3.4V.

To improve the device stability in this wide potential window, a possible solution is to change the duty cycle of the squared pulse signal. A shorter duty cycle reduces the total supplied energy for undesired oxidative reactions in the conjugated polymer and, at the same time, allows a longer relaxation of the system. For instance, a duty cycle of 0.4 (red line/circle, t_{ON}=10µs, t_{OFF}=15µs) slightly improves the device stability with a total loss of ~40% at 3.4V, while for a duty cycle of 0.3 (green line/square, t_{ON}=7.5µs, t_{OFF}=17.5µs), the OECT shows a more stable behaviour in the potential window of interest. In the latter conditions, a final ~6% decrease in the maximum transconductance is observed only when the OECT was sequentially cycled to a potential up to 3.4V. These findings are particularly important as they provide evidence that under these conditions, that is, 40kHz, duty cycle 0.3, the OECT channel is capable of supporting high oxidative potentials without an irreversible loss in its amplification performance, an essential requirement to perform in-line electrical monitoring of the cell layer during healing.

Next, the electrical wound-healing assay was performed by seeding MDCK II-pLifeAct cells on the OECT. Initial optimisation experiments were performed in a classic, static configuration using a glass well to contain the cell culture media. Figure 40a shows a typical frequency-dependent transistor response in the absence (dashed grey curve) and in the presence of a fully

confluent MDCK II-pLifeAct cell layer (solid black line). In the images below (black frame), the brightfield and the F-actin fluorescence pictures of a confluent cell layer are shown. The electrical wound to the cells was then generated by pulsing the electrode with 2.7V at 40kHz (duty cycle 0.3) for 30s. An identical pulsing protocol was repeated four times until a complete absence of fluorescence covering the transistor channel was observed. The F-actin fluorescence images (orange frame) shows the well-defined square shape of the wound corresponding to the size of the transistor channel (100 × 100µm^2), proving the ability of the OECT to create an electric wound in a well-confined area of the cell layer.

Following the formation of the wound, optical and electrical monitoring of the healing process is started, by using the same OECT employed for the generation of the wounding. Moreover, the electronic monitoring of the healing process was performed by using the OECT as a three-terminal device. Figure 40a shows the time evolution of the frequency dependent response of the OECT measured every 16min while cells were healing, shown by the gradual colour change of the curves from orange (wounded cell layer) to blue (healed cell layer). As the healing begins, slight variations in the cut-off frequency were measured, arising from the initial rearrangement of the cells in the proximity of the electrical wound, and the formation of two moving healing fronts. The initial stage of the healing process corresponds to the closely packed orange curves of Figure 40a. Subsequently, with the advancing of the healing fronts toward the middle of the wound a continuous decrease in the cut-off frequency is observed until completion of the healing, as revealed by the proximity of the blue curves. The electrical evolution of the healing process can be appreciated in more detail in the inset graph of Figure 35a, showing a well-defined sigmoidal trend with two steady state conditions corresponding to the start, with a cut-off frequency equal to ~600Hz, and the end of the healing, with a cut-off frequency equal to ~60Hz, respectively. The images of Figure 40a (blue frame) show the brightfield and fluorescence images of the fully healed cell layer. Encouraged by these findings, the OECT electrical wound-healing assay is then integrated with the microfluidics. Figure 40b shows the typical time evolution of the cell layer resistance obtained during the healing process of the cells. First, the cells were wounded on the transistor channel resulting in a complete loss of cell-

related impedance, as well as the actin fluorescence, in a well-defined manner, as shown before and in the inset fluorescence picture at time zero.

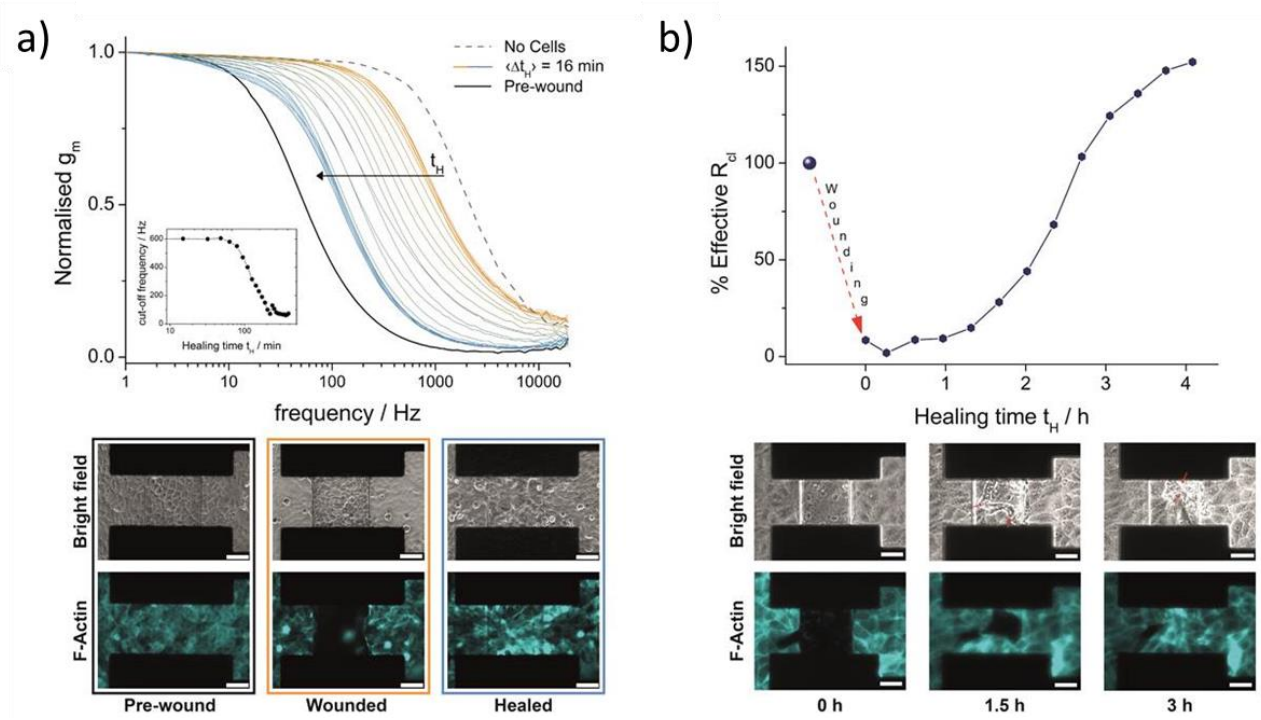

Figure 40: a) Typical time evolution of the OECT frequency-dependent response during the healing process of an electrical wound generated on a confluent cell layer of MDCK II-pLifeAct. A confluent layer of cells grown on the transistor channel induces a shift in the OECT cut-off frequency, from ~1400Hz (dashed grey line) to ~30Hz (solid black line). Following the generation of the electrical wound (2.7V at 40kHz, duty cycle 0.3, cycle time 30s), the cut-off frequency increases (orange line) due to loss of cells from the active area of the device. As the healing of the cells progresses, a continuous decrease in the cut-off frequency is monitored until completion (blue line). The inset graph shows the sigmoidal evolution in the cut-off frequency during the healing process. The data point at time zero is omitted for clarity. Below are shown brightfield and fluorescence images for the pre-wound (black frame), wounded (orange frame), and healed (blue frame) cell layer (scale bar, 50µm). b) Electrical wound-healing assay performed inside the microfluidic device. On the top, the temporal evolution of the Rcl during the healing process is shown. The bottom panel contains the brightfield and the F-actin fluorescence images at a different time during the healing process. In the brightfield images, the red arrows highlight the densely packed healing fronts incorporating the wounded cells and likely leading to the final increase of ~1.5-fold in the effective Rcl. (scale bar, 50µm).

It is also important to note from the brightfield image that, following electroporation, dead cells were still covering the transistor channel area although they were not responsible for

substantial resistive contributions (Rcl 10% of initial value) within the first hour of the healing process. As the healing front of the cells started to move toward the centre of the transistor channel, a continuous increase in the cell resistance is measured with a final Rcl ~1.5-fold higher than the starting resistance before the wound. This is attributed to the formation of a densely packed healing front (less permeable to ions/higher resistance) due to the incorporation of debris from the dead cells lying on top of the transistor channel. This is clearly visible in the brightfield images collected 1.5 and 3h after starting of the healing process as indicated by the red arrows.

The wound-healing assay developed in this section is a powerful tool to monitor with more accuracy the migration and the properties of the cells. Its implementation within a microfluidic chip is a step forward in the improvement of in vitro test. It fits better with the conditions of pressure and flow in the body. All organs in the body are soft and so, to make an OECT on a stretchable substrate would represent even a better modelling of in vivo real conditions. Furthermore, in the objective to follow the healing on top of the skin, the use of OECTs in an e-skin seems possible.

3.4. Development of OECT on a stretchable substrate

The development on a rigid substrate has been demonstrated in the previous sections for the development of a wound-healing assay. The process is adapted for a rigid substrate for classical applications but not for the integration of stretchable materials. In this purpose, the development of a stretchable OECT on PDMS is presented. A schematic of the resulting device is shown in Figure 41. In this section, the methods available in the literature for making PEDOT:PSS stretchable are identified. The optimisation of the formulation of PEDOT:PSS is then presented. The adaptation from the rigid process is explained to integrate only stretchable materials. The integration of the channel is discussed as an essential parameter to make a stretchable device. Finally, results of the stretchable device are presented.

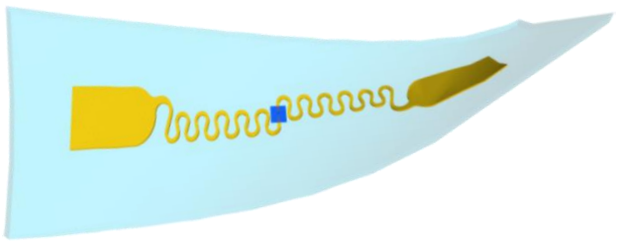

Figure 41: Resulting device modelled in 3D. The device is made out of stretchable interconnections with PEDOT:PSS in dark blue for the channel, encapsulated in PDMS. As a stretchable device, it can be bent and accommodated to 3D surfaces.

3.4.1. Review on enhancing stretchability of PEDOT:PSS

The stretchability of PEDOT:PSS has already been studied in the literature. Two additives have been proved to improve the stretchability of PEDOT:PSS. Chen *et al.* have characterised mechanically self-standing films of blends of PEDOT:PSS with polyvinyl alcohol (PVA)[131]. With more than 60% of PVA, the film endures a stretch by more than 90% before rupture. On the other hand, the addition of non-conducting polymer decreases the conductivity of the film. The conductivity decreases by a factor 10 between 0% and 70% PVA and then decreases drastically. So, there is a trade-off between the mechanical and the electrical properties. They suggest the best ratio of 30-40% of PEDOT:PSS in PVA for self-standing film, whereas a more important ratio of PEDOT:PSS around 70% might be preferred for thin films because the low resistivity cannot be compensated by a high thickness.

The second additive is a fluorosurfactant. The commercial name is known as Zonyl FS-300, sold by DuPont, but due to environmental issues with the biodegradability of the product, it has to be replaced with Capstone FS-30. Bao group in Stanford extensively studied the effect of this surfactant on the mechanical and electrical properties of PEDOT:PSS for applications as transparent electrodes, mainly for solar cells. The use of fluorosurfactant has several enhancing effects. First, it helps with the wettability of the solution on polymer hydrophobic substrates [132]. With a 1% Zonyl, it also increases the conductivity of the resulting film. The surfactant induces phase segregation of PEDOT and PSS, forming longer PEDOT-rich region, that favours the mobility of the holes[132]. This effect is similar to the addition of a co-solvent such as ethylene glycol. Finally, the most important for stretchable electronics, it greatly increases the stretchability of the PEDOT:PSS as a thin-film[133]. The mechanical and electrical behaviour of PEDOT:PSS on PDMS with the fluorosurfactant are displayed in Figure 42. Without Zonyl, the layer had an increase in the resistance by a factor 60 at 50% strain whereas it was only by a factor 2 with 1% of surfactant (Figure 42a).

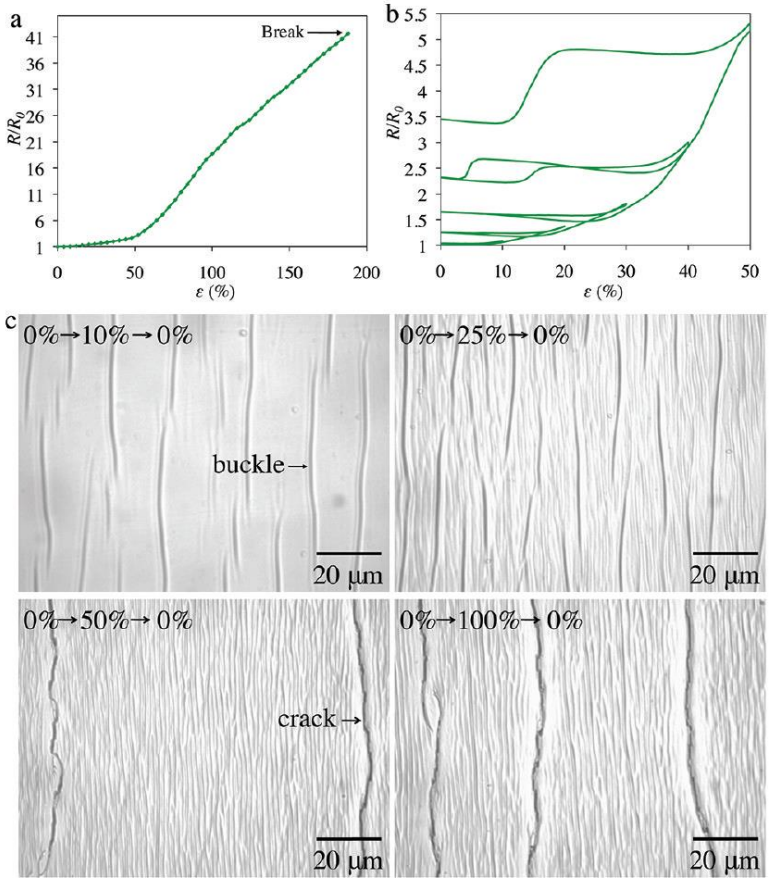

Figure 42: Stretchability of PEDOT:PSS deposited on PDSM with a fluorosurfactant. a) Resistance change in resistance as a function of strain. b) Cycling of the device and c) Micrograph of the layer during cycling measurement. The resistance of the PEDOT:PSS has increased by a factor 2 at 50% strain. There is an apparition of cracks between 25% and 50% strain that increases the resistance of the layer permanently. Reproduced from[133].

In Figure 42b, the cycling of the device has shown stable resistance until 20% strain. Then, the resistance starts to increase irreversibly due probably to the apparition of cracks particularly visible at 50% strain in Figure 42c.

The activation of the substrate is also a very important parameter; it has a huge impact on the final stretchability. Lipomi *et al.* have shown that a light activation completely changes the stretchability of the PEDOT:PSS[133]. While 3 minutes of an O_2 plasma at 150W led to an increase of the resistance of the layer by more than 50 times at 5%, the same plasma treatment but for 10 seconds, the device reached the same value of resistance at 50% strain. Moreover, a

UV/ozone treatment of the substrate for 20 minutes improved, even more, the stretchability of the PEDOT:PSS layer, multiplying its initial resistance by only a factor 2 at 50%. The mechanism of the behaviour of the mechanical behaviour of PDMS after activation is presented in Figure 43. When activated, the PDMS forms brittle material on its surface, close to silica. When stretched, these rigid areas break forming islands of rigid materials. The PEDOT:PSS on the island does not deform. Between the islands, however, the conducting polymer endures a lot of strain. It leads to the creation of the same cracks than the PDMS, and thus an increase in the resistance[133], [134].

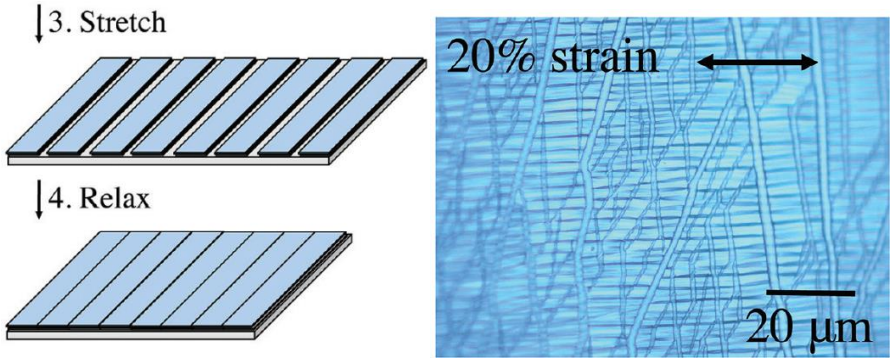

Figure 43: Mechanism proposed to explain the behaviour of PDMS under stretch after strong plasma treatment. The apparition of ductile areas decreases the stretchability of a thin layer on top, extracted from [133].

The use of additives is a known method to improve the stretchability of PEDOT:PSS deposited on PDMS. The use of PVA and Capstone, a fluorosurfactant is promising. With both additives, the stretchability is increased to reach around 30% strain without detrimental damage to the layer. In the purpose of a stretchable OECT, to make it compatible with the different materials composing the device, the study of the process of fabrication is necessary.

3.4.2. Formulation optimisation of PEDOT:PSS for stretchable properties

As mentioned in section 3.1.1.3, the formulation of PEDOT:PSS mixture for the OECT channel is based on work done by Sessolo *et al.* to improve its conductivity and adhesion[124]. This formulation has been developed for rigid/flexible OECTs, but not for a stretchable one. To increase the stretchability of PEDOT:PSS films, the two main chemicals introduced in the previous section were investigated: a fluorosurfactant (capstone®) and polyvinyl alcohol (PVA) since these two compounds are known[131]–[133]. The resistance of a layer of PEDOT:PSS mixture on PDMS was evaluated as a function of the strain for different amounts of additives. In Figure 31 the graphs of the different experiments for the PEDOT:PSS mixture optimisation.

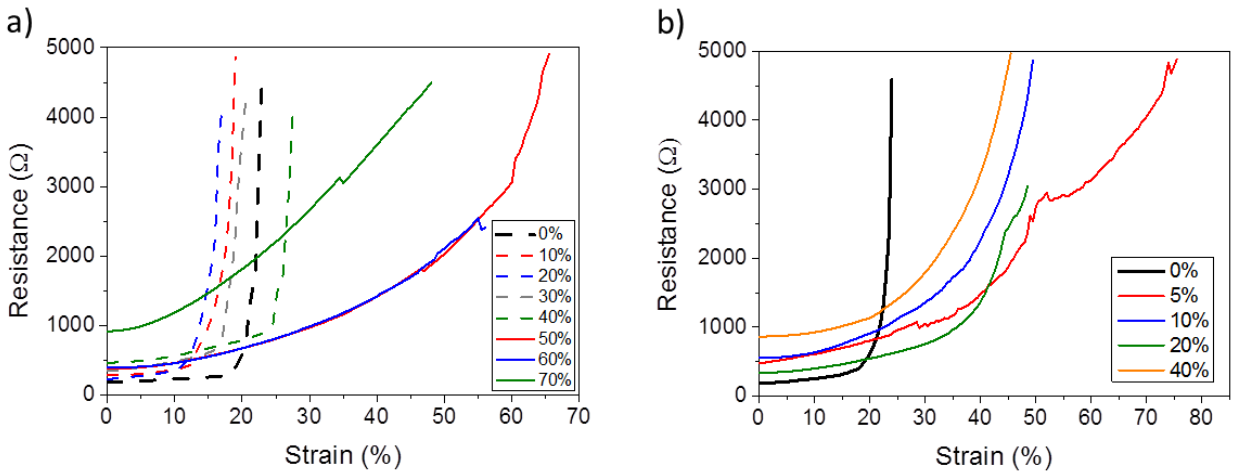

Figure 44: Optimisation of the formulation for the PEDOT:PSS layer spin-coated on a PDMS substrate. a) Resistance as a function of the strain for different wt% of PVA. b) Resistance as a function of the strain for different vol% of Capstone®. The samples were squares of 17mm by 25mm of PEDOT:PSS layer on PDMS.

As shown in Figure 44, without any additives, the formulation described previously had a stable resistance until 20% strain. After this value, the resistance increased rapidly, and the layer resistance was too high to provide good performance for OECT. The impact of PVA on the stretchability of the film was investigated with solutions from 0wt% to 70wt% without the

addition of GOPS (Figure 44a). Its addition resulted in an increase of resistance and provided no improvement for the stretchability. With regard to the literature, it appeared that the addition of PVA does not affect the mechanical properties before 40wt% of PVA[131]. The best mechanical properties were found with 50wt% PVA, but it appeared that the PEDOT:PSS mixture layer was delaminating from the PDMS substrate while stretching. This was most likely due to the absence of GOPS which acts as a cross-linker agent, helping with the adhesion of the film[135]. The impact of the addition of Capstone between 0vol% and 40vol% is available in Figure 44b.

The best ratio of Capstone is 20vol%; it showed high conductivity and an increase of the resistance at around 35% strain. A study of the polymer at the molecular level is needed to thoroughly understand the impact of the different additives on the mechanical and electrical properties.

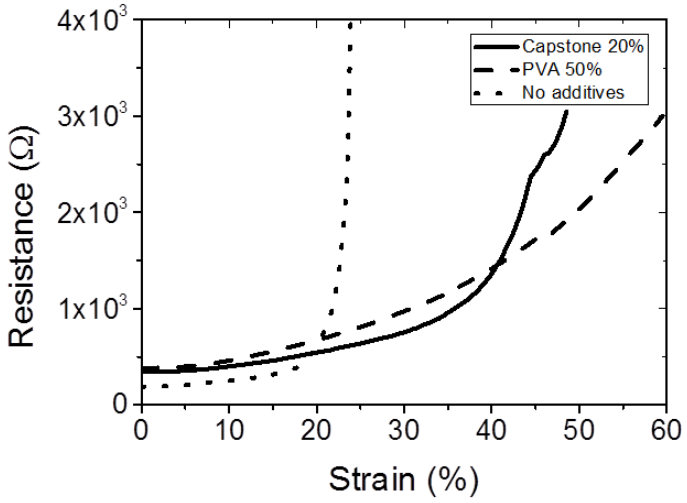

Figure 45: Ratios estimated to be the best for each additive. The addition of Capstone as a fluorosurfactant increases the stretchable properties of the PEDOT:PSS. Furthermore, the addition of PVA also enhances the mechanical properties, but ultimately appears to delaminate from the substrate under stretch. The samples are squares of 17 mm by 25 mm of PEDOT:PSS layer on PDMS.

A comparison with the best two ratios of additives is displayed in Figure 45. Since the PVA based solution delaminated under stretching, 20vol% Capstone was selected as an additive for

improving the mechanical properties of the active area. It resulted in an active area with high stretchability and a conductivity of 150S.cm^{-1}; in the same range than the value reported by the supplier (900S.cm^{-1}) [136]. This solution was spin coated on the device at the end of the fabrication process presented in the next section.

3.4.3. Process optimisation to integrate stretchable materials

The process developed is based on the most common way of making an OECT, namely the parylene-C (Pa-C) lift-off technique described previously. The use of the parylene layer as a sacrificial layer also avoids the use of photolithography directly on PDMS, which is difficult due to the adhesion of the photoresist on PDMS[51]. However, the existing process is not adapted for the etching of thick layer of Parylene and then PDMS. There are several parameters to adjust: the thickness of parylene, the thickness of photoresist, and the parameters for etching PDMS.

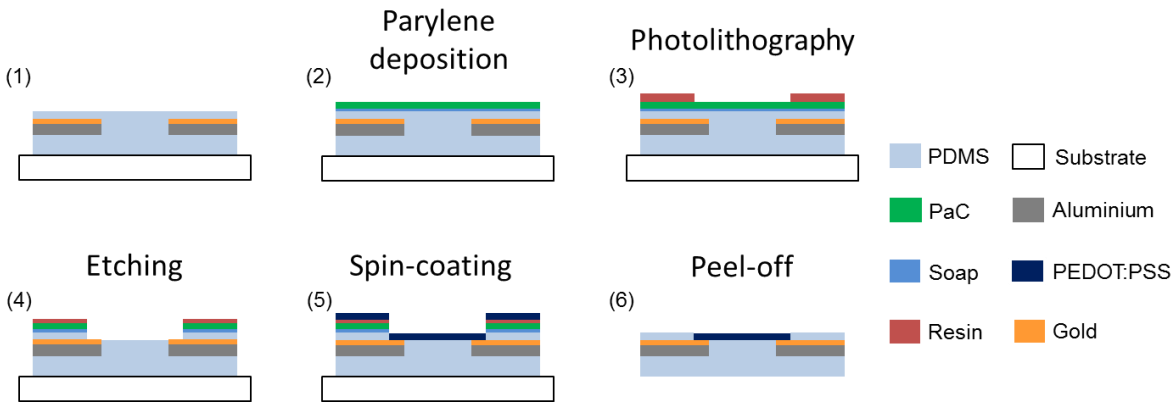

Figure 46: Schematic depicting the fabrication steps. The encapsulated lines are covered by parylene. The opening of the channel and contacts on pads are done by photolithography and reactive ion etching of parylene and the PDMS encapsulation layer. The PEDOT:PSS formulation is spin-coated, and the sacrificial parylene layer is removed to pattern the active area. The resulting device is a fully stretchable OECT including metallic lines, PEDOT:PSS and PDMS

A schematic of the fabrication process is depicted in Figure 46, where Pa-C was used as a sacrificial layer and support for the photolithography process.

1- Rather than using Pa-C as a second layer for the insulator which is not stretchable, a thin (8µm) PDMS spin-coated layer was used by mixing PDMS with hexane (1:1 in mass). The choice of 8µm of PDMS as an encapsulation layer is enough to ensure at least 50% of strain without delamination of the line. With 1-2µm of PDMS, it quickly led to the break of the encapsulation layer and to the delamination of the lines. With 8µm of PDMS, the failure of the device was observed before this effect occurred. With thicker layer, it was too long to open the channel at the etching step presented further. Instead of using pure aluminium for the interconnections, the aluminium was first covered with 100nm of gold to ensure superior electrical connection and biocompatibility. The aluminium has indeed a thin layer of oxide that induces a resistance between the PEDOT:PSS and the aluminium.
2- The encapsulated line was coated with a soap solution acting as an anti-adhesive. Next, a 4µm Pa-C layer was deposited and patterned by photolithography and plasma etching with an opening at the contact pads and in the channel. The PDMS encapsulation layer was first etched with a mixture of O_2 and SF_6[137], [138] and the Pa-C layer was then etched with a mixture of O_2 and CHF_3[124] to open the connections on the pads and on the channel. The PEDOT:PSS mixture was spin coated, and the sacrificial Pa-C layer was subsequently completely peeled-off from the PDMS device. The etching was highly exothermic, making the photoresist more brittle and the process of peel-off more difficult. The thickness of parylene was increased from 2µm to 4µm to make it more rigid and thus easier to remove.
3- The thickest layer (24µm) of AZ 9260 available on the supplier website was used, with two steps:

- Spin coating at 2400rpm for 60sec and baking 110°C for 80sec
- Spin coating at 2100rpm for 60sec and baking at 110°C for 160sec

Otherwise, the thickness of photoresist was too thin to etch the PDMS completely

4- For the etching of PDMS, a plasma of O_2 and SF_6 was used at a ratio 1:4 as described in the literature[137], [138]. 100sccm of SF_6 and 25sccm of O_2 at 70mTorr at 300W were used, corresponding to the maximum power pressure and flow of SF_6 allowed by the tool. The etch rate was around 0.35µm/min but was not entirely linear because of the heat created during the process. For a layer of 8µm PDMS, it needed around 20 minutes to be etched. The first device that as etched at room temperature needed 25 minutes to be etched, while even if the machine had a chiller, the temperature could go up to 30-40°C for the next ones and increased the etch rate.
5- The spin coating step was similar than for the rigid OECT, but the solution with 20% Capstone was used.
6- The peel-off was the same than for the standard OECT; a tape was used to remove the parylene layer and only leave the PEDOT PSS on the channel and the pads.

This process used the interconnections presented in chapter 2, but the integration of a transistor needs a modification of the device. The interconnections were cut in the middle to implement the channel made of PEDOT:PSS.

3.4.4. Transistor channel integration

Low resistance interconnections with high stretchability have been developed. The objective was to integrate an OECT with these lines. The strategy was to cut by laser the line in the middle to create a channel with the desired length. There was a major problem limiting the stretchability of the device, illustrated in Figure 47. When stretched, the PDMS and the interconnection were not elongated in the same way. The line was pulled back, leading to an empty gap even for strain inferior to 10%. Thus, it created an area where the PEDOT, which was on top of both materials, was highly stretched and then broke.

Figure 47 illustrates the various geometries of the channel tested to limit this effect:

a- The line for the channel was cut perpendicular to the direction of the stretch and called horizontal channel. The channel was pulled by the serpentine, and there was a failure.

b- The line was also cut perpendicular, but a long straight line was used after the end of the horseshoe to counter the pulling of the deformed horseshoe. It also showed a premature failure.

c- The channel was ended with a triangular shape, to prevent the displacement of the interconnections inside the PDMS. The channel was less affected by the strain; however, the gap was still observed.

d- The channel was cut parallel to the strain. This strategy has reduced the horizontal displacement of the line inside the PDMS. A small rotation of the line upon stretching was observed alongside with the apparition of cracks. However, they did not appear in the sensing area, in between the lines. Then, it did not impact the performance of the device.

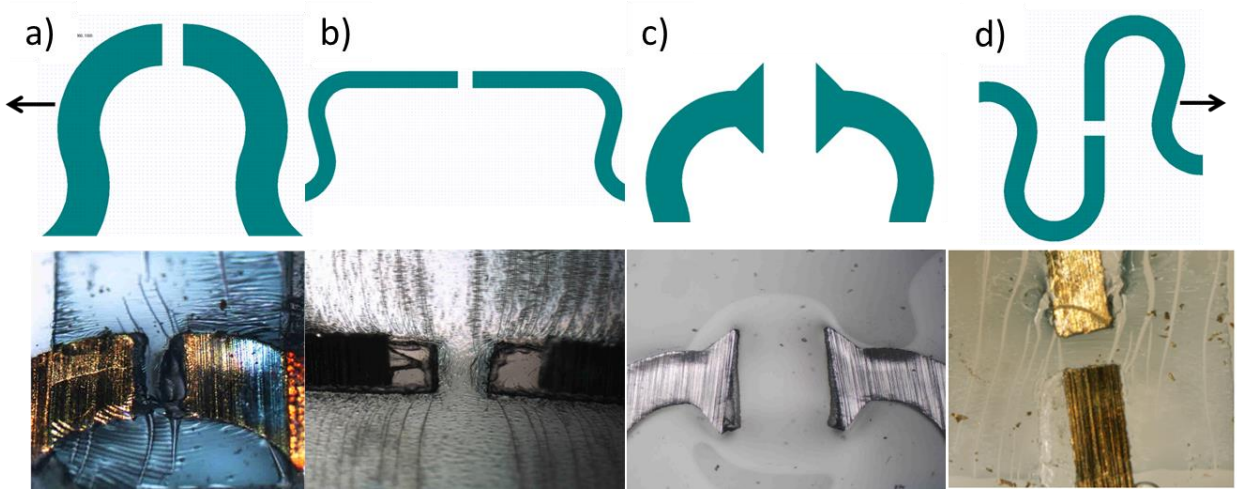

Figure 47: different configurations for the channel: a) horizontal channel 15% strain, b) long and straight horizontal channel 30% strain, c) triangular ended horizontal channel 15% strain, and d) vertical channel 30% strain. The arrows represent the directions of the stretch. Scale bar is 400µm.

This mismatch is a big problem when using materials with such a big difference in Young Modulus. With the same force applied, the resulting strain in the material is completely different, leading to incompatible movements and mechanical failure. To force the line to move with the PDSM substrate, (3-Mercaptopropyl)trimethoxysilane (MPTMS) was tested. It bonds Si groups to metal atoms[139]. However, it resulted in the same failure, probably because the force of deformation was too strong.

The resulting design kept for the channel was then vertical channel, and the final device is displayed in Figure 48. The channel was designed perpendicular to the strain direction to minimise the extension of its length during the strain.

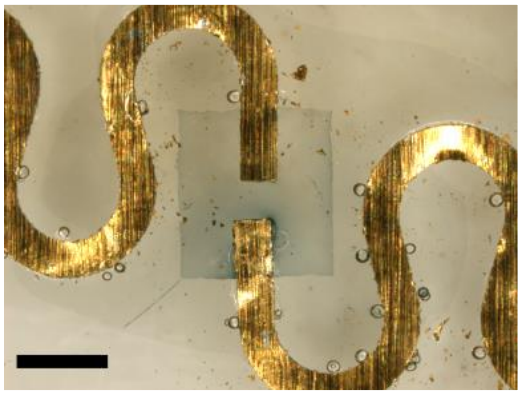

Figure 48: Zoom of the final device on the channel. In blue, the PEDOT, patterned by photolithography in a square shape. The size of the square is voluntarily very large compared to the channel size, to see more easily later the effect of the stretch on the PEDOT:PSS. Scale bar is 500µm.

3.4.5. Characterisation of the stretchable OECT

With these optimised metallic interconnections and PEDOT:PSS formulation designed for improved stretchability, a stretchable OECT was fabricated. A picture of a device under test is available in Figure 49.

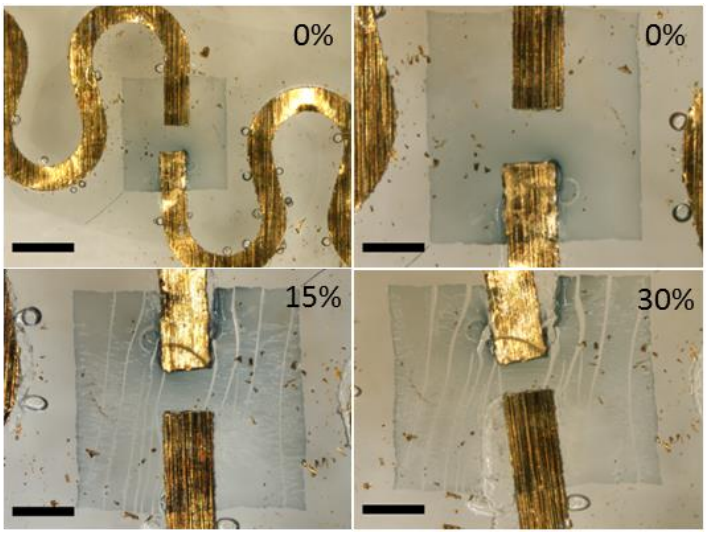

Figure 49: Picture of the channel at the end of the process for different strains. For the 0 % strain picture and 500µm for the others. Some cracks are appearing in the active area, but the channel zone is not affected. Scale bar is 1mm

A diminution of the channel length in 2D was observed due to the compression of PDMS on the side. Some cracks are appearing, but only out of the channel, keeping its integrity and so, its ability to successfully conduct current.

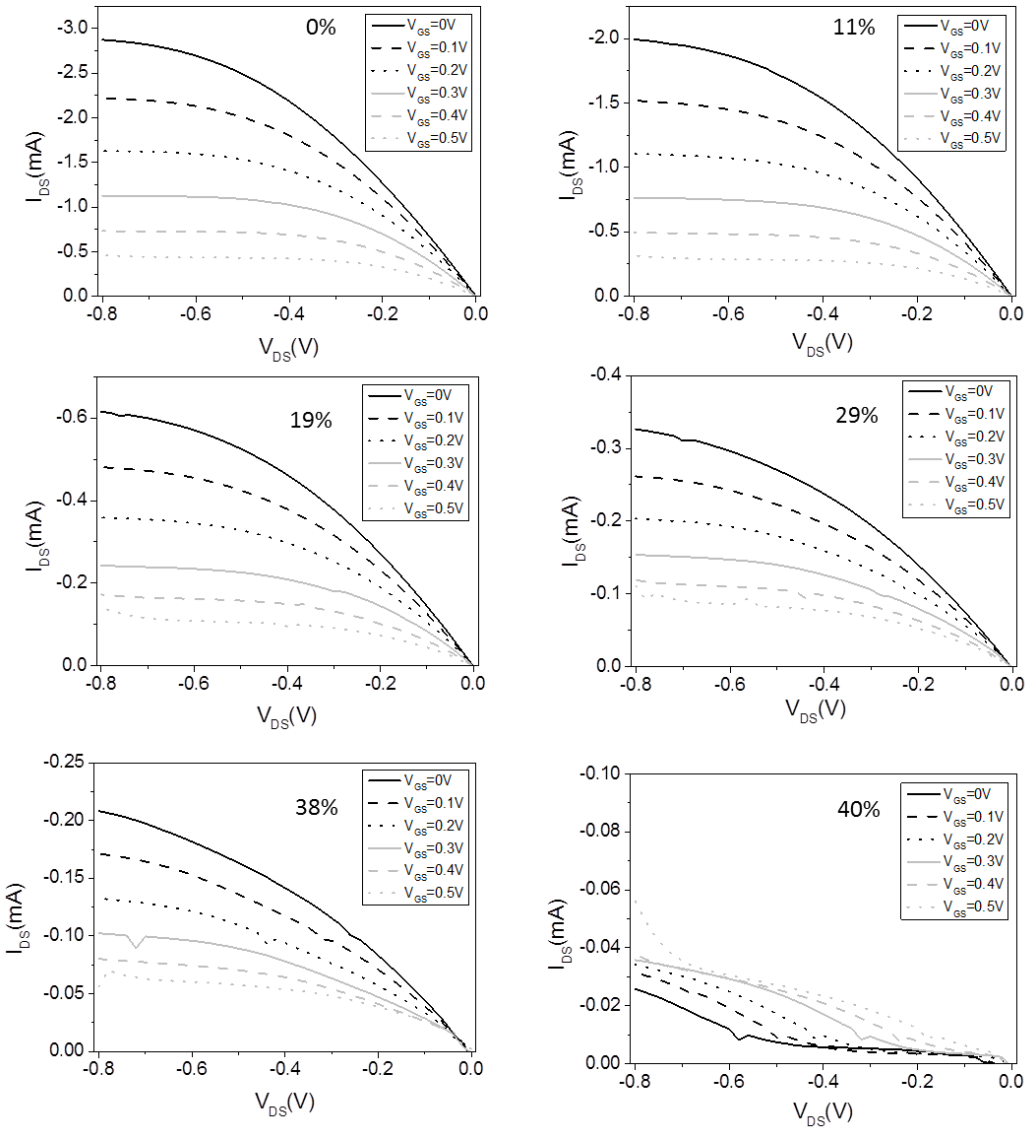

Figure 50: Output curves of the device with VGS varying from 0V to 0.5 for different strains. The OECT had initially a channel length of 250µm and a thickness of 300nm with an external Ag/AgCl gate. The device clearly displays transistor behaviour showing high current even at 38%. Nevertheless, the current has decreased by a factor 7.

A typical output characteristics from an OECT for different strains is presented in Figure 50, with a drain-to-source voltage (V_{DS}) swept from 0 to -0.8V, for a gate-to-source voltage (V_{GS}) ranging in magnitude from 0 to 0.5V in 0.1V increments. The length of the OECT channel was initially 250µm, the contact lines are 400µm wide, and the total device thickness was 300µm. For the best transistor, a maximum drain current magnitude around 2.8mA was obtained. The current

decreased while stretching, transistor behaviour with a current magnitude of 0.2mA was still observed until 38% strain.

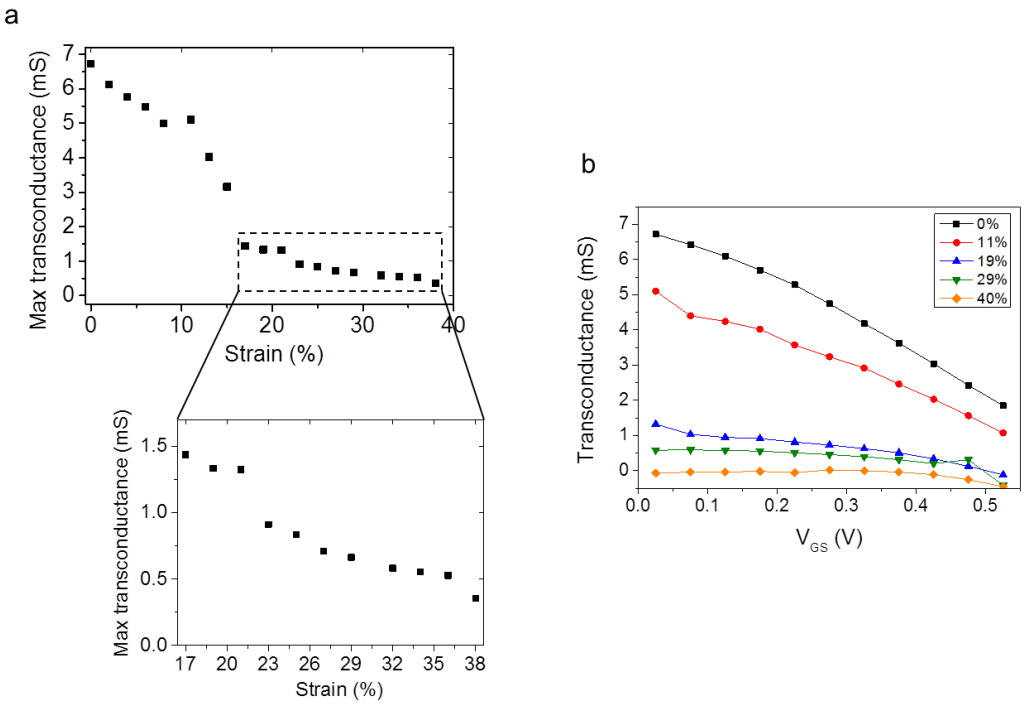

Figure 51: a) The maximum transconductance as a function of the strain extracted from the IV curves of the best performing device with an initial transconductance around 6.5mS at 0% strain. There was a noticeable reduction in the performance after 11% strain. Focussing on the zoom part in the graph of Figure c, for strains between 17% and 38%, the transconductance was diminishing slowly from 1.5mS to 0.35mS. After this value, it was not possible to record a proper output curve and therefore extract the transconductance. b) Transconductance as a function of V_{GS} associated with the output curves Figure 50. The maximum transconductance can reasonably be associated with the point between V_{GS} = 0V and V_{GS} = 0.05V.

The maximum transconductance associated with the output curves for each strain applied is displayed in Figure 51a. On this graph, only the maximum transconductance is displayed, which in our case, corresponded to the gain between a gate voltage magnitude of 0V and 0.05V as displayed in Figure 51b.

In Figure 51a, a slight decrease was observed down to 5mS at an elongation of 11%, after which, there was a significant drop between 11% and 17% where the transconductance felt to 1.5mS, and finally a slow decrease to 0.35mS until 38% elongation.

The maximum transconductance of 6.5mS was comparable to rigid based OECTs fabricated on glass[116]. The drop in OECT performance after 11% strain has been observed previously. For strain higher than 10%, cracks started to appear in the PEDOT:PSS films and so, it is fair to assume that the elastic limit has been reached, thereby entering the plastic region[133]. This deterioration in performance was not seen in Figure 44b, where the PEDOT:PSS mixture film resistance was fairly stable and lower than 1kΩ until 40% strain. As a result, the drastic reduction of transconductance can be attributed to the interface between the PEDOT:PSS layer and the metal. Since these two materials had different mechanical properties (Young's Modulus), there was an accumulation of stress at this interface which was detrimental to the overall performance of the OECT.

Many devices were displaying the same performance than the one presented previously. However and as seen in Figure 52, performances could drop faster. The initial IV was showing good results initially, and the maximum transconductance dropped linearly with the strain until around 20%. Then, it decreased suddenly, and it was not possible to extract any transconductance from the output curve. The main hypothesis is that between 15% and 20%, many cracks were appearing in the PEDOT:PSS layer, and sometimes, there could be some defects that lead to the apparition of cracks within the channel. This could be confirmed by coupling these electrical measurements with microscopy techniques on top of the tensile table.

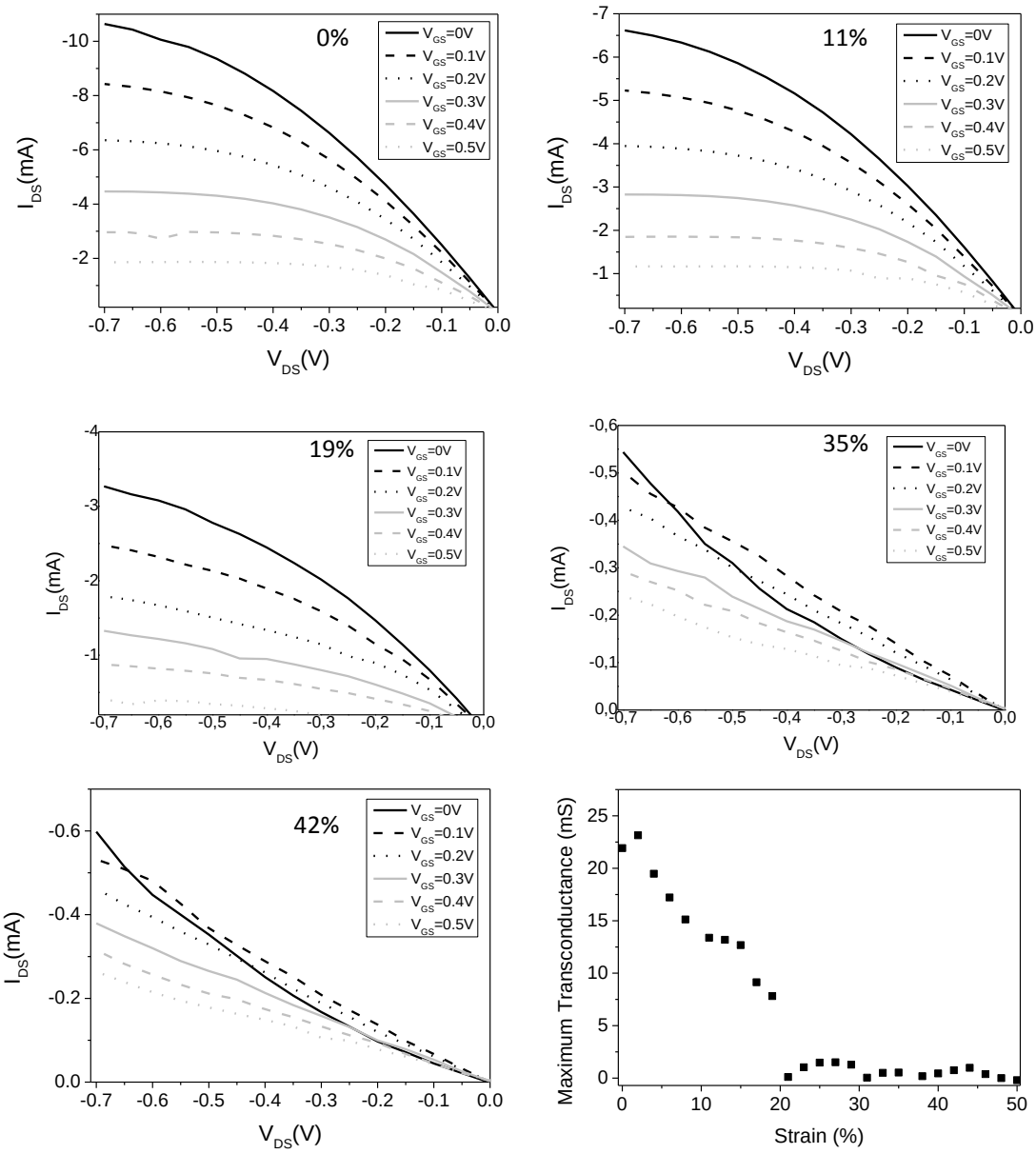

Figure 52: Output curves for a device featuring a channel length of 250µm and a 500nm-thick layer of PEDOT:PSS. The device showed good performance until 19% strain and then suddenly dropped. The first measurement with V_{GS}=0V was completely different from the other datasets, resulting in negative transconductance in some cases. The other curves are still showing transistor behaviour. The transconductance plot has been extracted from V_{GS}=0V and V_{GS}=0.05V.

3.5. Conclusion on the stretchable OECT

A process to pattern a stretchable electrochemical transistor has been developed. By taking advantage of the interconnections, the process is based on the lift-off of a sacrificial Parylene-C layer by replacing non-stretchable materials with PDMS, patterned by photolithography and dry etching. This process is a proof of the compatibility of the devices and tools presented with standard microfabrication techniques; it avoids any pre-strain step and contains only stretchable materials.

The resulting device displays similar performance than a standard OECT until 11% strain, with good transconductance and output characteristics until 38%. However, due to the mechanical properties mismatch between the rigid interconnections and the PDMS, the integration of thin layer polymer (PEDOT:PSS) at the interface is damaged during elongation. This limitation has been countered by an appropriate design, but there is still a drop of performance after 11% strain while the PEDOT:PSS has shown more stretchability.

Fully stretchable sensors in this configuration are more adapted with thin layer interconnections, following the elongation of the substrate. Thus, some modifications could be brought to improve the stretchability of the device:

- Re-design the structure of the device entirely to avoid this mismatch and maybe limit the displacement of the PDMS to the vicinity of the interconnections.
- Work on the transition from the interconnections to the PDMS, using glue. This glue would stick the interconnections to the PDMS.
- Use a substrate with a gradient of Young modulus, rigid in the polymeric active area and stretchable in the interconnections. It would mimic the bridge-island structure

4. Development of a stretchable IR sensor

An objective of an e-skin in prosthetics is to reproduce the capabilities of the skin on a robotic arm for instance. The use of pressure sensors for giving the feeling of touch is an active topic of research, and the transmission of the response of the sensors to the brain has been intensively studied[140]. The topic of this chapter deals with the integration of the feeling of temperature and especially for the detection of non-contact heat sources. Thus, it would be possible to detect the temperature before being too close from the object and injuring the artificial skin. The objective of this chapter is to develop infrared sensors with more than 30% stretchability.

A review of the temperature sensors has identified the pyroelectric materials as an adequate choice for the e-skin application. The PVDF is a polymeric material presenting these properties. It possesses the particularity of inducing an electrical field with a change of temperature that disappears when the temperature is kept stable. To avoid the mismatch of Young Modulus within the material, a rigid-island strategy is adopted, and the process is adapted in consequence. Then, methods for the characterisation of the devices are explained. Finally, various characteristics of the device are presented:

- The direct temperature sensing through the measurement of its capacitance
- The dynamic sensing of temperature change by the measurement of induced voltage
- The response to infrared illumination
- The properties under strain

Section 4.1 introduces the different method for temperature sensing and justifies the choice of pyroelectric measurement and the use of poly[(vinylidenefluoride-co-trifluoroethylene] (PVDF-TrFE) as an active material for the sensor.

Section 4.2 presents the design of the sensor and particularly, the choice of the rigid-island method for this sensor.

Section 4.3 is dedicated to the presentation of the methods used for the characterisation of the device.

Section 4.4 presents the characterisation of the device.

Section 4.5 concludes on the results presented and details the advantages of the use of the interconnections developed for this sensor.

4.1. Overview of devices and material for IR sensing

In this section, the different methods for thermal sensing are introduced. The pyroelectric materials, as a choice for the sensor, are presented, and their potential for the e-skin is explained.

4.1.1. Different types of thermal sensors

A classic thermal infrared sensor is constructed around the absorption of a black body material on a thermal sensor. The material absorbs the infrared radiation and produces heat. This heat source is placed on a heat-sensitive material, with different properties depending on its temperature. There are several types of sensors generally used for temperature measurement.

- The thermocouple lies on the Seebeck effect. A junction of two different metals exposed at a hot temperature creates a difference of potential between the two metals placed at a known cold temperature. This voltage is related to the temperature difference. It is also possible to make a thermopile, a device that comprises multiple small thermocouples in series for a higher output voltage, thus, a higher sensitivity.
- The resistance temperature detector (RTD) is based on materials which have a predictable change in resistance depending on the temperature. These materials are mostly metals such as platinum or copper.

- Thermistors are made out of ceramic semiconducting materials. One type is negative temperature coefficient (NTC) thermistors; they are semiconducting materials with metal oxides mixture. When the temperature increased, the electrons can move more easily from the valence band to the conduction band, decreasing its overall resistance. Others are positive temperature coefficient (PTC) materials and possess a brutal rise in resistance in a certain range temperature
- Some temperature sensors can exploit the properties of semiconductor junctions to determine the temperature. When passing a constant current through the junction, the resulting voltage is a linear function of the temperature
- The pyroelectric detectors are based on a pyroelectric material that can generate a voltage when there is a change of temperature. Compared to other material, these detectors do not need to be powered. The response delivers directly a voltage that is conveniently measured.

The temperature detection techniques based on the use of very rigid metals or semiconductors might be difficult to use for making devices stretchable; while some polymeric pyroelectric materials are available, giving more flexibility for mechanical properties and for processing. The detection of temperature induced in pyroelectric materials is due to its particular crystal organisation.

4.1.2. Piezoelectric and pyroelectric materials

Piezoelectricity is the capacity of a material to turn mechanical stresses such as sound waves, touch or vibrations into an electrical field. Crystals that exhibit natural crystalline structure with centrosymmetry usually show piezoelectricity effect. At the molecular level, the symmetry provides stability and electrical neutrality. When atoms are not symmetric within the unit cell, due to the distribution of the electrons, the structure exhibits a natural dipole at least in a single cell[141]. If the distribution of the dipoles is random, the crystal does not naturally show piezoelectric properties. It needs a specific process step of “poling” to align the dipoles. It is

possible to stretch it or to apply a high electrical field to force the polarisation. Once the polarisation is done, some materials, so-called ferroelectric can retain the polarisation before Curie temperature. For other materials, the stress is kept to maintain the dipoles oriented.

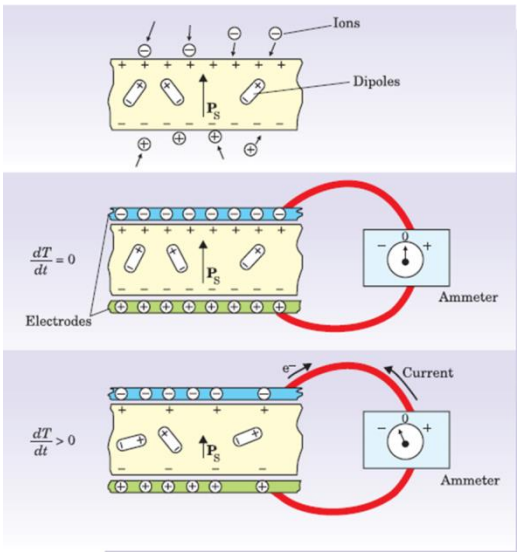

Figure 53: Mechanism of pyroelectricity. Due to the relaxation of the global dipolar moment Ps, a voltage is induced to keep the neutrality of the device through the relaxation of the charges at the interface of the material. Reproduced from [142].

Some of these piezoelectric materials also exhibit pyroelectric properties. The material contains the preferentially oriented dipoles at a stable state at a certain temperature. Figure 53 illustrates the mechanism of the creation of voltage by pyroelectricity. Initially, in between two electrodes, the device is stable, and the potential between two electrodes is 0. When a change of temperature appears, a voltage is induced through the electrodes[143]. This voltage is transient and created due to the change of charges at the interface of the material for a dipolar state. When the dipolar moment is changing through temperature or pressure on the material, the global neutrality is not the same, leading to a movement within the charges on the surface. To keep the neutrality at the interface of the electrodes, electrons are moving from one electrode to the other one. Once the temperature stable, the device is stable again, and no voltage is induced.

This device has the advantage of being very sensitive to the change in temperature, and a simple measure of the voltage can be performed. However, the voltage induced is not permanent. So, dynamic measurement is essential to measure the change of temperature. However, the dipolar moment of the device is closely related to the change of temperature. So, a direct determination of the temperature can be made by measuring the dipolar moments.

The PVDF is the most used polymer for its pyroelectric properties.

4.1.3. PVDF as pyroelectric material

In this work, the copolymer PVDF-TrFE was used as a pyroelectric material. The PVDF and its copolymers are widely used due to their mechanical flexibility, low temperature of crystallisation, ferroelectric and piezoelectric properties[144], [145]. The PVDF is also well known for its strong piezoelectric responsivity, first reported by Kawai *et al.*[146].

The PVDF and its copolymers can present four different crystalline phases[147], [148]:

- The α phase, obtained with the crystallisation from the liquid state. It is a not polar phase and thus not piezoelectric.
- The β phase, the pyroelectric phase with strongest piezoelectric and pyroelectric properties, obtained from stretching α-phased PVDF or at crystallisation at high pressure and temperature.
- The γ phase, obtained by addition of a polar solvent or by baking PVDF from the α phase at high temperature.
- The δ phase, made by electrical or mechanical poling of the α phase.

The PVDF is a semi-crystalline polymer. As described before, the crystallised phases presented previously are surrounded by amorphous polymer phases[149]. The β phase has the highest alignment of hydrogen and fluor and thus, the strongest dipolar moment. However, the alignment between the chains is random, so the global dipolar moment is neutral.

Depending on the process used for the deposition of the PVDF, the crystallisation leads to different structures, but only one presents the crystalline structure suitable for pyroelectric properties (β-phase)[141]. Nevertheless, the PVDF does not crystallise naturally in the good phase; it needs to be annealed and/or stretched[147]. In order to allow the direct crystallisation of the β-phase from the solvated state, it is possible to use PVDF-TrFE copolymers[141], [150]. Once it has crystallised, it is possible to pole the copolymer layer in order to create the pyroelectric properties by applying a high electric field across the layer[141], [151], [152].

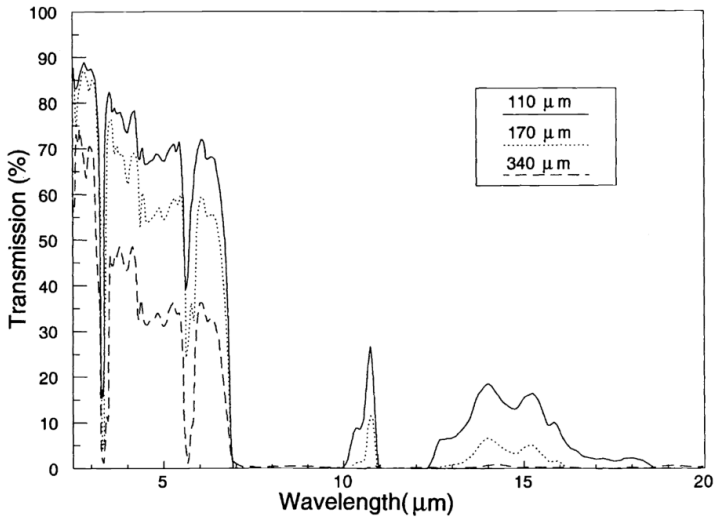

Figure 54: Absorption spectrum of PVDF-TrFE for different thickness. There is a strong absorption after 7μm. Reproduced from [153].

In addition, the absorption spectrum of this material shows a high absorption for wavelength after 7μm[153]. From Wien's displacement law, the maximum of emission matches with temperatures below 140°C. Previous work has shown the feasibility of IR sensor with PVDF in far infrared[153], [154]. Pecora *et al.* have also shown the operation of a flexible PVDF-TrFE pyroelectric sensor under absorption of a specific radiation[155] and Graz *et al.* have done a flexible sensor based on the absorption of PVDF in far-infrared to detect the approach of a human finger[25].

So the PVDF is well adapted for detection of human body for example[156], dealing with low temperature and low emission. The aim of the e-skin is to detect high-temperature surfaces before touching it. Thus, a layer absorbing higher temperature radiations and then lower wavelength is more appropriate. For the detection of far infrared radiations, one solution is to use special conditions of evaporation to deposit porous gold as known as black-gold[157], [158]. For near-infrared, another solution is to use an electrode that has absorption properties in the desired wavelength band: below 7µm.

4.1.4. Potential in infrared sensing for e-skin

An easy way for making infrared sensor includes the deposition of an absorbing infrared layer on top of a temperature sensor. The absorption in the layer creates a local increase of the heat that is sensed by the thermal sensor. The sensor is easy to fabricate, but, it is not possible to distinguish an infrared radiation from the effect of the outside temperature. The calculation of the temperature from an infrared radiation needs a constant temperature, with a proper calibration. The measurement takes advantage of the difference of power emitted, illustrated by Figure 18 from chapter 1. The power emitted increases with the temperature. Moreover, the exact calculation of the temperature depends on the material. The emissivity of the surface has to be taken into account. The human skin has the same problem; the determination of the exact temperature is not possible. However, by approaching the hand from a hot surface, it is possible to feel the heat and determine if the temperature is higher than the ambient.

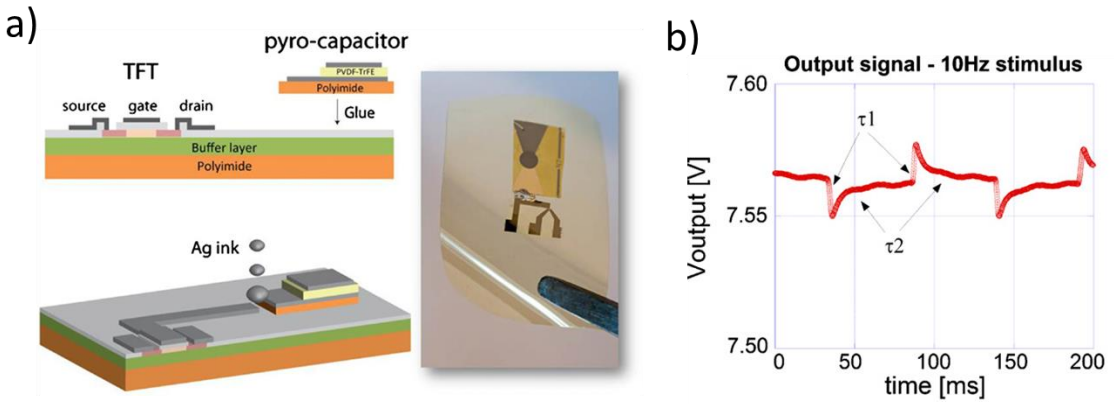

Figure 55: A flexible pyroelectric infrared sensor. a) Design of the device and b) Output curve to a laser of 5mW at 632nm. Reproduced from [155].

Stretchable and flexible infrared sensors in e-skin are still marginal. The only mention in the literature is from Lumelski *et al.* They developed a flexible e-skin based on infrared LED coupled with a detector for proximity detection based on the reflection of the LED, capable of sensing an object up to 20cm. This work is less interesting for pure infrared sensing. As mentioned before, people have already done flexible temperature and visible radiation temperature sensor with PVDF-TrFE [25], [155], but not stretchable. An example of a flexible temperature sensor by Pecora *et al.* is displayed Figure 55[155]. In Figure 55a, the device is made out of a printed transistor connected to the pyroelectric capacitor. The device shows a voltage induced by a temperature change. The measurement of the device under illumination of 5mW of a laser at a wavelength of 632nm is displayed in Figure 55b. The device shows only a low response of about 1mV under illumination. This is probably because the silver layer reflects the signal partially and the PVDF-TrFE absorption at this wavelength is particularly low.

The sensor designed during this thesis intends to replace the top electrode by using an absorbing and conducting material. The absorption of the sensor aimed to be in the near infrared, to ensure sensing of temperature near 100°C.

4.2. Design and fabrication of the sensor

This section presents the design of the sensor. The device was based on the blocks developed in the previous chapters.

Contrary to the design of the OECT, which had the PEDOT:PSS deposited on the device for a fully stretchable device, the IR sensor take the full advantage of the rigid metallic interconnections by using the rigid-island approach. A schematic of the device is displayed in Figure 56. The interconnections were connected in the middle to a round-shape island of 5mm diameter and on the other side to a pad used to take the signal. The PVDF-TrFE was deposited, constituting the bottom electrode. The top electrode, made of stretchable PEDOT:PSS took the signal and also provided the stretchability between the active area and the other part of the interconnection carrying the signal from the top electrode.

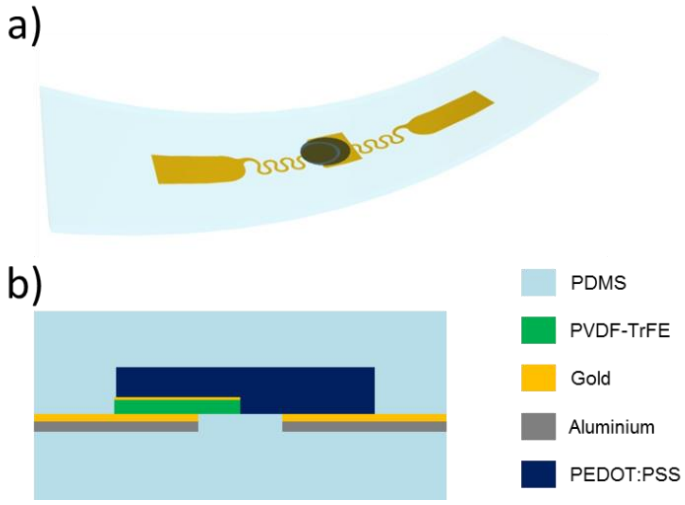

Figure 56: Schematics of the temperature sensor device. a) 3D view of the device. In the middle, the active area of the sensor and on the sides, the pads are collecting the measured signal. They were linked with stretchable gold interconnections. b) Side view of the stack, the layer of PVDF was sandwiched between two gold electrodes, and the top electrode was covered with PEDOT:PSS to ensure stretchability.

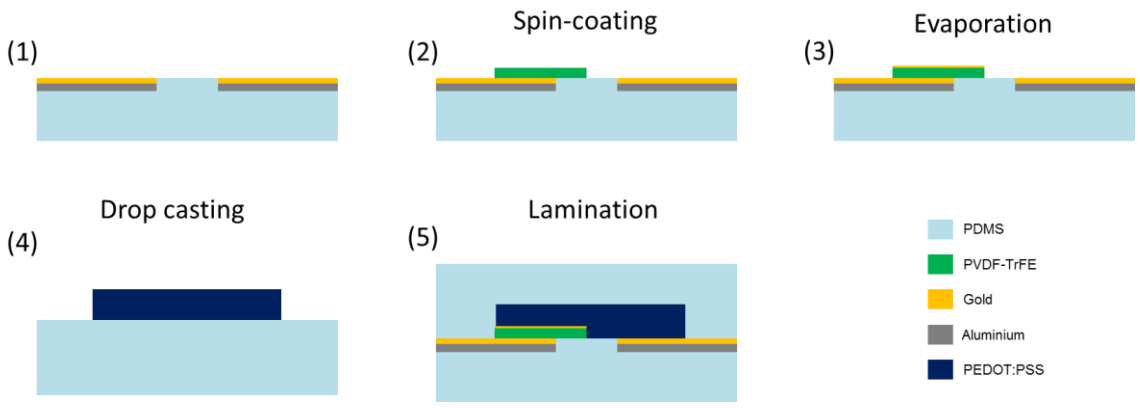

Figure 57: Fabrication process of the IR sensor. The PVDF-TrFE was spin-coated, and a layer of gold was evaporated through a shadow mask. The PEDOT:PSS was drop-casted on a PDMS empty substrate and laminated on top of the device.

A schematic of the fabrication of the device is depicted in Figure 57:

1- The interconnections of chapter 2 were not encapsulated directly with PDMS
2- The PVDF-TrFE was spin-coated at 1500rpm, from a solution of 10% in Methyl Ethyl Ketone for a thickness of 3µm through a Kapton mask. The device was then annealed at 150°C for 30 minutes
3- 100nm of gold was evaporated on top of the PVDF-TrFE through a shadow to get a proper electrical contact when the top PEDOT:PSS electrode was laminated on top
4- The formulation from chapter 3 of PEDOT:PSS was drop-casted on an empty PDMS substrate after plasma treatment (25W, no gas) and was baked at 110°C for 1h.
5- This PEDOT:PSS on PDMS is laminated after plasma treatment (25W, no gas) to ensure sealing of the device. The PEDOT:PSS was not spin coated directly on the substrate because the subsequent device was conductive, so no measurement of capacitance would have been possible due to short-cut.

4.3. Methodology of characterisation

The real-time measurement of the capacitance was done with an Agilent 4263B LCR meter, calibrated with a 47pF capacitance. The system is highly resistive, so the capacitance was extracted by measuring the parallel capacitance.

The real-time measurement of the temperature was done by placing a KTY81-210 silicone temperature sensor on the device. The resistance of the sensor was related to the temperature with a homemade Matlab program by interpolation of the calibrated values from the datasheet.

For real-time measurement of the temperature, the heat source was an electronic heat gun with an adjustable and controllable temperature. The output was set up at 80°C and placed in the direction of the sample at 10cm. For static measurement of the capacitance as a function of the temperature, a hot plate was used, and the corresponding temperature was taken from the temperature sensor after 5 minutes stabilisation required for the hotplate to have a stable temperature.

The real-time measurement of the voltage was done by using a Keithley 2636A Source unit connected to both electrodes without applied current.

Stretching measurement was done by using the tensile table coupled with the above-mentioned methods and equipment.

4.4. Sensor characterisation under temperature change and under IR illumination

This section presents the characterisation of the device through different measurements:

- Direct temperature sensing through the measurement of its capacitance
- Sensing of temperature change by direct voltage measurement induced after poling
- The voltage response of the poled device under infrared illumination
- The properties under strain

The device shows two modes of operation:

- By measuring the capacitance, it is possible to determine the temperature directly. It just needs a proper calibration. The device can be poled, or not.
- By poling the device, it is possible to detect a change of temperature. Through the relaxation of dipoles, a voltage is induced when the temperature changes. This voltage is only a temporary response and cannot give an absolute value of the temperature.

4.4.1. Device characterisation under temperature change through capacitance measurement

Figure 58a presents a graph of the capacitance and the temperature as a function of time for one device. The change of capacitance followed closely the change of temperature from the temperature sensor which validates the temperature sensing through the capacitance measurement.

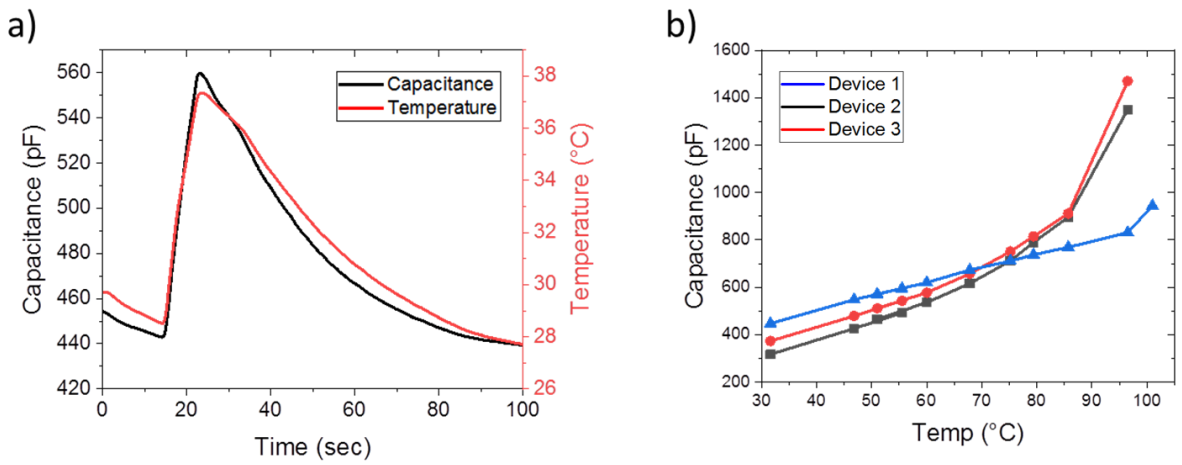

Figure 58: Electrical characterisation of the sensor with a temperature change. a) Capacitance change regarding the temperature change of the device b) Capacitance as a function of the temperature for 3 devices. There was a linear response within a range of temperature.

The capacitance as a function of the temperature from ambient temperature to 100°C is displayed in Figure 58b. The device showed a very linear response to a temperature below 60°C with a sensitivity of 7.2pF/°C for the device 3 and 7.71pF/°C for the device 2. Then above 60°C, the capacitance started to deviate from the trend and the above 100°C the capacitance was not measurable. The device 1 showed a higher initial capacitance, but a sensitivity of 5.95pF/°C. It was lower than for the other devices, but the linear range was broader: between 30°C and 90°C. So without poling, it was possible to use the device as a temperature sensor by measuring its capacitance.

4.4.2. Device characterisation under temperature change through voltage measurement after poling

The device showed a linear response to temperature change without poling through the measurement of the capacitance. However, pyroelectric materials are mostly used for their ability to sense a change in temperature, and not absolute temperature, by poling the device[159]. Moreover, the measurement of the capacitance is not direct; it requires a complicated circuit to extract the value. After poling of the device, the measurement of a voltage is less invasive and does not need a complicated setup.

The device was poled with an aluminium electrode laminated on top. The setup was provided by the company IRLYNX and made out of a sinusoidal generator with an amplifier. The devices were poled at 700Vpp with 10 periods of a signal at a frequency of 0.5Hz. This voltage was the limit for the poling of the device. Higher voltage resulted in the burning of the device.

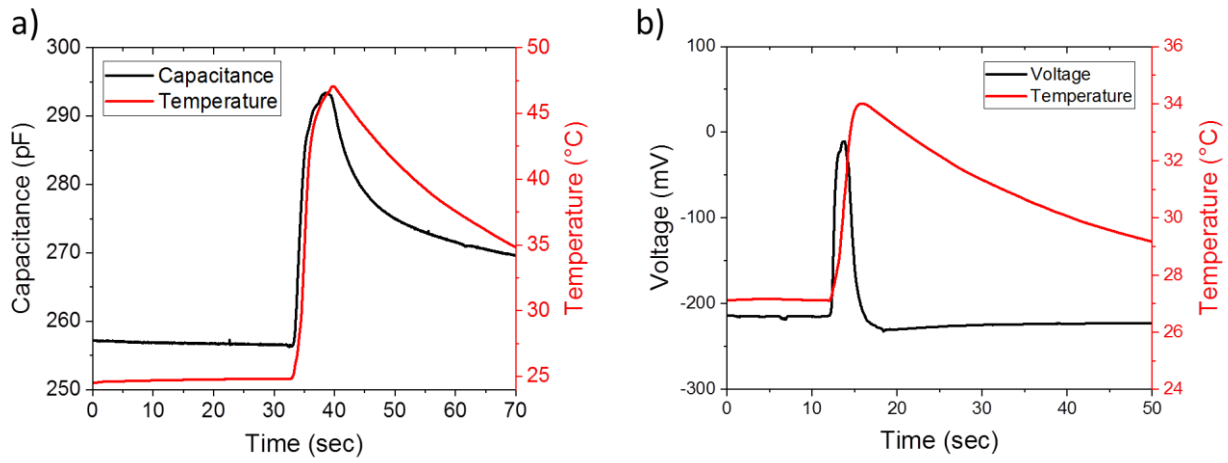

Figure 59: Characterisation of a device after poling. a) Change of the capacitance and b) voltage generated due to the change of temperature, the baseline was at -200mV and was brought to 0. The change of capacitance was less important than before poling. However, when the temperature was increased, there was a voltage created contrary to without poling

Figure 59 presents the graphs of the characterisation after the poling of the device. Figure 59a shows the change in capacitance as a function of the temperature. The sensitivity of the

capacitance has decreased to reach 1.6pF/°C. The voltage created due to the poling is displayed in Figure 59b, called pyroelectricity. The voltage sensed through the electrodes was stable, and a peak of 200mV was measured when the temperature was increased by 7°C by the heat gun. This voltage represented the derivative of the temperature change. From the baseline, the voltage increased when the temperature was going higher and decreases when the temperature was decreasing. During the cooling, the voltage was slightly lower than the baseline.

The device was most likely not optimally poled. First, the capacitance was expected to be higher than the initial one. Indeed, the poling orients the dipoles in the same direction, so, the capacitance should have increased. Moreover, the values of the peak of voltage induced by temperature change were lower than what was found in the literature at a similar thickness[159].

4.4.3. Voltage measurement under IR illumination

The poled device can be used for temperature sensing. For the infrared temperature sensor, the absorption of the top electrode was studied. Then, the device under illumination of IR radiation was measured.

The gold is a commonly used electrode, which shows a high electrical conductivity but presents poor IR absorption properties. Moreover, as mentioned before, the PVDF does not absorb infrared wavelength below 7µm. A replacement electrode must have absorption in the IR to absorb an IR radiation, low resistivity to carry the signal and finally, stretchability to be integrated for e-skin application. The properties of PEDOT:PSS has already shown high stretchability and conductivity. In addition, a thick layer of PEDOT:PSS (thicker than 10µm) does not transmit any radiation between 600nm and 1400nm(Figure 60a). For its properties of stretchability, the formulation of PEDOT:PSS with a fluorosurfactant described in chapter 3 was used.

The response of the sensor to the illumination under a LED at a wavelength of 830nm is displayed in Figure 60b. The intensity of the illumination was measured at 0.3mW/mm² which gives a power of 5.88mW on the 19mm² surface of the sensor. The LED was kept on for 10 seconds and then turned off. The non-poled device has not shown any voltage response to the illumination. The poled device, on the contrary, displayed a very sharp reaction. As soon as the LED was turned on, a peak of voltage was measured. The peak represented a dynamic response; it showed a rapid change of temperature. As the change of temperature was quick, it would be interesting to see if the intensity of the peak is proportional to the power sent through the LED. The peak amplitude is 13mV, which is ten times better than the flexible device reported in the literature at 632 nm for similar energy[155]. There was also the reversed peak when the LED was turned off, with an amplitude of -12mV, so almost the same magnitude. This sharp peak showed that when the LED was turned off, the dissipation was also almost instantaneous.

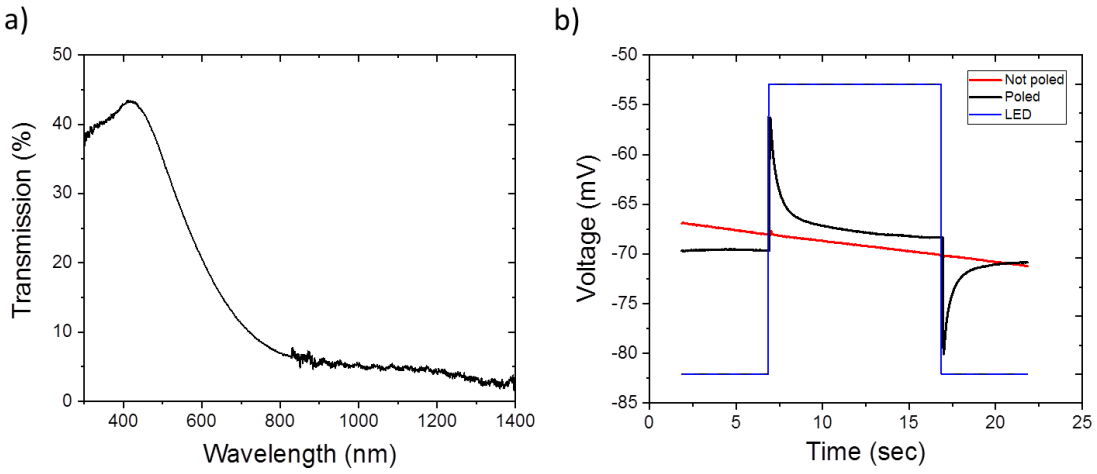

Figure 60: a) Absorption spectrum of a PEDOT:PSS thick layer. b) Device under infrared illumination at 830nm. The PEDOT:PSS absorbs the radiation, creating a local heat source that induces a voltage for a poled device. The non-poled device did not create any voltage.

So, the device showed satisfying sensitivity to a LED lighting, but still, need to be close enough to get a sufficient energy. Some optimisations are still possible: the use of an infrared dye inside the PEDOT:PSS for the top electrode has already shown similar results. The PEDOT:PSS is not a strong IR absorber. Then, the electrode needs to have a sufficient thickness to show good

absorption, and the heat is dissipated through the whole electrode. The use of a dye would allow the top electrode to be thinner. Then, the heat would be more concentrated and closer to the active material. Moreover, with a better poling, an increase in the sensitivity by a factor 10 could be expected.

4.4.4. Characterisation under stretching

The pyroelectricity generated of a poled device from 0% to 10% is shown in Figure 61. When stretched, the device displayed a very important noise, with an amplitude of 50mV. This noise was then too high to measure any change of temperature and was even worst for infrared sensing, having a lower response. However, once the device went back to 0% strain, the voltage went back to normal. This might be improved by a better poling of the device, but needs to be investigated. Therefore, further characterisation of the non-poled device under strain was carried out.

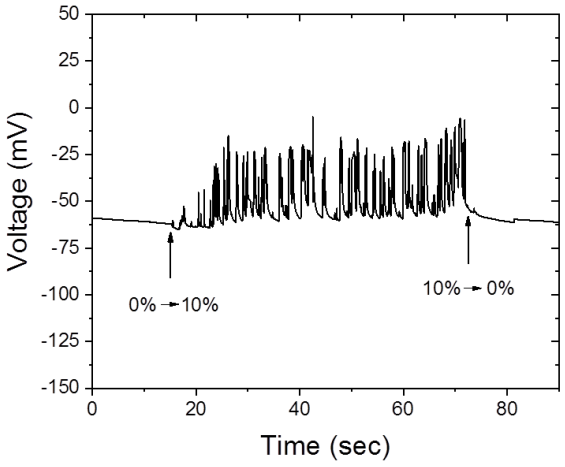

Figure 61: Pyroelectric response of a poled device to the stretch, the voltage was measured on the device from 0% to 10% stretch.

Characterisation of the capacitance as a function of the temperature (non-poled devices) is displayed at different strains in Figure 62. The device had the same behaviour with temperature change at 0% stretch (Figure 62a) and 35% (Figure 62b). It means that the change of resistance due to the stretch of PEDOT:PSS layer had no impact on the capacitance measurement.

The measurement of the capacitance of a non-poled device at the ambient temperature as a function of the deformation is displayed in Figure 62c. The capacitance decreased by only 3% between 0 and 35% strain. Then, it decreased from 430pF to 400pF between 35% and 40%. Further measurement of the capacitance after 40% was then impossible to read because of rupture of PEDOT:PSS after 40%.

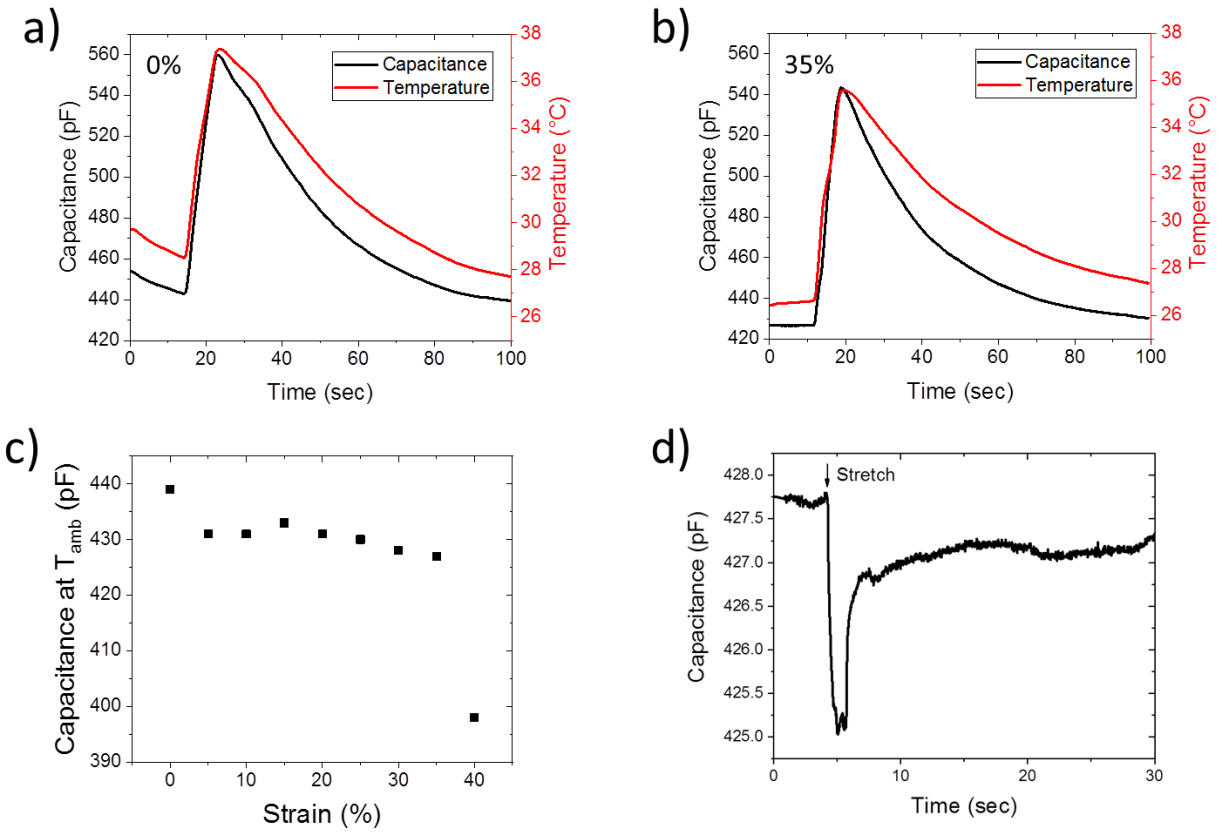

Figure 62: Stretching of a non-poled device for temperature sensing. a,b) Response of the sensor to an increase of temperature at 0 and 35%. c) Capacitance at ambient temperature as a function of the strain. The device did not show a significant change in the response until 35%. Then, there was a drop in the capacitance which decreased the sensitivity. d) Capacitance at ambient temperature of a device stretched from 25% to 35%

The graph of the change of capacitance of a non-poled device, from 25% to 35% strain at a constant temperature, is displayed in Figure 62d. There was a transient drop of 3pF capacitance when the device was stretched by 5%. This is due to the piezoelectric properties of the PVDF-TrFE. The pressure and the strain had the same effect than the temperature on its response. Then, when the displacement was finished, the capacitance almost came back to its initial value, losing 0.8pF which was equivalent to an error of around 0.5°C for this sensor. This loss could indicate an irreversible deformation.

4.5. Conclusion on the stretchable temperature sensor

The final device presented had a temperature sensing sensitivity of 7pF/°C at no strain. No change in its performance was noticed up to 35% strain. Sensing of infrared radiations was possible after poling. However, optimisation is possible to be able to measure pyroelectric voltage properly under stretch. So, the fabricated device was more adapted to temperature sensing through the measure of capacitance. This device was fully compatible with the e-skin approach. It can be integrated into a matrix and can mimic the properties of the skin.

Moreover, this chapter showed that the rigid-island approach is well adapted to the interconnections developed during this work.

5. Conclusion and outlook

The development of sensors capable of reproducing human skin capabilities is a stimulating topic of research. The integration of pressure sensors within an artificial skin has been made possible by using stretchable sensors. However, the fabrication of stretchable temperature sensors and more particularly non-contact temperature sensing has not been extensively covered.

This work presented activities on stretchable electronics. It demonstrated the development of stretchable electronics and more specifically for sensing application in e-skin. Due to the favourable mechanical flexibility and theoretical potential stretchability, the development of sensors based on organic materials was focused in this work. The stretchability targeted for applications in e-skin has been established at 30%. The aim is to get low interconnection resistance with limited variation during the stretch in order to not alter the sensor signal. The development of two stretchable sensors was presented:

- An organic electrochemical transistor, enabling the measure of physiological parameters.
- An infrared temperature sensor, enabling the measure of the temperature in a non-contact approach.

Chapter 1 presented an overview of stretchable electronics to understand the challenges; and to choose the materials and technologies for the development of stretchable interconnections. The best solution has been identified through the horseshoe-shaped metallic interconnections. No stretchability exceeding 100% has been demonstrated in the literature, but it allows low resistance and high stability while stretching. The fabrication processes are based on photolithography and were tunable to the dedicated application. For the integration of the active sensors, a classic technique – so-called island architecture - is to stiffen an area and work only on the stretchability of the interconnections. Another approach is to use intrinsically stretchable materials deposited for instance on a pre-strained substrate. This gives good stretchability but is not easily compatible with the classic techniques of microfabrication.

In chapter 2, the process and the characterisation of low resistance and stretchable interconnections patterned with a laser was detailed. The device was stretchable by 80% with an increase in resistance by 1%. This outcome represents state-of-the-art achievement. It presented comparable stretchability as already reported, but with unprecedented stable and low resistance in the milliohms range, due to the use of bare metallic foil. Moreover, the fabrication process was fast and easy to integrate into microfabrication processes. This low resistance under stretch is required for the fabrication of high-performance stretchable sensors.

In chapter 3, the development of a stretchable OECT has been demonstrated. The development of this device on a rigid substrate for wound-healing was presented in a first approach. This work was an introduction to demonstrate the sensing potential of OECTs and what are the challenges in using this device. State-of-the-art formulation and process has been optimised to make OECT stretchable. Compared to literature, the electrical performances obtained are comparable to rigid devices at no strain. The device was stretchable until 38%, but the transconductance was not firmly stable while stretching. Indeed, the fabrication of this sensor is challenging due to the heterogeneity in Young Modulus at the interface between the various materials used; for instance between rigid metal and soft polymer. A proper engineering of the transition metal/polymer has to be carried out to reduce the mechanical mismatch and get smooth transition.

In the final chapter, PVDF-TrFE was used to fabricate a stretchable temperature sensor. This infrared sensor aimed to be integrated directly in an electronic skin. This sensor showed promising results, as for instance, a 35% stretchability without any change in the performance. The interconnections developed through this thesis were adequate for the development of the IR temperature sensor. Compared to the OECT, the design of the infrared sensor appeared more adapted to the use of the bulk metal interconnections. The rigid island formed did not cause the problems of Young modulus mismatch found with the integration of the active material in between the rigid metal and the soft substrate. The rigid interconnections were stiff and perfectly adapted serving as mechanical island that carried the active materials.

The next step of this work is to integrate the sensors in a matrix to use it in the e-skin model as displayed in Figure 2. The infrared sensor can be used for pressure and temperature with also the detection of infrared. First, it is necessary to work on the dissociation of these different effects. Indeed, as a pyroelectric material, the PVDF-TrFE has also a sensitive response to pressure and strain. But, in the aim of integrating these devices with other pressure and touch sensors, it would be possible to decouple at least temperature from these effects. Indeed, the use of touch and pressure sensors stable with the temperature would allow to predict the response of the PVDF-TrFE to these stimulations. Moreover, it is also not possible to detect the infrared preferentially over the temperature response. However, a heat source at a high temperature emits a high power density of infrared radiations. Thus, the sensor would feel a strong heating. In the case of an e-skin, anyway, the skin would feel very high temperature and know there is a hazard.

The development of a stretchable infrared sensor is a crucial step of the development of the e-skin. Integration in a matrix is the next challenge. The interconnections developed in this work are stretchable in one direction, but not in the perpendicular axis. However, some works have already been done to adapt the use of the serpentines in all the directions and can be easily adapted for the present interconnections. Moreover, the design of a matrix implies a device to address each sensor, with the fabrication of stretchable thin films transistors as active matrix for example. If multiple sensing layers are used in a stack configuration with each layer addressing a specific sensing capability; recorded signal has to transmit from one layer to another through vertical interconnections in order to collect all the data. These vertical interconnections have to be developed by inserting conventional metallic wires in between layers. As an alternative, the recorded signals could be transfer by light, through stretchable waveguides to carry the information[160].

Scientific contributions

Peer-reviewed journal articles:

"Laser-patterned metallic interconnections for all stretchable organic electrochemical transistors**",** *Bastien Marchiori, Roger Delattre, Stuart Hannah, Sylvain Blayac, Marc Ramuz*

Scientific Reports, (2018), volume 8, Article number: 8477, DOI: 10.1038/s41598-018-26731-8

"Organic transistor platform with integrated microfluidics for in-line multi-parametric in vitro cell monitoring", *Vincenzo F. Curto, Bastien Marchiori, Adel Hama, Anna-Maria Pappa, Magali P. Ferro, Marcel Braendlein, Jonathan Rivnay, Michel Fiocchi, George G. Malliaras, Marc Ramuz and Róisín M. Owens*

Microsystems & Nanoengineering - Nature (2017) 3, 17028; DOI:10.1038/micronano.2017.28

"Saccharomyces boulardii CNCM I-745 restores intestinal barrier integrity by regulation of E-cadherin recycling", *Chloé Terciolo, Aurélie Dobric, Mehdi Ouaissi, Carole Siret, Gilles Breuzard, Françoise Silvy, Bastien Marchiori, Sébastien Germain, Renaté Bonier, Adel Hama, Roisin Owens, Dominique Lombardo, Véronique Rigot, Frédéric André*

Journal of Crohn's and Colitis, (2017), vol. 11, no 8, p. 999-1010; doi:10.1093/ecco-jcc/jjx030

"Effect of E cigarette emissions on tracheal cells monitored at the air-liquid interface using an organic electrochemical transistor", *Magali P Ferro, Lara Leclerc, Mohamad Sleiman, Bastien Marchiori, Jérémie Pourchez, Roisin M. Owens and Marc Ramuz*

Journal article accepted with revisions in Advanced Biosystems

"PVDF-TrFE based stretchable infrared temperature sensor for e-skin application", *Bastien Marchiori, Stuart Hannah, Sylvain Blayac, Marc Ramuz*

Journal article in Preparation

"Serpentine shaped metal with active material for high surface area electrodes", *Mohamed Nasreldin, Bastien Marchiori, Marc Ramuz, Roger Delattre, Thierry Djenizian*

Journal article in Preparation

Oral contributions:

"New Process for the Patterning of Fully Stretchable Organic Biosensors—Application to the Organic Electrochemical Transistor", *Bastien Marchiori, Roger Delattre, Sylvain Blayac, Marc Ramuz*

Oral presentation at the MRS Spring Meeting 2018, Phoenix, United States of America

"New process for a fully stretchable Organic Electrochemical Transistor", *Bastien Marchiori, Roger Delattre, Sylvain Blayac, Marc Ramuz*

Oral presentation at the E-MRS Spring Meeting 2017, Strasbourg, France

References

[1] V. Kaushik *et al.*, 'Textile-Based Electronic Components for Energy Applications: Principles, Problems, and Perspective', *Nanomaterials*, vol. 5, no. 3, pp. 1493–1531, Sep. 2015.

[2] Y. Liu, M. Pharr, and G. A. Salvatore, 'Lab-on-Skin: A Review of Flexible and Stretchable Electronics for Wearable Health Monitoring', *ACS Nano*, vol. 11, no. 10, pp. 9614–9635, Oct. 2017.

[3] S. Lai, A. Zucca, P. Cosseddu, F. Greco, V. Mattoli, and A. Bonfiglio, 'Ultra-conformable Organic Field-Effect Transistors and circuits for epidermal electronic applications', *Org. Electron.*, vol. 46, pp. 60–67, Jul. 2017.

[4] W. W. Lee, J. Cabibihan, and N. V. Thakor, 'Bio-mimetic strategies for tactile sensing', in *SENSORS, 2013 IEEE*, 2013, pp. 1–4.

[5] E. García Breijo, B. G.-L. Pérez, and P. Cosseddu, Eds., *Organic sensors: materials and applications*. London, United Kingdom: The Institution of Engineering and Technology, 2017.

[6] R. D. Sontheimer, 'Skin Is Not the Largest Organ', *J. Invest. Dermatol.*, vol. 134, no. 2, pp. 581–582, Feb. 2014.

[7] M. L. Hammock, A. Chortos, B. C.-K. Tee, J. B.-H. Tok, and Z. Bao, '25th Anniversary Article: The Evolution of Electronic Skin (E-Skin): A Brief History, Design Considerations, and Recent Progress', *Adv. Mater.*, vol. 25, no. 42, pp. 5997–6038, Nov. 2013.

[8] L. Cai *et al.*, 'Super-stretchable, Transparent Carbon Nanotube-Based Capacitive Strain Sensors for Human Motion Detection', *Sci. Rep.*, vol. 3, Oct. 2013.

[9] G. Kettlgruber *et al.*, 'Intrinsically stretchable and rechargeable batteries for self-powered stretchable electronics', *J. Mater. Chem. A*, vol. 1, no. 18, p. 5505, 2013.

[10] R.-H. Kim *et al.*, 'Waterproof AlInGaP optoelectronics on stretchable substrates with applications in biomedicine and robotics', *Nat. Mater.*, vol. 9, no. 11, pp. 929–937, Nov. 2010.

[11] D. Ruh *et al.*, 'Stretchable Optoelectronic Circuits Embedded in a Polymer Network', *Adv. Mater.*, vol. 26, no. 11, pp. 1706–1710, Mar. 2014.

[12] R. C. Webb *et al.*, 'Ultrathin conformal devices for precise and continuous thermal characterisation of human skin', *Nat. Mater.*, vol. 12, no. 10, pp. 938–944, Sep. 2013.

[13] D.-H. Kim *et al.*, 'Epidermal Electronics', *Science*, vol. 333, no. 6044, pp. 838–843, Aug. 2011.

[14] W. Clippinger, R. Avery, and B. R. Titus, 'A sensory feedback system for an upper-limb amputation prosthesis', *Bull Prosthet. Res*, no. 247, 1974.

[15] V. J. Lumelsky, M. S. Shur, and S. Wagner, 'Sensitive skin', *IEEE Sens. J.*, vol. 1, no. 1, pp. 41–51, 2001.

[16] T. Someya, 'A large-area, flexible pressure sensor matrix with organic field-effect transistors for artificial skin applications', *Proc. Natl. Acad. Sci.*, vol. 101, no. 27, pp. 9966–9970, Jun. 2004.

[17] T. Someya *et al.*, 'Conformable, flexible, large-area networks of pressure and thermal sensors with organic transistor active matrixes', *Proc. Natl. Acad. Sci. U. S. A.*, vol. 102, no. 35, pp. 12321–12325, 2005.

[18] T. Sekitani, Y. Noguchi, K. Hata, T. Fukushima, T. Aida, and T. Someya, 'A Rubberlike Stretchable Active Matrix Using Elastic Conductors', *Science*, vol. 321, no. 5895, pp. 1468–1472, Sep. 2008.

[19] T. Sekitani *et al.*, 'Stretchable active-matrix organic light-emitting diode display using printable elastic conductors', *Nat. Mater.*, vol. 8, no. 6, pp. 494–499, Jun. 2009.

[20] T. Sekitani, Y. Noguchi, K. Hata, T. Fukushima, T. Aida, and T. Someya, 'A Rubberlike Stretchable Active Matrix Using Elastic Conductors', *Science*, vol. 321, no. 5895, pp. 1468–1472, Sep. 2008.

[21] S. C. B. Mannsfeld *et al.*, 'Highly sensitive flexible pressure sensors with microstructured rubber dielectric layers', *Nat. Mater.*, vol. 9, no. 10, pp. 859–864, Oct. 2010.

[22] M. Shimojo, A. Namiki, M. Ishikawa, R. Makino, and K. Mabuchi, 'A Tactile Sensor Sheet Using Pressure Conductive Rubber With Electrical-Wires Stitched Method', *IEEE Sens. J.*, vol. 4, no. 5, pp. 589–596, Oct. 2004.

[23] A. Shirinov, 'Pressure sensor from a PVDF film', *Sens. Actuators Phys.*, vol. 142, no. 1, pp. 48–55, Mar. 2008.

[24] D. J. Lichtenwalner, A. E. Hydrick, and A. I. Kingon, 'Flexible thin film temperature and strain sensor array utilizing a novel sensing concept', *Sens. Actuators Phys.*, vol. 135, no. 2, pp. 593–597, Apr. 2007.

[25] I. Graz *et al.*, 'Flexible active-matrix cells with selectively poled bifunctional polymer-ceramic nanocomposite for pressure and temperature sensing skin', *J. Appl. Phys.*, vol. 106, no. 3, p. 34503, Aug. 2009.

[26] T. Q. Trung and N.-E. Lee, 'Flexible and Stretchable Physical Sensor Integrated Platforms for Wearable Human-Activity Monitoring and Personal Healthcare', *Adv. Mater.*, vol. 28, no. 22, pp. 4338–4372, Jun. 2016.

[27] C. Yu, Z. Wang, H. Yu, and H. Jiang, 'A stretchable temperature sensor based on elastically buckled thin film devices on elastomeric substrates', *Appl. Phys. Lett.*, vol. 95, no. 14, p. 141912, 2009.

[28] C. Wang *et al.*, 'User-interactive electronic skin for instantaneous pressure visualization', *Nat. Mater.*, vol. 12, no. 10, pp. 899–904, Oct. 2013.

[29] M. Segev-Bar, A. Landman, M. Nir-Shapira, G. Shuster, and H. Haick, 'Tunable Touch Sensor and Combined Sensing Platform: Toward Nanoparticle-based Electronic Skin', *ACS Appl. Mater. Interfaces*, vol. 5, no. 12, pp. 5531–5541, Jun. 2013.

[30] J. Kim *et al.*, 'Stretchable silicon nanoribbon electronics for skin prosthesis', *Nat. Commun.*, vol. 5, p. 5747, Dec. 2014.

[31] C. K. Chiang and C. R. Fincher, 'Electrical Conductivity in Doped Polyacetylene', *Phys. Rev. Lett.*, vol. 39, no. 17, pp. 1098–1101, 1977.

[32] D.-S. Leem, A. Edwards, M. Faist, J. Nelson, D. D. C. Bradley, and J. C. de Mello, 'Efficient Organic Solar Cells with Solution-Processed Silver Nanowire Electrodes', *Adv. Mater.*, vol. 23, no. 38, pp. 4371–4375, Oct. 2011.

[33] O. Ostroverkhova, Ed., *Handbook of organic materials for optical and (opto)electronic devices: properties and applications*. Oxford: Woodhead Publishing, 2013.

[34] J. Jang and S. H. Han, 'High-performance OTFT and its application', *Curr. Appl. Phys.*, vol. 6, pp. e17–e21, Aug. 2006.

[35] G. C. McConnell, H. D. Rees, A. I. Levey, C.-A. Gutekunst, R. E. Gross, and R. V. Bellamkonda, 'Implanted neural electrodes cause chronic, local inflammation that is correlated with local neurodegeneration', *J. Neural Eng.*, vol. 6, no. 5, p. 56003, Oct. 2009.

[36] V. S. Polikov, P. A. Tresco, and W. M. Reichert, 'Response of brain tissue to chronically implanted neural electrodes', *J. Neurosci. Methods*, vol. 148, no. 1, pp. 1–18, Oct. 2005.

[37] M. R. Abidian, K. A. Ludwig, T. C. Marzullo, D. C. Martin, and D. R. Kipke, 'Interfacing Conducting Polymer Nanotubes with the Central Nervous System: Chronic Neural Recording using Poly(3,4-ethylenedioxythiophene) Nanotubes', *Adv. Mater.*, vol. 21, no. 37, pp. 3764–3770, Oct. 2009.

[38] J. A.K., G. Pavankumar, P. C. Ramamurthy, D. Roy Mahapatra, and G. Hegde, 'Understanding degradation phenomena in organic electronic devices', 2015, p. 93600S.

[39] S. Y. Son *et al.*, 'High-Field-Effect Mobility of Low-Crystallinity Conjugated Polymers with Localised Aggregates', *J. Am. Chem. Soc.*, vol. 138, no. 26, pp. 8096–8103, Jul. 2016.

[40] S. Ogata, J. Li, N. Hirosaki, Y. Shibutani, and S. Yip, 'Ideal shear strain of metals and ceramics', *Phys. Rev. B*, vol. 70, no. 10, Sep. 2004.

[41] N. Kim *et al.*, 'Highly Conductive PEDOT:PSS Nanofibrils Induced by Solution-Processed Crystallisation', *Adv. Mater.*, vol. 26, no. 14, pp. 2268–2272, Apr. 2014.

[42] *Polymer Microscopy*. New York, NY: Springer New York, 2008.

[43] G. Wang *et al.*, 'Aggregation control in natural brush-printed conjugated polymer films and implications for enhancing charge transport', *Proc. Natl. Acad. Sci.*, vol. 114, no. 47, pp. E10066–E10073, Nov. 2017.

[44] I. D. Johnston, D. K. McCluskey, C. K. L. Tan, and M. C. Tracey, 'Mechanical characterisation of bulk Sylgard 184 for microfluidics and microengineering', *J. Micromechanics Microengineering*, vol. 24, no. 3, p. 35017, Mar. 2014.

[45] K. Khanafer, A. Duprey, M. Schlicht, and R. Berguer, 'Effects of strain rate, mixing ratio, and stress–strain definition on the mechanical behavior of the polydimethylsiloxane (PDMS) material as related to its biological applications', *Biomed. Microdevices*, vol. 11, no. 2, pp. 503–508, Apr. 2009.

[46] T. K. Kim, J. K. Kim, and O. C. Jeong, 'Measurement of nonlinear mechanical properties of PDMS elastomer', *Microelectron. Eng.*, vol. 88, no. 8, pp. 1982–1985, Aug. 2011.

[47] The Essential Chemical Industry, 'Polymers: an overview', 2013. [Online]. Available: http://www.essentialchemicalindustry.org/polymers/polymers-an-overview.html. [Accessed: 07-Oct-2018].

[48] S. Wagner and S. Bauer, 'Materials for stretchable electronics', *MRS Bull.*, vol. 37, no. 3, pp. 207–213, Mar. 2012.

[49] J.-H. Ahn and J. H. Je, 'Stretchable electronics: materials, architectures and integrations', *J. Phys. Appl. Phys.*, vol. 45, no. 10, p. 103001, Mar. 2012.

[50] J. N. Lee, C. Park, and G. M. Whitesides, 'Solvent Compatibility of Poly(dimethylsiloxane)-Based Microfluidic Devices', *Anal. Chem.*, vol. 75, no. 23, pp. 6544–6554, Dec. 2003.

[51] W. Chen, R. H. W. Lam, and J. Fu, 'Photolithographic surface micromachining of polydimethylsiloxane (PDMS)', *Lab Chip*, vol. 12, no. 2, pp. 391–395, 2012.

[52] G. D. Moon *et al.*, 'Highly Stretchable Patterned Gold Electrodes Made of Au Nanosheets', *Adv. Mater.*, vol. 25, no. 19, pp. 2707–2712, May 2013.

[53] W. J. Hyun, S. Lim, B. Y. Ahn, J. A. Lewis, C. D. Frisbie, and L. F. Francis, 'Screen Printing of Highly Loaded Silver Inks on Plastic Substrates Using Silicon Stencils', *ACS Appl. Mater. Interfaces*, vol. 7, no. 23, pp. 12619–12624, Jun. 2015.

[54] J. Jiang *et al.*, 'Fabrication of Transparent Multilayer Circuits by Inkjet Printing', *Adv. Mater.*, vol. 28, no. 7, pp. 1420–1426, Feb. 2016.

[55] T.-H. Kim *et al.*, 'Kinetically controlled, adhesiveless transfer printing using microstructured stamps', *Appl. Phys. Lett.*, vol. 94, no. 11, p. 113502, Mar. 2009.

[56] Norgren, 'Chemical Resistance Chart', *Chemical Resistance Chart*. [Online]. Available: http://cdn.norgren.com/pdf/Chem%20Resis%20Man.pdf. [Accessed: 02-Sep-2018].

[57] Y. Cheng, R. Wang, J. Sun, and L. Gao, 'A Stretchable and Highly Sensitive Graphene-Based Fiber for Sensing Tensile Strain, Bending, and Torsion', *Adv. Mater.*, vol. 27, no. 45, pp. 7365–7371, Dec. 2015.

[58] N. Lu and S. Yang, 'Mechanics for stretchable sensors', *Curr. Opin. Solid State Mater. Sci.*, vol. 19, no. 3, pp. 149–159, Jun. 2015.

[59] S. Yang, E. Ng, and N. Lu, 'Indium Tin Oxide (ITO) serpentine ribbons on soft substrates stretched beyond 100%', *Extreme Mech. Lett.*, vol. 2, pp. 37–45, Mar. 2015.

[60] D. S. Gray, J. Tien, and C. S. Chen, 'High-Conductivity Elastomeric Electronics', *Adv. Mater.*, vol. 16, no. 5, pp. 393–397, Mar. 2004.

[61] H. Hocheng and C.-M. Chen, 'Design, Fabrication and Failure Analysis of Stretchable Electrical Routings', *Sensors*, vol. 14, no. 7, pp. 11855–11877, Jul. 2014.

[62] M. Gonzalez, F. Axisa, M. V. Bulcke, D. Brosteaux, B. Vandevelde, and J. Vanfleteren, 'Design of metal interconnects for stretchable electronic circuits', *Microelectron. Reliab.*, vol. 48, no. 6, pp. 825–832, Jun. 2008.

[63] Y.-Y. Hsu, M. Gonzalez, F. Bossuyt, F. Axisa, J. Vanfleteren, and I. De Wolf, 'The effects of encapsulation on deformation behavior and failure mechanisms of stretchable interconnects', *Thin Solid Films*, vol. 519, no. 7, pp. 2225–2234, Jan. 2011.

[64] D. Brosteaux, Fabrice Axisa, M. Gonzalez, and J. Vanfleteren, 'Design and Fabrication of Elastic Interconnections for Stretchable Electronic Circuits', *IEEE Electron Device Lett.*, vol. 28, no. 7, pp. 552–554, Jul. 2007.

[65] Y. Zhang *et al.*, 'Experimental and Theoretical Studies of Serpentine Microstructures Bonded To Prestrained Elastomers for Stretchable Electronics', *Adv. Funct. Mater.*, vol. 24, no. 14, pp. 2028–2037, Apr. 2014.

[66] J. Vanfleteren, 'Stretchable Electronics for Smart Textiles', presented at the COLAE Seminar, University of Gent, 25-Apr-2012.

[67] A. Jahanshahi *et al.*, 'Stretchable Circuits with Horseshoe Shaped Conductors Embedded in Elastic Polymers', *Jpn. J. Appl. Phys.*, vol. 52, no. 5S1, p. 05DA18, May 2013.

[68] F. Axisa, F. Bossuyt, T. Vervust, and J. Vanfleteren, 'Laser based fast prototyping methodology of producing stretchable and conformable electronic systems', in *Electronics System-Integration Technology Conference, 2008. ESTC 2008. 2nd*, 2008, pp. 1387–1390.

[69] N. Bowden, S. Brittain, A. G. Evans, J. W. Hutchinson, and G. M. Whitesides, 'Spontaneous formation of ordered structures in thin films of metals supported on an elastomeric polymer', *Nature*, vol. 393, no. 6681, pp. 146–149, 1998.

[70] M. Watanabe, H. Shirai, and T. Hirai, 'Wrinkled polypyrrole electrode for electroactive polymer actuators', *J. Appl. Phys.*, vol. 92, no. 8, pp. 4631–4637, Oct. 2002.

[71] S. P. Lacour, S. Wagner, Z. Huang, and Z. Suo, 'Stretchable gold conductors on elastomeric substrates', *Appl. Phys. Lett.*, vol. 82, no. 15, pp. 2404–2406, Apr. 2003.

[72] S. Wagner *et al.*, 'Electronic skin: architecture and components', *Phys. E Low-Dimens. Syst. Nanostructures*, vol. 25, no. 2–3, pp. 326–334, Nov. 2004.

[73] A. Hirsch, H. O. Michaud, A. P. Gerratt, S. de Mulatier, and S. P. Lacour, 'Intrinsically Stretchable Biphasic (Solid-Liquid) Thin Metal Films', *Adv. Mater.*, vol. 28, no. 22, pp. 4507–4512, Jun. 2016.

[74] Y. Sun, W. M. Choi, H. Jiang, Y. Y. Huang, and J. A. Rogers, 'Controlled buckling of semiconductor nanoribbons for stretchable electronics', *Nat. Nanotechnol.*, vol. 1, no. 3, pp. 201–207, Dec. 2006.

[75] B. Y. Ahn *et al.*, 'Omnidirectional Printing of Flexible, Stretchable, and Spanning Silver Microelectrodes', *Science*, vol. 323, no. 5921, pp. 1585–1593, 2009.

[76] C. Lv, H. Yu, and H. Jiang, 'Archimedean spiral design for extremely stretchable interconnects', *Extreme Mech. Lett.*, vol. 1, pp. 29–34, Dec. 2014.

[77] H.-B. Lee *et al.*, 'Mogul-Patterned Elastomeric Substrate for Stretchable Electronics', *Adv. Mater.*, vol. 28, no. 16, pp. 3069–3077, Apr. 2016.

[78] S. P. Lacour, D. Chan, S. Wagner, T. Li, and Z. Suo, 'Mechanisms of reversible stretchability of thin metal films on elastomeric substrates', *Appl. Phys. Lett.*, vol. 88, no. 20, p. 204103, May 2006.

[79] Y. Kim *et al.*, 'Stretchable nanoparticle conductors with self-organized conductive pathways', *Nature*, vol. 500, no. 7460, pp. 59–63, Jul. 2013.

[80] K.-Y. Chun *et al.*, 'Highly conductive, printable and stretchable composite films of carbon nanotubes and silver', *Nat. Nanotechnol.*, vol. 5, no. 12, pp. 853–857, Dec. 2010.

[81] D. J. Lipomi *et al.*, 'Skin-like pressure and strain sensors based on transparent elastic films of carbon nanotubes', *Nat. Nanotechnol.*, vol. 6, no. 12, pp. 788–792, Oct. 2011.

[82] M. Park *et al.*, 'Highly stretchable electric circuits from a composite material of silver nanoparticles and elastomeric fibres', *Nat. Nanotechnol.*, vol. 7, no. 12, pp. 803–809, Dec. 2012.

[83] F. Xu and Y. Zhu, 'Highly Conductive and Stretchable Silver Nanowire Conductors', *Adv. Mater.*, vol. 24, no. 37, pp. 5117–5122, Sep. 2012.

[84] N. Matsuhisa *et al.*, 'Printable elastic conductors with a high conductivity for electronic textile applications', *Nat. Commun.*, vol. 6, p. 7461, Jun. 2015.

[85] S.-W. Jung *et al.*, 'Stretchable Organic Thin-Film Transistors Fabricated on Elastomer Substrates Using Polyimide Stiff-Island Structures', *ECS Solid State Lett.*, vol. 4, no. 1, pp. P1–P3, 2015.

[86] R. Li, M. Li, Y. Su, J. Song, and X. Ni, 'An analytical mechanics model for the island-bridge structure of stretchable electronics', *Soft Matter*, vol. 9, no. 35, p. 8476, 2013.

[87] H. C. Ko *et al.*, 'A hemispherical electronic eye camera based on compressible silicon optoelectronics', *Nature*, vol. 454, no. 7205, pp. 748–753, Aug. 2008.

[88] S. P. Lacour, S. Wagner, R. J. Narayan, T. Li, and Z. Suo, 'Stiff subcircuit islands of diamondlike carbon for stretchable electronics', *J. Appl. Phys.*, vol. 100, no. 1, p. 14913, Jul. 2006.

[89] M. Amjadi, K.-U. Kyung, I. Park, and M. Sitti, 'Stretchable, Skin-Mountable, and Wearable Strain Sensors and Their Potential Applications: A Review', *Adv. Funct. Mater.*, vol. 26, no. 11, pp. 1678–1698, Mar. 2016.

[90] T. Yamada *et al.*, 'A stretchable carbon nanotube strain sensor for human-motion detection', *Nat. Nanotechnol.*, vol. 6, no. 5, pp. 296–301, May 2011.

[91] H. S. White, G. P. Kittlesen, and M. S. Wrighton, 'Chemical derivatization of an array of three gold microelectrodes with polypyrrole: fabrication of a molecule-based transistor', *J. Am. Chem. Soc.*, vol. 106, no. 18, pp. 5375–5377, 1984.

[92] M. Ramuz, A. Hama, M. Huerta, J. Rivnay, P. Leleux, and R. M. Owens, 'Combined Optical and Electronic Sensing of Epithelial Cells Using Planar Organic Transistors', *Adv. Mater.*, vol. 26, no. 41, pp. 7083–7090, Nov. 2014.

[93] R. Nave, [Online]. Available: http://hyperphysics.phy-astr.gsu.edu/hbase/wien.html. [Accessed: 23-Jul-2018].

[94] M. Lapczyna, K. P. Chen, P. R. Herman, H. W. Tan, and R. S. Marjoribanks, 'Ultra high repetition rate (133 MHz) laser ablation of aluminum with 1.2-ps pulses', *Appl. Phys. A*, vol. 69, no. 1, pp. S883–S886, 1999.

[95] J.-H. Klein-Wiele and P. Simon, 'Sub-100nm pattern generation by laser direct writing using a confinement layer', *Opt. Express*, vol. 21, no. 7, p. 9017, Apr. 2013.

[96] O. J. Ohara, M. Nagakubo, N. Kawahara, and T. Hattori, 'High aspect ratio etching by infrared laser induced micro bubbles', in *Micro Electro Mechanical Systems, 1997. MEMS'97, Proceedings, IEEE., Tenth Annual International Workshop on*, 1997, pp. 175–179.

[97] J. T. Kim, J. Pyo, J. Rho, J.-H. Ahn, J. H. Je, and G. Margaritondo, 'Three-Dimensional Writing of Highly Stretchable Organic Nanowires', *ACS Macro Lett.*, vol. 1, no. 3, pp. 375–379, Mar. 2012.

[98] S. Zhang, E. Hubis, G. Tomasello, G. Soliveri, P. Kumar, and F. Cicoira, 'Patterning of Stretchable Organic Electrochemical Transistors', *Chem. Mater.*, vol. 29, no. 7, pp. 3126–3132, Apr. 2017.

[99] Y. H. Kim, C. Sachse, M. L. Machala, C. May, L. Müller-Meskamp, and K. Leo, 'Highly Conductive PEDOT:PSS Electrode with Optimised Solvent and Thermal Post-Treatment for ITO-Free Organic Solar Cells', *Adv. Funct. Mater.*, vol. 21, no. 6, pp. 1076–1081, Mar. 2011.

[100] S. H. Eom *et al.*, 'Polymer solar cells based on inkjet-printed PEDOT:PSS layer', *Org. Electron.*, vol. 10, no. 3, pp. 536–542, May 2009.

[101] W. Hong, Y. Xu, G. Lu, C. Li, and G. Shi, 'Transparent graphene/PEDOT–PSS composite films as counter electrodes of dye-sensitized solar cells', *Electrochem. Commun.*, vol. 10, no. 10, pp. 1555–1558, Oct. 2008.

[102] J. Rivnay *et al.*, 'Structural control of mixed ionic and electronic transport in conducting polymers', *Nat. Commun.*, vol. 7, p. 11287, Apr. 2016.

[103] E. Stavrinidou *et al.*, 'Direct Measurement of Ion Mobility in a Conducting Polymer', *Adv. Mater.*, vol. 25, no. 32, pp. 4488–4493, Aug. 2013.

[104] X. Cui and D. C. Martin, 'Electrochemical deposition and characterisation of poly (3, 4-ethylenedioxythiophene) on neural microelectrode arrays', *Sens. Actuators B Chem.*, vol. 89, no. 1–2, pp. 92–102, 2003.

[105] H. W. Heuer, R. Wehrmann, and S. Kirchmeyer, 'Electrochromic Window Based on Conducting Poly (3, 4-ethylenedioxythiophene)–Poly (styrene sulfonate)', *Adv. Funct. Mater.*, vol. 12, no. 2, pp. 89–94, 2002.

[106] M. M. de Kok *et al.*, 'Modification of PEDOT:PSS as hole injection layer in polymer LEDs', *Phys. Status Solidi A*, vol. 201, no. 6, pp. 1342–1359, May 2004.

[107] S. Venkatraman *et al.*, 'In Vitro and In Vivo Evaluation of PEDOT Microelectrodes for Neural Stimulation and Recording', *IEEE Trans. Neural Syst. Rehabil. Eng.*, vol. 19, no. 3, pp. 307–316, Jun. 2011.

[108] E. Bihar, T. Roberts, M. Saadaoui, T. Hervé, J. B. De Graaf, and G. G. Malliaras, 'Inkjet-Printed PEDOT:PSS Electrodes on Paper for Electrocardiography', *Adv. Healthc. Mater.*, vol. 6, no. 6, p. 1601167, Mar. 2017.

[109] P. Leleux *et al.*, 'Conducting Polymer Electrodes for Electroencephalography', *Adv. Healthc. Mater.*, vol. 3, no. 4, pp. 490–493, Apr. 2014.

[110] P. Lin, F. Yan, and H. L. W. Chan, 'Ion-Sensitive Properties of Organic Electrochemical Transistors', *ACS Appl. Mater. Interfaces*, vol. 2, no. 6, pp. 1637–1641, Jun. 2010.

[111] M. Sessolo, J. Rivnay, E. Bandiello, G. G. Malliaras, and H. J. Bolink, 'Ion-Selective Organic Electrochemical Transistors', *Adv. Mater.*, vol. 26, no. 28, pp. 4803–4807, Jul. 2014.

[112] D. J. Macaya, M. Nikolou, S. Takamatsu, J. T. Mabeck, R. M. Owens, and G. G. Malliaras, 'Simple glucose sensors with micromolar sensitivity based on organic electrochemical transistors', *Sens. Actuators B Chem.*, vol. 123, no. 1, pp. 374–378, Apr. 2007.

[113] D. Khodagholy *et al.*, 'Organic electrochemical transistor incorporating an ionogel as a solid state electrolyte for lactate sensing', *J. Mater. Chem.*, vol. 22, no. 10, p. 4440, 2012.

[114] N. Coppedè, G. Tarabella, M. Villani, D. Calestani, S. Iannotta, and Z. Andrea, 'Human Stress Monitoring Through an Organic Cotton-Fiber Biosensor', *J. Mater. Chem. B*, vol. 2, no. 34, pp. 5620–5626.

[115] S. Tria, L. Jimison, A. Hama, M. Bongo, and R. Owens, 'Sensing of EGTA Mediated Barrier Tissue Disruption with an Organic Transistor', *Biosensors*, vol. 3, no. 1, pp. 44–57, Jan. 2013.

[116] D. Khodagholy *et al.*, 'High transconductance organic electrochemical transistors', *Nat. Commun.*, vol. 4, Jul. 2013.

[117] D. Khodagholy *et al.*, 'In vivo recordings of brain activity using organic transistors', *Nat. Commun.*, vol. 4, no. 1, Dec. 2013.

[118] A. Campana, T. Cramer, D. T. Simon, M. Berggren, and F. Biscarini, 'Electrocardiographic Recording with Conformable Organic Electrochemical Transistor Fabricated on Resorbable Bioscaffold', *Adv. Mater.*, vol. 26, no. 23, pp. 3874–3878, Jun. 2014.

[119] Y. Xia and J. Ouyang, 'PEDOT:PSS films with significantly enhanced conductivities induced by preferential solvation with cosolvents and their application in polymer photovoltaic cells', *J. Mater. Chem.*, vol. 21, no. 13, p. 4927, 2011.

[120] A. M. Nardes, R. A. J. Janssen, and M. Kemerink, 'A Morphological Model for the Solvent-Enhanced Conductivity of PEDOT:PSS Thin Films', *Adv. Funct. Mater.*, vol. 18, no. 6, pp. 865–871, Mar. 2008.

[121] T. Takano, H. Masunaga, A. Fujiwara, H. Okuzaki, and T. Sasaki, 'PEDOT Nanocrystal in Highly Conductive PEDOT:PSS Polymer Films', *Macromolecules*, vol. 45, no. 9, pp. 3859–3865, May 2012.

[122] B. Fan, X. Mei, and J. Ouyang, 'Significant Conductivity Enhancement of Conductive Poly(3,4-ethylenedioxythiophene):Poly(styrenesulfonate) Films by Adding Anionic Surfactants into Polymer Solution', *Macromolecules*, vol. 41, no. 16, pp. 5971–5973, Aug. 2008.

[123] S. Zhang, P. Kumar, A. S. Nouas, L. Fontaine, H. Tang, and F. Cicoira, 'Solvent-induced changes in PEDOT:PSS films for organic electrochemical transistors', *APL Mater.*, vol. 3, no. 1, p. 14911, Jan. 2015.

[124] M. Sessolo *et al.*, 'Easy-to-Fabricate Conducting Polymer Microelectrode Arrays', *Adv. Mater.*, vol. 25, no. 15, pp. 2135–2139, Apr. 2013.

[125] J. A. DeFranco, B. S. Schmidt, M. Lipson, and G. G. Malliaras, 'Photolithographic patterning of organic electronic materials', *Org. Electron.*, vol. 7, no. 1, pp. 22–28, Feb. 2006.

[126] F. Algahtani, K. B. Thulasiram, N. M. Nasir, and A. S. Holland, 'Four point probe geometry modified correction factor for determining resistivity', presented at the SPIE Micro+Nano Materials, Devices, and Applications, Melbourne, Victoria, Australia, 2013, p. 89235D.

[127] C. R. Keese, J. Wegener, S. R. Walker, and I. Giaever, 'Electrical wound-healing assay for cells in vitro', *Proc. Natl. Acad. Sci. U. S. A.*, vol. 101, no. 6, pp. 1554–1559, 2004.

[128] J. Wegener, C. R. Keese, and I. Giaever, 'Recovery of adherent cells after in situ electroporation monitored electrically', *Biotechniques*, vol. 33, no. 2, pp. 348–357, 2002.

[129] J. Teissie, M. Golzio, and M. P. Rols, 'Mechanisms of cell membrane electropermeabilization: A minireview of our present (lack of ?) knowledge', *Biochim. Biophys. Acta BBA - Gen. Subj.*, vol. 1724, no. 3, pp. 270–280, Aug. 2005.

[130] P. Tehrani, A. Kanciurzewska, X. Crispin, N. Robinson, M. Fahlman, and M. Berggren, 'The effect of pH on the electrochemical over-oxidation in PEDOT:PSS films', *Solid State Ion.*, vol. 177, no. 39–40, pp. 3521–3527, Jan. 2007.

[131] C. Chen *et al.*, 'Mechanical characterisations of cast Poly(3,4-ethylenedioxythiophene):Poly(styrenesulfonate)/Polyvinyl Alcohol thin films', *Synth. Met.*, vol. 161, no. 21–22, pp. 2259–2267, Nov. 2011.

[132] M. Vosgueritchian, D. J. Lipomi, and Z. Bao, 'Highly Conductive and Transparent PEDOT:PSS Films with a Fluorosurfactant for Stretchable and Flexible Transparent Electrodes', *Adv. Funct. Mater.*, vol. 22, no. 2, pp. 421–428, Jan. 2012.

[133] D. J. Lipomi, J. A. Lee, M. Vosgueritchian, B. C.-K. Tee, J. A. Bolander, and Z. Bao, 'Electronic Properties of Transparent Conductive Films of PEDOT:PSS on Stretchable Substrates', *Chem. Mater.*, vol. 24, no. 2, pp. 373–382, Jan. 2012.

[134] H. Hillborg, J. F. Ankner, U. W. Gedde, G. D. Smith, H. K. Yasuda, and K. Wikstrom, 'Crosslinked polydimethylsiloxane exposed to oxygen plasma studied by neutron reflectometry and other surface specific techniques', *Polymer*, vol. 41, pp. 6851–6863, 2000.

[135] M. ElMahmoudy, S. Inal, A. Charrier, I. Uguz, G. G. Malliaras, and S. Sanaur, 'Tailoring the Electrochemical and Mechanical Properties of PEDOT:PSS Films for Bioelectronics', *Macromol. Mater. Eng.*, vol. 302, no. 5, p. 1600497, May 2017.

[136] 'Provided by Clevios PH1000 maker, Haraeus'. [Online]. Available: http://www.clevios.com/index.php?page_id = 3671.

[137] M. P. Anenden, M. Svehla, N. H. Lovell, and G. J. Suaning, 'Process development for dry etching polydimethylsiloxane for neural electrodes', in *Engineering in Medicine and Biology Society, EMBC, 2011 Annual International Conference of the IEEE*, 2011, pp. 2977–2980.

[138] M.-E. Vlachopoulou, G. Kokkoris, C. Cardinaud, E. Gogolides, and A. Tserepi, 'Plasma Etching of Poly(dimethylsiloxane): Roughness Formation, Mechanism, Control, and Application in the Fabrication of Microfluidic Structures', *Plasma Process. Polym.*, vol. 10, no. 1, pp. 29–40, Jan. 2013.

[139] Y.-L. Loo, R. L. Willett, K. W. Baldwin, and J. A. Rogers, 'Interfacial Chemistries for Nanoscale Transfer Printing', *J. Am. Chem. Soc.*, vol. 124, no. 26, pp. 7654–7655, Jul. 2002.

[140] L. E. Osborn *et al.*, 'Prosthesis with neuromorphic multilayered e-dermis perceives touch and pain', *Sci. Robot.*, vol. 3, no. 19, p. eaat3818, 2018.

[141] R. G. Kepler, 'Piezoelectricity, pyroelectricity, and ferroelectricity in organic materials', *Annu. Rev. Phys. Chem.*, vol. 29, no. 1, pp. 497–518, 1978.

[142] L. Carlioz, J. Delamare, S. Basrour, and G. Poulin, 'Hybridization of magnetism and piezoelectricity for an energy scavenger based on temporal variation of temperature', in

2008 Symposium on Design, Test, Integration and Packaging of MEMS/MOEMS, Nice, France, 2008, pp. 311–313.

[143] B. Ploss, B. Ploss, F. G. Shin, H. L. W. Chan, and C. L. Choy, 'Pyroelectric Activity of Ferroelectric PT/PVDF-TRFE', *IEEE Trans. Dielectr. Electr. Insul.*, vol. 7, no. 4, Aug. 2000.

[144] S. Ebnesajjad, 'Introduction to fluoropolymers: materials, technology and applications', William Andrew, 2013.

[145] J. G. Bergman, J. H. McFee, and G. R. Crane, 'PYROELECTRICITY AND OPTICAL SECOND HARMONIC GENERATION IN POLYVINYLIDENE FLUORIDE FILMS', *Appl. Phys. Lett.*, vol. 18, no. 5, pp. 203–205, Mar. 1971.

[146] H. KAWAI, 'The piezoelectricity of poly (vinylidene fluoride)', *J. Appl. Phys.*, no. 8, pp. 975–976, 1969.

[147] Y. Takahashi, Y. Matsubara, and H. Tadokoro, 'Mechanisms for crystal phase transformations by heat treatment and molecular motion in poly (vinylidene fluoride)', *Macromolecules*, vol. 15, no. 2, pp. 334–338, 1982.

[148] R. Gregorio, 'Determination of the α, β, and γ crystalline phases of poly(vinylidene fluoride) films prepared at different conditions', *J. Appl. Polym. Sci.*, vol. 100, no. 4, pp. 3272–3279, May 2006.

[149] E. Giannetti, 'Semi-crystalline fluorinated polymers', *Polym. Int.*, vol. 50, no. 1, pp. 10–26, 2001.

[150] W. Li, Y. Zhu, D. Hua, P. Wang, X. Chen, and J. Shen, 'Crystalline morphologies of P(VDF-TrFE) (70/30) copolymer films above melting point', *Appl. Surf. Sci.*, vol. 254, no. 22, pp. 7321–7325, Sep. 2008.

[151] K. Koga and H. Ohigashi, 'Piezoelectricity and related properties of vinylidene fluoride and trifluoroethylene copolymers', *J. Appl. Phys.*, vol. 59, no. 6, pp. 2142–2150, Mar. 1986.

[152] E. Bihler, G. Neumann, G. Eberle, and W. Eisenmenger, 'Influence of charge injection on the formation of remanent polarisation in P (VDF-TrFE) copolymers', in *Electrical Insulation and Dielectric Phenomena, 1990. Annual Report., Conference on*, 1990, pp. 140–145.

[153] M. Levesque, M. Cote, S. Lelievre, and P. Galarneau, 'P (VDF-TrFE) infrared detectors and array', in *Infrared Technology XX*, 1994, vol. 2269, pp. 124–131.

[154] N. Fujitsuka *et al.*, 'Monolithic pyroelectric infrared image sensor using PVDF thin film', *Sens. Actuators Phys.*, vol. 66, no. 1–3, pp. 237–243, 1998.

[155] A. Pecora, L. Maiolo, F. Maita, and A. Minotti, 'Flexible PVDF-TrFE pyroelectric sensor driven by polysilicon thin film transistor fabricated on ultra-thin polyimide substrate', *Sens. Actuators Phys.*, vol. 185, pp. 39–43, Oct. 2012.

[156] R. Freitag and H. Meixner, 'PVDF sensor array for human body detection', in *Electrets, 1988.(ISE 6) Proceedings., 6th International Symposium on (IEEE Cat. No. 88CH2593-2)*, 1988, pp. 374–378.

[157] D. J. Advena, V. T. Bly, and J. T. Cox, 'Deposition and characterisation of far-infrared absorbing gold black films', *Appl. Opt.*, vol. 32, no. 7, pp. 1136–1144, 1993.

[158] J. Lehman, E. Theocharous, G. Eppeldauer, and C. Pannell, 'Gold-black coatings for freestanding pyroelectric detectors', *Meas. Sci. Technol.*, vol. 14, no. 7, pp. 916–922, Jul. 2003.

[159] S. Hannah, A. Davidson, I. Glesk, D. Uttamchandani, R. Dahiya, and H. Gleskova, 'Multifunctional sensor based on organic field-effect transistor and ferroelectric poly(vinylidene fluoride trifluoroethylene)', *Org. Electron.*, vol. 56, pp. 170–177, May 2018.

[160] M. Ramuz, B. C.-K. Tee, J. B.-H. Tok, and Z. Bao, 'Transparent, Optical, Pressure-Sensitive Artificial Skin for Large-Area Stretchable Electronics', *Adv. Mater.*, vol. 24, no. 24, pp. 3223–3227, Jun. 2012.

Résumé des parties en français

Introduction

Le développement de l'électronique flexible et extensible a ouvert la possibilité à de nombreuses nouvelles applications. Les systèmes électroniques que l'on peut porter sur soi sont généralement flexibles et très minces, ils peuvent se conformer aux surfaces 3D. Les dispositifs extensibles peuvent être encore plus efficaces, et subir toute déformation. Pour une application sur la peau, cette propriété est obligatoire. La peau peut s'étirer jusqu'à 15% et bouge constamment. Ces technologies sont donc particulièrement adaptées au développement de capteurs et d'actionneurs distribués directement sur la peau humaine.

La sensation de toucher et de pression dans la peau artificielle a été largement étudiée, mais l'intégration de capacités de détection de température reste un défi, et en particulier la détection sans contact. Cette thèse a pour objectif de comprendre les stratégies de fabrication de dispositifs étirables ; et ensuite, de fournir les outils pour fabriquer des capteurs étirables pour les intégrer dans une peau artificielle. Les différentes composantes d'un capteur extensible sont analysées pour sélectionner les matériaux et les méthodes appropriés à cette application. De nouveaux procédés de fabrication facile et rapide de dispositifs hautement étirables sont introduits. Pour comprendre les défis et développer les procédés de fabrication de capteurs extensibles, un transistor électrochimique organique (OECT) étirable et performant est fabriqué. Son intégration sur la peau permettrait de détecter divers paramètres physiologiques. Ensuite, la fabrication d'un capteur infrarouge extensible avec des performances similaires à celles des dispositifs électroniques rigides est démontrée.

Le chapitre 1 passe en revue les capteurs étirables déjà existants pour la peau électronique. Une étude des dispositifs extensibles est réalisée pour comprendre la structure de la conception de tels systèmes. Un capteur extensible comprend 3 blocs avec différentes stratégies pour rendre l'ensemble du capteur extensible: le substrat pour porter le dispositif, les interconnexions

intégrées dans le substrat pour transmettre le signal, et la zone active entre les interconnexions pour générer ce signal.

Le chapitre 2 décrit une méthode pour réaliser des interconnexions étirables hautement conductrices. Ce procédé permet la fabrication d'interconnexions métalliques épaisses pour une résistivité minimale sous étirement et ainsi une qualité du signal élevée.

Le chapitre 3 présente l'intégration des interconnexions compatibles avec les procédés de micro fabrication classiques et son application à des capteurs organiques, ave la fabrication d'un transistor électrochimique organique.

Le chapitre 4 est consacré à la fabrication du capteur de température et infrarouge étirable. En utilisant les connaissances développées dans les chapitres précédents, le capteur montre des résultats prometteurs pour une intégration dans une peau électronique.

Résumé du chapitre 1: Etat de l'art sur les capteurs pour l'électronique souple

Ce chapitre donne un aperçu général du travail effectué pour fabriquer des dispositifs électroniques étirables destinés à des applications en peau électronique. La définition de dispositif étirable, dans cette thèse, doit être comprise par la capacité d'un objet (plus précisément d'un dispositif ou d'un matériau) à être élastiquement allongé sans être inélastiquement, ou définitivement déformé. Un dispositif étirable conserve par définition sa fonctionnalité jusqu'à un certain allongement définissant son extensibilité. Une étude des différents dispositifs étirables pour la peau électronique est effectuée dans la première section. Les différents éléments d'un tel système étirable sont identifiés et analysés. Une sélection des matériaux pour le substrat, les interconnexions et la zone active est effectuée. Les matériaux et les procédés sont choisis en fonction des applications. Ensuite, une introduction aux deux capteurs développés pendant cette thèse est fournie afin d'en comprendre les défis.

Les composants électroniques étirables sont les circuits électriques et électroniques qui sont élastiquement ou inélastiquement extensibles de plus de quelques pourcents tout en maintenant leurs fonctions initiales. Pour ce faire, les dispositifs ont tendance à être généralement fins. Comparés aux systèmes électroniques conventionnels rigides, en formats planaires, les systèmes électroniques étirables peuvent être étirés, compressés, pliés et déformés selon des formes quelconques sans défaillance électrique ou mécanique des circuits. Pour cette raison, les systèmes électroniques extensibles ont de nombreuses applications importantes et émergentes dans de nouveaux domaines inspirés par le vivant, mous et incurvés, tels que les caméras oculaires électroniques ou la peau artificielle, capable d'une intégration mécaniquement invisible sur la peau humaine. Le corps humain est mou, toujours en mouvement et en évolution. Sa peau peut être étirée pendant les mouvements jusqu'à 15% [2]. Les systèmes électroniques doivent donc correspondre aux propriétés mécaniques de la peau pour s'adapter au corps. De plus, cette évolution conduira à des systèmes électroniques plus imperceptibles, plus confortables à utiliser. Par exemple, les capteurs extensibles pour des

applications biomédicales incluent diverses capacités de détection telles que la température, le toucher / pression, l'électrocardiogramme et la détection de mouvement. Des appareils électroniques étirables peuvent également être attachés à n'importe quel organe du corps pour surveiller ou assister les organes pour les soins de santé. Des capteurs très minces et flexibles ont déjà été intégrés et ont montré un bon contact avec la peau [3].

Un capteur étirable, et plus globalement un dispositif étirable, est construit autour de 3 composants: un substrat, des interconnexions et un matériau actif.

- Le substrat est le premier matériau à choisir. Il doit être étirable car il s'agit du matériau qui subit directement la déformation, et contient le capteur. Le substrat doit être compatible avec le procédé de fabrication du dispositif final. L'extensibilité du substrat: sa capacité à se déformer avant qu'il ne casse ou ne perde ses propriétés initiales est essentielle.

- Les interconnexions, sont définit l'extensibilité et la conductivité de l'interconnexion. Il est important d'avoir une conductivité élevée pour que le signal délivré par le capteur soit précis. Ainsi, une étude de la conductivité relative à l'extensibilité de ces interconnexions est la clé pour choisir les matériaux et les techniques adaptés à cette application.

- Le matériau actif de détection: les matériaux inorganiques et organiques sont des candidats potentiels pour cette fonction. Les matériaux inorganiques étant rigides, la stratégie appropriée consiste donc à intégrer un matériau rigide dans une matrice étirable. En ce qui concerne les matériaux organiques, ceux-ci possèdent naturellement une meilleure extensibilité que les métaux. Il est possible d'améliorer la capacité d'étirement du dispositif global par différentes techniques et d'étudier la stratégie permettant de minimiser les contraintes subies par le matériau actif conduisant à sa rupture. Cette contrainte est causée par l'application d'une force: une tension qui tire le matériau. Le matériau a un certain degré de résistance à la contrainte avant d'être étiré.

La fabrication d'un dispositif étirable est toujours construite autour d'une même logique. Le substrat est fabriqué indépendamment des interconnexions. Ensuite, en fonction du matériau utilisé, une stratégie est choisie pour intégrer les interconnexions au sein de ce substrat. Enfin, le matériau actif est déposé et défini en utilisant des techniques de micro-fabrication [5].

Le but de ce travail est de développer et de fabriquer des capteurs électroniques extensibles pour des applications en peau artificielle. Par exemple, un OECT étirable – utilisé pour la détection de signaux physiologiques - a été développé. De plus, un capteur sensible à la température a été fabriqué, possédant une capacité à détecter une émission infrarouge, afin de reproduire la capacité du corps humain à ressentir la température, même sans contact direct avec cette dernière. Tous ces dispositifs doivent être capables de s'étirer de plus de 15% pour être intégrés dans une peau électronique. Ainsi, un objectif de 30% a été défini pour nos capteurs; et une extensibilité accrue améliorera d'autant plus la fiabilité de l'appareil. Un problème avec les dispositifs étirables, cependant, est la disponibilité limitée de matériaux conducteurs métalliques, de semi-conducteurs et plus généralement de dispositifs ayant les mêmes propriétés électriques que les systèmes électroniques rigides.
Outre un certain degré de flexibilité, les matériaux organiques sont potentiellement peu coûteux et faciles à intégrer dans une fabrication à grande échelle. Pour la détection, cette flexibilité mécanique et leur conductivité ionique / électronique mixte sont également mieux adaptées à la détection de signaux en interaction avec le corps, pour des mesures physiologiques [5].Par conséquent, le développement de capteurs organiques a été choisi comme axe de ce travail avec deux capteurs:

• L'OECT est un capteur qui correspond à la vision de peau électronique. Il peut être utilisé comme capteur multitâche pour mesurer des paramètres physiologiques du corps.

• Un capteur infrarouge pour la mesure de température contact / sans contact, qui vise à être intégré à la peau électronique, en particulier pour les applications en prothétiques et en robotiques.

Résumé du chapitre 2: développement et caractérisation d'interconnexions étirables fabriquées par découpe laser

Le développement d'interconnexions métalliques en forme de fer à cheval est plus efficace pour les matériaux métalliques épais. Ces matériaux ont l'avantage d'être très conducteurs. Cependant, la littérature ne fournit pas de procédé de fabrication optimisé pour les métaux épais. La technologie étudiée dans le chapitre 1 est soit basée sur la photolithographie, coûteuse et fastidieuse; soit sur la découpe laser de films minces sur un substrat polymère flexible. De plus, la littérature n'établit pas de règles claires pour la conception des interconnexions en forme de fer à cheval.

L'objectif de ce chapitre est de développer un procédé simple et rapide permettant la fabrication d'interconnexions métalliques possédant une faible résistance et une extensibilité maximale. Dans ce but, un procédé de fabrication basé sur de la découpe laser permettant la fabrication d'interconnexions métalliques encapsulées dans du PDMS est décrit. Différents matériaux pour les interconnexions sont étudiés et la forme est optimisée pour une extensibilité maximale.

Des interconnexions avec une faible résistance et stables sous étirement ont été fabriquées. Leur faible résistance permet une mesure précise pour des capteurs. Le procédé utilisé est compatible avec les techniques de micro-fabrication et le dispositif final est plat et prêt pour la prochaine étape d'intégration du capteur. Les interconnexions sont extensibles jusqu'à 80%, ce qui est plus que l'objectif de 30%. Cependant, les mesures en cyclage montrent environ 90 cycles d'étirement avant la rupture de la ligne. Ces performances sont suffisantes pour des tests en laboratoire, mais doivent être améliorées pour les applications de peau électronique. Une amélioration de l'étirement est possible grâce à une étude de la couche d'encapsulation.

Résumé du chapitre 3: développement d'un OECT étirable pour des applications de capteur biologique et de peau électronique

L'OECT est un capteur qui permet plusieurs mesures et qui peut être intégré dans une peau pour mesurer les paramètres en temps réel du corps humain. De plus, le processus est bien maîtrisé et l'intégration du PEDOT:PSS au-dessus des interconnexions est un défi technologique pour la fabrication de dispositifs organiques totalement étirables. L'OECT est un transistor souvent à base PEDOT dopé avec du PSS en tant que matériau actif. Ce polymère est conducteur et largement utilisé pour sa capacité à convertir un flux ionique en flux de courant.

Un procédé pour structurer un transistor électrochimique étirable a été développé. En utilisant les interconnexions du chapitre 2, le procédé de fabrication repose une couche sacrificielle de Parylène-C et sur le remplacement des matériaux non étirables par du PDMS, définis par photolithographie et gravure plasma. Ce procédé constitue une preuve de la compatibilité des dispositifs et des outils présentés avec les techniques de micro-fabrication standard. Il évite toute étape de pré-étirement et ne contient que des matériaux étirables.

Le dispositif résultant affiche des performances similaires à celles d'une OECT standard jusqu'à 11% de déformation, avec une bonne transconductance et de bonnes caractéristiques de sortie jusqu'à 38%. Cependant, en raison du déséquilibre des propriétés mécaniques entre les interconnexions rigides et le PDMS, le polymère en couche mince (PEDOT:PSS) à l'interface est endommagé pendant l'étirement. Une conception appropriée du canal a permis de contrer cette limitation, mais les performances ont encore baissé après une déformation de 11%, alors que le PEDOT: PSS a montré plus d'extensibilité sur PDMS.

Résumé du chapitre 4: développement et caractérisation d'un capteur température/infrarouge étirable

Un objectif de l'e-skin sur des prothèses est de reproduire les capacités de la peau sur un bras robotique. L'utilisation de capteurs de pression pour donner la sensation du toucher est un sujet de recherche très actif et la transmission de la réponse des capteurs au cerveau a fait l'objet d'études approfondies [140]. Ce chapitre traite de l'intégration de la sensation de température et en particulier de la détection de sources de chaleur sans contact. Ainsi, il serait possible de détecter la température avant d'être trop près de l'objet et d'endommager la peau artificielle. L'objectif de ce chapitre est de développer des capteurs infrarouges avec une extensibilité supérieure à 30%. Un examen des capteurs de température a permis d'identifier les matériaux pyroélectriques comme un choix adéquat pour l'application de peau électronique. Le PVDF est un matériau polymère présentant ces propriétés. Il possède la particularité d'induire un champ électrique avec un changement de température qui disparaît lorsque la température est maintenue stable. Pour éviter le décalage du module d'Young dans le matériau, une stratégie d'îlots rigides est adoptée et le procédé de fabrication est adapté en conséquence. Ensuite, les méthodes de caractérisation des dispositifs sont expliquées. Enfin, différentes caractéristiques du dispositif sont présentées:

- la détection directe de température grâce à la mesure de capacité
- La détection dynamique du changement de température par la mesure de tension induite
- la réponse à une illumination infrarouge
- ses propriétés sous étirement

Le dispositif final présente une sensibilité à la détection de la température de 7pF/ °C sans contrainte. Aucun changement dans ses performances n'a été observé jusqu'à 35% d'étirement. La détection des radiations infrarouges est possible après polarisation du capteur. Cependant, son optimisation est requise pour pouvoir mesurer correctement la tension pyroélectrique sous étirement.

Conclusion

Le développement de capteurs capables de reproduire les capacités de la peau humaine est un sujet de recherche stimulant. L'intégration de capteurs de pression dans une peau artificielle a été rendue possible grâce à l'utilisation de capteurs étirables. Cependant, la fabrication de capteurs de température étirables et plus la détection de température sans contact n'a pas été largement étudiée.

Ce travail a présenté les activités en rapport avec l'électronique étirable. Il a mis en évidence le développement de l'électronique extensible et plus spécifiquement pour des applications de détection dans la peau électronique. En raison de la flexibilité mécanique et de l'extensibilité potentielle des matériaux organiques, le développement de capteurs organiques a été choisi pour ce travail. L'objectif d'extensibilité des capteurs a été établi à 30%. Le but est d'obtenir une faible résistance d'interconnexion avec une variation limitée pendant l'étirement afin de ne pas altérer le signal du capteur. Le développement de deux capteurs étirables a été présenté:

• Un transistor électrochimique organique, permettant la mesure de paramètres physiologiques.

• Un capteur de température infrarouge, permettant la mesure de la température dans une approche sans contact.

Le chapitre 1 a présenté un aperçu de l'électronique étirable pour en comprendre les défis, et pour choisir les matériaux et les technologies pour le développement d'interconnexions étirables. La meilleure solution identifiée repose sur des interconnexions métalliques en forme de fer à cheval. Aucune extensibilité supérieure à 100% n'a été démontrée dans la littérature, mais elle permet une faible résistance et une grande stabilité lors de l'étirement. Pour l'intégration des capteurs actifs, une technique classique – dite à architecture d'île - consiste à rigidifier une zone et à ne travailler que sur l'extensibilité des interconnexions. Une autre approche consiste à utiliser des matériaux intrinsèquement étirables déposés par exemple sur

un substrat précontraint. Cela donne une bonne extensibilité mais n'est pas facilement compatible avec les techniques dites classiques de micro fabrication.

Dans le chapitre 2, le procédé de fabrication et la caractérisation des interconnexions étirables à faible résistance coupés au laser ont été décrits. Le dispositif était étirable à 80% avec une augmentation de résistance de 1%. Il présentait une extensibilité comparable à celle déjà rapportée, mais avec une stabilité sans précédent et une résistance faible de l'ordre du milliohms, du fait de l'utilisation de feuilles métalliques épaisses. De plus, sa fabrication était rapide et facile à intégrer aux procédés de micro fabrication. Cette faible résistance à l'étirement est nécessaire pour la fabrication de capteurs extensibles de haute performance.

Au chapitre 3, le développement d'un OECT extensible a été démontré. Le développement de ce dispositif sur un substrat rigide pour la cicatrisation des plaies a été présenté dans une première approche. Ce travail était une introduction pour démontrer le potentiel de détection des OECT et quels sont les défis liés à l'utilisation de ce dispositif. La formulation et le procédé à la pointe de la technologie ont été optimisés pour rendre cet OECT étirable. Par rapport à la littérature, les performances électroniques obtenues sans contraintes sont comparables à des dispositifs rigide. Le dispositif était extensible jusqu'à 38%, mais la transconductance n'était pas stable lors de l'étirement. En effet, la fabrication de ce capteur est difficile en raison de l'hétérogénéité du module de Young à l'interface entre les différents matériaux utilisés; par exemple entre un métal rigide et un polymère souple. Une ingénierie appropriée à la transition métal / polymère doit être réalisée pour réduire les inégalités mécaniques et obtenir une transition en douceur.

Dans le dernier chapitre, le PVDF-TrFE a été utilisé pour fabriquer un capteur de température étirable. Ce capteur infrarouge avait pour objectif d'être intégré directement dans une peau électronique. Ce capteur a montré des résultats prometteurs, avec une extensibilité de 35% sans aucune modification des performances. Les interconnexions développées dans le cadre de cette thèse étaient an adéquation avec le développement du capteur de température infrarouge. Par rapport à l'OECT, la conception du capteur infrarouge est apparue plus adaptée à l'utilisation d'interconnexions métalliques épaisse. L'îlot rigide formé ne posait pas les problèmes d'incompatibilité de module d'Young rencontrés avec l'intégration du matériau actif

entre le métal rigide et le substrat étirable. Les interconnexions étaient rigides et parfaitement adaptées, servant d'îlot mécanique portant le matériau actif.

La prochaine étape de ce travail consiste à intégrer les capteurs dans une matrice afin de l'utiliser dans le modèle de peau électronique illustré par la figure 2. Le capteur peut être utilisé pour la pression et la température, ainsi que pour la détection infrarouge. Cependant, il est nécessaire de travailler sur la dissociation de ces différents effets. En effet, en tant que matériau piézoélectrique, le PVDF-TrFE a également une réponse à la pression et aux contraintes. Mais, dans le but d'intégrer ces dispositifs à d'autres capteurs de pression et de contact, Il serait possible de découpler au moins la température de ces effets. En effet, l'utilisation de capteurs tactiles et de pression stables à la température permettrait de prédire la réponse du PVDF-TrFE à ces stimulations. De plus, il n'est également pas possible de détecter l'infrarouge de préférence sur la réponse en température. Cependant, une source de chaleur à haute température émet une densité de puissance élevée des rayonnements infrarouges. Ainsi, le capteur sentirait un échauffement. Quoi qu'il en soit, dans le cas d'une peau électronique, la peau sentirait une source très chaude et comprendrait un danger. Le développement d'un capteur infrarouge étirable est une étape cruciale au développement de la peau électronique. L'intégration en matrice de capteur est le prochain défi. Les interconnexions développées dans ce travail sont extensibles dans une direction mais pas dans l'axe perpendiculaire. Cependant, certains travaux ont déjà été réalisés pour adapter l'utilisation des serpentins dans toutes les directions et peuvent être facilement adaptés aux interconnexions actuelles. De plus, la conception d'une matrice implique un dispositif pour adresser chaque capteur, avec la fabrication de transistors à films minces étirables, comme matrice active par exemple. Si plusieurs couches de détection sont utilisées dans une configuration d'empilement, chaque couche s'adressant à une capacité de détection spécifique, le signal enregistré doit être transmis d'une couche à une autre par des interconnexions verticales afin de collecter toutes les données. Ces interconnexions verticales doivent être développées en insérant des fils métalliques conventionnels entre les couches. Alternativement, les signaux enregistrés pourraient être transférés par la lumière, à travers des guides d'ondes extensibles pour porter les informations [160].

Annexe 1: LabVIEW code to make the stretching test

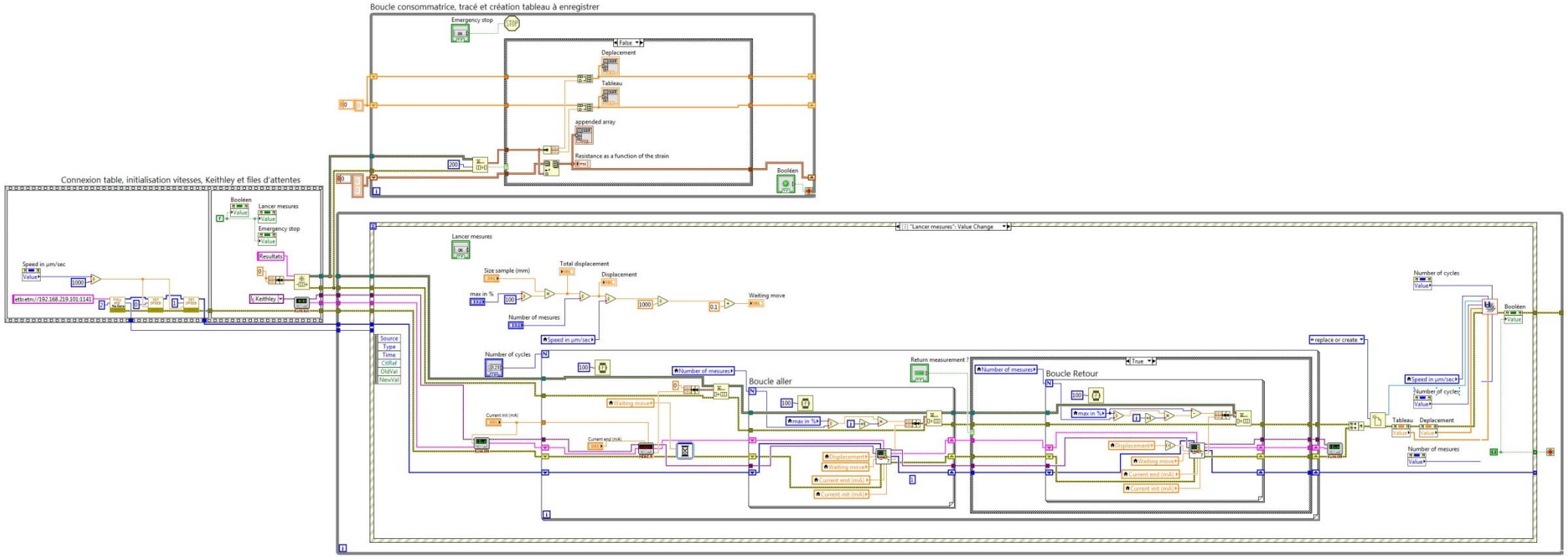

Annexe 2: Code developed to design horseshoe interconnections

This code is developed in Ruby, which is compatible with KLayout. It designs serpentines with pads connectors, with desired parameters Alpha, Radius, Width, L, number of serpentines, and width of the connection between the pad and the serpentines.

module MyMacro

```
#Initialization
#Create a new view (mode 1) with an empty layout
main_window = RBA::Application::instance.main_window
layout = main_window.create_layout(1).layout
layout_view = main_window.current_view
#Set the database unit (shown as an example, the default is 0.001)
layout.dbu = 0.01
#Create a layer (in this sample layer 1, datatype 0)
layer_index = layout.insert_layer(RBA::LayerInfo::new(1, 0))
#Add a cell (in this case "TOP")
cell_index = layout.add_cell("TOP")
cell = layout.cell(cell_index)

# Definition of the horseshoe parameters
w = 400*100   #Width line in µm divided by database unit
a = 20        #Angle alpha in deg
r = 800*100   #Radius of the arc of circle in µm divided by database unit
L = 800*100   #Length of connection between 2 horseshoe in µm divided by database unit

#Internal parameters for the design
alpha=a*Math::PI / 180      #Radians
ar= Math::PI + 2*a*Math::PI / 180     #Radians+ half circle
ac= (a*Math::PI / 180)
rint = r-w/2      #Internal circle  radius
rext = r+w/2      #External circle radius
rconnecteur=rext*5      #Radius of the connector to the pad
nboucles = 10     #Number of horseshoe
n=100       #Precision for the number of point in the arc of circle
da= ar/n     #Angle of the precision
a=0
b=0
d=0

#Calculous of the coordinates for the first motif
#Points of the external circle
fa=Math::cos(alpha) *rext *(-1)
fo=Math::sin(alpha) *rext *(-1)
#1st point of the connection
ao=Math::cos(alpha) *L
aa=Math::sin(alpha) *L
```

```
la=fa+aa
lo=fo-ao
#2nd point rectangle
bo=Math::sin(alpha) *rint
ba=Math::cos(alpha) *rint
ca=la-ba
co=lo-bo
#Last point circle
car= ca-ba
cor=co+bo
#Other point rectangle
dar=Math::sin(alpha) *L
dor=Math::cos(alpha) *L
ra=car+dar
ro=cor+dor
#Back of the first motif
wa=ra-Math::cos(alpha)*w
wo=ro+Math::sin(alpha)*w
far=Math::cos(alpha) *rint*(-1)
forr=Math::sin(alpha) *rint *(-1)
aor=Math::cos(alpha) *L
aar=Math::sin(alpha) *L
lar=far+aar
lor=forr-aor
dpa= a+fa

#Distance between 2 motifs
d=dpa + ra

# Left pad
pts = []
p1a=wa-ba
p1o= wo+bo
arp= Math::PI + alpha
dap= arp/n
acp= alpha
p2a=p1a-(rconnecteur-rint-w)

#Drawing 1st motif and left pad
serpentines and connection
for i in 0..n
pts.push(RBA::Point::from_dpoint(RBA::DPoint::new(p1a+rint * Math::cos(i*dap-acp), p1o+rint * Math::sin(i*dap-acp))))
end
for i in 0..n
pts.push(RBA::Point::from_dpoint(RBA::DPoint::new(p2a+rconnecteur * Math::cos((n-i)*Math::PI/n), p1o+rconnecteur *
Math::sin((n-i)*Math::PI/n))))
end
for i in 0..n
pts.push(RBA::Point::from_dpoint(RBA::DPoint::new(p1a+rext * Math::cos((n-i)*alpha/n-acp), p1o+rext * Math::sin((n-
i)*alpha/n-acp))))
end
cell.shapes(layer_index).insert(RBA::Polygon::new(pts))
#Circle of the pad
pts=[]
cpa=p1a-rint-3000*100
for i in 0..n
pts.push(RBA::Point::from_dpoint(RBA::DPoint::new(cpa+3000*100 * Math::cos(i*2*Math::PI/n), 3000*100 *
Math::sin(i*2*Math::PI/n))))
end
```

```
cell.shapes(layer_index).insert(RBA::Polygon::new(pts))
#Rectangle pad
cell.shapes(layer_index).insert(RBA::Box::new(cpa, -3000*100, cpa-9000*100, 3000*100))
for j in 0..nboucles
pts = []

#dernier point du cercle de centre (a,b)
fa=Math::cos(alpha) *rext *(-1) +a
fo=Math::sin(alpha) *rext *(-1)

#pour le premier point du rectangle
ao=Math::cos(alpha) *L
aa=Math::sin(alpha) *L
la=fa+aa
lo=fo-ao

#Coordonnées du centre de la boucle 2
#Pour le premier point du rectangle
bo=Math::sin(alpha) *rint
ba=Math::cos(alpha) *rint
ca=la-ba
co=lo-bo

#Coordonnées du dernier point du cercle
car= ca-ba
cor=co+bo

#coordonnées du point du rectangle au dessus
dar=Math::sin(alpha) *L
dor=Math::cos(alpha) *L
ra=car+dar
ro=cor+dor

#Creation de la structrureretour
wa=ra-Math::cos(alpha)*w
wo=ro+Math::sin(alpha)*w
far=Math::cos(alpha) *rint*(-1) +a
forr=Math::sin(alpha) *rint *(-1)
aor=Math::cos(alpha) *L
aar=Math::sin(alpha) *L
lar=far+aar
lor=forr-aor
for i in 0..n
pts.push(RBA::Point::from_dpoint(RBA::DPoint::new(a+rext * Math::cos(i*da-ac), b+rext * Math::sin(i*da-ac))))
end
pts.push(RBA::Point::new(la,lo))
#Boucle 2
for i in 0..n
pts.push(RBA::Point::from_dpoint(RBA::DPoint::new(ca+rint * Math::cos(i*da-ac), co+rint * Math::sin(-(i*da-ac)))))
end
pts.push(RBA::Point::new(ra,ro))
pts.push(RBA::Point::new(wa,wo))
for i in 0..n
pts.push(RBA::Point::from_dpoint(RBA::DPoint::new(ca+rext * Math::cos((n-i)*da-ac), co+rext * Math::sin(-((n-i)*da-ac)))))
end
pts.push(RBA::Point::new(lar,lor))
pts.push(RBA::Point::new(far,forr))
for i in 0..n
pts.push(RBA::Point::from_dpoint(RBA::DPoint::new(a+rint * Math::cos((n-i)*da-ac), rint * Math::sin((n-i)*da-ac))))
```

```
end

#Polygone
cell.shapes(layer_index).insert(RBA::Polygon::new(pts))
a=a-d+1
end

# Ajout du pad à droite
p1a=a+d
p1o=0
#dernier rectangle
pts = []
r11a=p1a+rint*Math::cos(alpha)
r11o=p1o-rint*Math::sin(alpha)
r12a=p1a+rext*Math::cos(alpha)
r12o=p1o-rext*Math::sin(alpha)
r21a=r11a-L*Math::sin(alpha)
r21o=r11o-L*Math::cos(alpha)
r22a=r12a-L*Math::sin(alpha)
r22o=r12o-L*Math::cos(alpha)
pts.push(RBA::Point::new(r11a,r11o))
pts.push(RBA::Point::new(r12a,r12o))
pts.push(RBA::Point::new(r22a,r22o))
pts.push(RBA::Point::new(r21a,r21o))
cell.shapes(layer_index).insert(RBA::Polygon::new(pts))

#dernier arc de cercle + rectangle
pts=[]
centrea=r22a+rint*Math::cos(alpha)
centreo=r22o-rint*Math::sin(alpha)
for i in 0..n
pts.push(RBA::Point::from_dpoint(RBA::DPoint::new(centrea+rint * Math::cos(-(n-i)*da+ac), centreo+rint * Math::sin(-(n-
i)*da+ac))))
end
r3a=centrea+rint*Math::cos(alpha)-L*Math::sin(alpha)
r3o=centreo+rint*Math::sin(alpha)+L*Math::cos(alpha)
pts.push(RBA::Point::new(r3a,r3o))
r4a=r3a+w*Math::cos(alpha)
r4o=r3o+w*Math::sin(alpha)
pts.push(RBA::Point::new(r4a,r4o))
for i in 0..n
pts.push(RBA::Point::from_dpoint(RBA::DPoint::new(centrea+rext * Math::cos(-i*da+ac), centreo+rext * Math::sin(-i*da+ac))))
end
cell.shapes(layer_index).insert(RBA::Polygon::new(pts))

#connecteur
# Ajout du pad à gauche
pts = []
r5a= r4a+ba
r5o= r4o+bo
arp= Math::PI + alpha
dap= arp/n
acp= alpha
p2a=r5a+(rconnecteur-rint-w)

#serpentin jusqu'à 90° puis connection
for i in 0..n
pts.push(RBA::Point::from_dpoint(RBA::DPoint::new(r5a+rint * Math::cos((n-i)*dap), r5o+rint * Math::sin((n-i)*dap))))
end
```

```
for i in 0..n
pts.push(RBA::Point::from_dpoint(RBA::DPoint::new(p2a+rconnecteur * Math::cos(i*Math::PI/n), r5o+rconnecteur *
Math::sin(i*Math::PI/n))))
end
for i in 0..n
pts.push(RBA::Point::from_dpoint(RBA::DPoint::new(r5a+rext * Math::cos(i*alpha/n+Math::PI), r5o+rext *
Math::sin(i*alpha/n+Math::PI))))
end
cell.shapes(layer_index).insert(RBA::Polygon::new(pts))

#cercle pad
pts=[]
cpa=r5a+rint+3000*100
for i in 0..n
pts.push(RBA::Point::from_dpoint(RBA::DPoint::new(cpa+3000*100 * Math::cos(i*2*Math::PI/n), 3000*100 *
Math::sin(i*2*Math::PI/n))))
end
cell.shapes(layer_index).insert(RBA::Polygon::new(pts))

#rectangle pad
cell.shapes(layer_index).insert(RBA::Box::new(cpa, -3000*100, cpa+9000*100, 3000*100))

#End
layout_view.select_cell(cell_index, 0)
layout_view.add_missing_layers
layout_view.zoom_fit
end
```

École Nationale Supérieure des Mines

de Saint-Étienne

NNT : Communiqué le jour de la soutenance

Bastien MARCHIORI

Stretchable electronics towards the fabrication of organic sensors for electronic skin

Speciality : Microelectronics

Keywords : Stretchable, sensors, e-skin

Abstract :

Stretchable electronics concern electrical and electronic circuits that are elastically or inelastically stretchable by more than a few percents while retaining function. In order to achieve this, devices tend to be laminar and usually thin. Compared with rigid, hard conventional electronic systems in planar formats, stretchable electronic systems can be stretched, compressed, bent, and deformed into arbitrary shapes without electrical or mechanical failure within the circuits. Currently, stretchable electronic systems have many important and emerging applications in new, soft and curved bio-inspired areas, such as tuneable electronic eye cameras or artificial skin capable of mechanically invisible integration onto human skin. These sensors would be integrated on robotic or prosthetic hands to recreate the same sensing capabilities than the skin: touch, pressure and temperature. The aim of this thesis is to identified strategies and materials to make stretchable devices with stretching capabilities similar to the one of the skin (~15%) with performance close to rigid devices. In this purpose, a microfabrication process to fabricate organic sensors has been developed. The devices are based on laser cut bulk metallic stretchable interconnections with maximum elongation of 80% in PDMS matrix. Then, these tools have been used to fabricate a biosensor: the organic electrochemical transistor (OECT). The transistor is based on a conducting polymer and is able to sense physiological signal. A temperature sensor has also been developed, able to sense infrared signal, like the human skin. These devices can stand up to 30% strain and can be integrated into a matrix for artificial skin applications.

École Nationale Supérieure des Mines

de Saint-Étienne

NNT : Communiqué le jour de la soutenance

Bastien MARCHIORI

Développement de l'électronique étirable pour la fabrication de capteurs organiques pour la peau électronique

Spécialité: Microélectronique

Mots-clefs: étirable, capteurs, peau électronique

Résumé :

Le domaine de l'électronique étirable concerne les circuits électriques et électroniques qui sont élastiquement ou inélastiquement étirables par plus de quelques pourcents tout en gardant leur intégrité mécanique et électrique. Actuellement, les dispositifs électroniques étirables ont de nouvelles applications émergentes, notamment pour les intégrer sur la peau. Ces systèmes, se présentent sous la forme d'une peau artificielle, qui peut intégrer des capteurs. Ces capteurs, peuvent être aussi intégrés sur des mains robotiques, ou des prothèses, pour recréer les mêmes propriétés que la peau : toucher, pression et température. Le but de ce travail est d'identifier les stratégies et les matériaux permettant de fabriquer des dispositifs étirables possédant une capacité d'étirement comparable à celle de la peau (~15%) avec des performances proches de l'électronique rigide. Pour cela, un procédé de micro fabrication permettant de fabriquer des capteurs organiques a été développé. Les systèmes développés sont basé sur des interconnections métalliques en forme de serpentin permettant un étirement jusqu'à 80%. Ensuite, ces différents outils ont été utilisés pour fabriquer un dispositif biomédical : le transistor électrochimique organique (OECT). Ce transistor utilise un polymère conducteur pour capter des signaux physiologiques. Enfin, un capteur température a été développé. Il peut aussi capter des signaux infrarouges, à la manière de la peau humaine. Ces dispositifs peuvent supporter des déformations jusqu'à 30% de sa longueur initiales et peuvent donc être intégrer sous forme de matrice pour une utilisation sur la peau artificielle.